



COMPACT ULTRAFAST FREQUENCY
COMBS

Thesis presented to the *Faculty of Science* for the degree of
Doctor of Science

Sargis Hakobyan

M. Sc. in Physics

Accepted on 29.11.2017 by the jury:

Prof. Thomas Südmeyer Director

Prof. Eric Cormier Examiner

Dr. Stéphane Schilt Examiner

Dr. Bojan Resan Examiner

Dr. Valentin Wittwer Examiner

Neuchâtel, 2017

IMPRIMATUR POUR THESE DE DOCTORAT

La Faculté des sciences de l'Université de Neuchâtel
autorise l'impression de la présente thèse soutenue par

Monsieur Sargis HAKOBYAN

Titre:

“Compact Ultrafast Frequency Combs”

sur le rapport des membres du jury composé comme suit:

- Prof. Thomas Südmeyer, directeur de thèse, Université de Neuchâtel, Suisse
- Dr Stéphane Schilt, Université de Neuchâtel, Suisse
- Prof. Eric Cormier, Université de Bordeaux, CELIA, France
- Dr Bojan Resan, Fachhochschule Nordwestschweiz, Suisse
- Dr Valentin Wittwer, Université de Neuchâtel, Suisse

Neuchâtel, le 30 janvier 2018

Le Doyen, Prof. R. Bshary



Keywords - Mot-clés

Keywords

Femtosecond laser, modelocked laser, diode-pumped solid-state laser (DPSSL), optical frequency comb, carrier envelope offset (CEO), self-referencing, phase stabilization, frequency noise, phase noise, opto-optical modulation (OOM), waveguide laser.

Mots-clés

Laser femtoseconde, laser à verrouillage de modes, laser à corps solide pompé par diode, peigne de fréquence optique, décalage de fréquence entre porteuse et enveloppe, auto-référencement, stabilisation de phase, bruit de fréquence, bruit de phase, modulation opto-optique (OOM), laser à guide d'onde

Acronyms

AC	Alternating current
AOFS	Acousto-optic frequency shifter
AOM	Acousto-optic modulator
CEO	Carrier-envelope offset
CW	Continuous wave
DBR	Distributed Bragg reflector
DC	Direct current
DPSSL	Diode-pumped solid-state laser
EOM	Electro-optic modulator
FN-PSD	Frequency-noise power spectral density
FWHM	Full-width half-maximum
HR	Highly reflective
HVA	High voltage amplifier
OC	Output coupler
OOM	Opto-optical modulator
PBS	Polarizing beam splitter
PCF	Photonic crystal fiber

PD	Photodiode
PI	Proportional integral
PID	Proportional integral derivative
PM	Polarization maintaining
PPLN	Periodically polled lithium niobate
PZT	Piezoelectric transducer
RBW	Resolution bandwidth
RF	Radio frequency
RIN	Relative intensity noise
SC	Supercontinuum
SESAM	Semiconductor saturable absorber mirror
SHG	Second harmonic generation
SM	Single mode
SNR	Signal-to-noise ratio
ULE	Ultra low expansion
VECSEL	Vertical External-Cavity Surface-Emitting Laser
VHG	Volume holographic grating
WG	Waveguide

Abstract

Optical frequency combs provide a direct and phase-coherent link between the optical spectral region of the electromagnetic spectrum (i.e., hundreds of THz frequencies) and the radio-frequency domain (MHz-GHz frequencies). As a result, they constitute a unique and powerful tool for various applications such as broadband high-resolution molecular spectroscopy, optical metrology, astrophysics, optical clocks, fundamental science and many other fields of research. Frequency combs with a high repetition rate are of particular interest for applications that can benefit from a high power per comb mode and a lower spectral density of comb modes, which makes the selection and filtering of a single optical line easier, and increases the signal-to-noise ratio in sensitive measurements.

Modelocked diode-pumped solid-state lasers (DPSSLs) are a perfect solution to generate high-power high repetition rate frequency combs. In this thesis, a 1-GHz comb based on a 1- μm DPSSL has been developed, with multi-watt output power and sub-100 fs pulse durations. This laser is an important step towards the development of compact cost-efficient frequency combs since it is pumped by a low-cost highly multimode pump laser diode. The optical spectrum of the laser has been fully stabilized by phase-locking both the repetition rate frequency to a radio-frequency (RF) reference signal by means of a piezoelectrical transducer controlling the cavity length of the laser, and the carrier-envelope offset (CEO) frequency using the traditional method of feedback to the pump current. This was achieved using a home-made high-bandwidth current

modulator for fast control of the pump power, as CEO stabilization is particularly challenging in high-repetition rate combs and requires a large stabilization bandwidth to compensate for the generally larger CEO frequency noise.

A detailed study of the noise properties of the comb is presented, enabling the identification of the dominant noise sources and their subsequent partial reduction. For instance, the limitation in the frequency noise of the comb lines arising at low Fourier frequencies from the noise floor of the RF reference signal used in the repetition rate stabilization was circumvented by locking a comb line to an optical reference, namely an ultra-stable Hz-level continuous-wave laser. As a result, a GHz frequency comb with ~ 150 -kHz comb mode linewidth was obtained with 2.1 W of average output power from the oscillator. The standard CEO stabilization method by feedback to the pump power is typically limited in bandwidth by the laser cavity dynamics, becoming a significant limiting factor in high-repetition rate combs. To overcome this limitation, the first opto-optical modulation (OOM) of a semiconductor saturable absorber mirror (SESAM) in a GHz DPSSL comb is reported in this thesis. With this SESAM-OOM, the stabilization bandwidth of the Yb:CALGO DPSSL was twice as large than the traditional gain modulation.

Another highly promising technology for GHz combs are waveguide lasers. As a first step towards such systems, Yb-doped waveguide lasers have been studied in CW and Q-switched operations. Waveguide lasers are one of the most attractive systems for fully integrated chip-based pulsed lasers. A highly-efficient Yb:YAG channel waveguide laser was demonstrated in this work, which can deliver Q-switched pulses with μJ pulse energies and an output power of up to 5.6 W. This achievement was made possible by recent progresses in fs-laser-written waveguide fabrication at Hamburg University and SESAM growth techniques at ETH Zurich with advanced structural designs. These lasers are very promising systems for various applications such as a seed source for nonlinear processes, Lidar systems, and micro-machining.

Résumé

Les peignes de fréquences optiques fournissent un lien direct et cohérent entre les domaines optiques (fréquence de quelques centaines de THz) et micro-ondes (fréquence dans les MHz ou GHz) du spectre électromagnétique. Ils constituent un outil unique et puissant pour de nombreuses applications telles que la spectroscopie moléculaire à haute-résolution et à large spectre, la métrologie optique, l'astrophysique, les horloges atomiques, la physique fondamentale et de nombreux autres domaines de recherche. Les peignes de fréquence avec un haut taux de répétition sont d'un intérêt particulier pour les applications pouvant bénéficier d'une puissance modale élevée et d'une faible densité de modes, qui facilite la sélection et le filtrage des modes individuels et augmente le rapport signal sur bruit dans des mesures sensibles.

Les lasers à verrouillage de mode à corps solide pompés par diode représentent une approche avantageuse pour la réalisation de peignes de fréquence de haute puissance et à taux de répétition élevé. Dans cette thèse, un peigne avec un taux de répétition de 1 GHz a été développé à partir d'un laser à verrouillage de mode émettant à une longueur d'onde de 1 μm . Le laser émet plus de 2 W de puissance moyenne dans des impulsions inférieures à 100 fs. Ce laser représente une étape importante vers la réalisation de peignes de fréquence compacts et économiquement avantageux puisqu'il est pompé par une diode laser multimode de bas coût. Le spectre du laser a été entièrement stabilisé par le verrouillage en phase simultané du taux de répétition sur une

référence radiofréquence (RF) à l'aide d'un élément piézo-électrique contrôlant la longueur de la cavité, et du décalage de fréquence entre porteuse et enveloppe (carrier-envelope offset - CEO - en anglais) par la méthode traditionnelle de rétroaction sur le courant de la diode de pompe. Cela a été réalisé à l'aide d'une électronique de modulation spécifiquement développée pour atteindre une haute bande passante de modulation qui est requise pour réduire le bruit généralement élevé du battement CEO dans les lasers à haut taux de répétition. Une analyse détaillée des propriétés de bruit du peigne est présentée, qui a permis d'identifier les sources de bruit dominantes et de réduire leur impact. Ainsi, la limitation apparaissant à basses fréquences de Fourier dans le bruit de fréquence d'une raie optique, qui provient du plancher de bruit de la référence RF utilisée dans la stabilisation du taux de répétition, a été repoussée en stabilisant une raie optique du peigne sur une référence optique. La référence optique est un laser ultra-stable avec une largeur de raie de quelques hertz. Ainsi, un peigne de fréquence avec un taux de répétition de 1 GHz, une puissance moyenne de 2.1 W et une largeur des raies optiques d'env. 150 kHz a été démontré. La méthode traditionnelle de stabilisation du battement CEO par rétroaction sur le courant de la diode de pompe est limitée en termes de bande passante par la dynamique de la cavité laser. Cela constitue une limitation majeure dans les peignes de fréquence à haut taux de répétition. Pour repousser cette limite, la première stabilisation du battement CEO dans un peigne de fréquence avec un taux de répétition dans la gamme du GHz par modulation opto-optique (OOM) d'un miroir saturable est présentée dans cette thèse. Avec cette méthode, la bande passante de stabilisation du laser Yb:CALGO a été augmentée d'un facteur 2 par rapport à l'approche traditionnelle utilisant une modulation du gain.

Une autre technologie attractive pour la réalisation de peignes de fréquence GHz sont les lasers à guide d'onde. Comme premier pas dans cette direction, des lasers à guide d'onde dopés à l'ytterbium ont été étudiés en régime d'émission continue et en mode déclenché (Q-switched). Les lasers à guide d'onde

constituent l'une des technologies les plus prometteuses pour la réalisation de lasers impulsions intégrés. Un laser à guide d'onde Yb:YAG de haute efficacité est démontré dans ce travail, délivrant des impulsions en mode déclenché avec une énergie de plusieurs μJ par impulsion et une puissance moyenne de 5.6 W. Ces performances ont été rendues possibles par les récents progrès réalisés dans les techniques de gravure de guides d'onde par lasers femtosecondes développées à l'université de Hambourg et dans la croissance de miroirs saturables à semi-conducteurs à l'ETH Zürich. Les lasers développés constituent une source attractive pour de nombreuses applications telles que pour des processus non-linéaires, des lidars, ou pour le micro-usinage.

Contents

1	Introduction and motivation	1
1.1	Lasers	3
1.1.1	Continuous wave lasers	3
1.1.2	Modelocked lasers	7
1.2	Frequency combs	9
1.2.1	Carrier Envelope Offset frequency detection	11
1.3	Stabilization of frequency combs	13
1.4	Outline of the thesis	14
2	High-power Yb:YAG waveguide lasers	17
2.1	Introduction	17
2.2	Dielectric waveguide fabrication methods	18
2.2.1	Ion-exchange	18
2.2.2	Liquid-phase epitaxy	19
2.2.3	Femtosecond laser inscription	20
2.3	Yb:YAG waveguide lasers	22

2.3.1	Fabrication	23
2.3.2	Experimental setup	24
2.3.3	Laser results	27
2.3.4	Conclusion	31
3 GHz repetition rate Yb:CALGO frequency comb		33
3.1	Introduction	33
3.2	1-GHz Yb:CALGO modelocked laser	35
3.2.1	Design	35
3.2.2	Laser performance	39
3.3	CEO frequency detection	40
3.4	Full stabilization of the frequency comb	44
3.4.1	Static and dynamic comb control	44
3.4.2	Stabilization schemes	46
3.5	Characterization of the fully stabilized comb	50
3.5.1	Frequency noise of the phase-locked comb parameters	50
3.5.2	CEO noise source analysis	53
3.5.3	Frequency stability	55
3.5.4	Characterization of an optical comb mode	56
3.6	Conclusion	61
4 GHz comb stabilization to an optical reference		65
4.1	Motivation	65

Contents

4.2	Further investigation on f_{rep} noise	70
4.3	Comb stabilization to an optical reference	73
4.4	Conclusion	77
5	Opto-optical stabilization of f_{CEO}	79
5.1	Introduction	79
5.2	OOM-SESAM stabilization of f_{CEO} in the 1-GHz Yb:CALGO laser	82
5.2.1	Experimental setup	82
5.2.2	Stabilization results	88
5.2.3	Conclusion	91
6	Conclusion and outcomes	93
	Bibliography	97
	Curriculum Vitae	111
	Acknowledgments	113

List of Figures

1.1	Fabry-Perot cavity, basic sechema of a laser	3
1.2	Overview of the center emission wavelengths of some commonly used laser gain crystals or glasses.	5
1.3	Cavity mode interference resulting in pulse formation in the time domain.	8
1.4	Time domain representation (top) and corresponding optical spectrum (bottom) of a modelocked laser frequency comb. In this particular example, the carrier-envelope phase $\Delta\varphi$ changes by $\pi/2$ from pulse to pulse, resulting in a CEO frequency of one fourth of the repetition rate.	10
1.5	Measurement principle of the self-referenced f -to- $2f$ interferometry, method for CEO frequency detection, showing the resulting generated beat signals at f_{CEO} and $f_{\text{rep}}-f_{\text{CEO}}$ (formulas highlighted in red and blue, respectively).	12
2.1	The main steps of the fabrication process of glass integrated channel waveguides by ion-exchange.	19
2.2	Images of a waveguide fabricated by liquid-phase epitaxy.	20
2.3	Femtosecond laser inscription of a waveguide.	22

2.4	Schematic of the fs-laser writing mechanism.	24
2.5	Experimental setup of the CW and Q-switched Yb:YAG waveguide lasers.	25
2.6	Picture of the waveguide laser in CW operation.	26
2.7	Output power (P_{out}) versus pump power (P_{pump}) for the CW laser configuration.	28
2.8	(a,b) Average output power P_{av} and pulse energy E_{p} versus pump power (P_{pump}) for the Q-switched laser configuration. (c,d) Optical spectra	29
2.9	Single Q-switched pulse and Q-switched pulse train	30
2.10	Pulse duration (τ_{p}) and repetition rate (f_{rep}) of the WG laser versus pump power (P_{pump})	30
2.11	Overview of the reported results on Q-switched, Q-switch mode-locked and modelocked channel waveguide lasers.	32
3.1	a) P_{out} and Voltage drop vs the pump current I_{pump} of the diode array, b) optical spectrum and M^2 measurement of the diode array	36
3.2	Scheme of the Yb:CALGO GHz laser	37
3.3	a) Picture of the overall Yb:CALGO laser cavity, b) Zoom on the SESAM mounted onto the PZT.	38
3.4	a) Average output power vs pump power for CW and modelocked (ML) operations. b) Optical spectrum of the laser in ML operation. c) Normalized radio-frequency (RF) spectrum of the laser in ML operation. d) Autocorrelation (AC) trace of an optical pulse of the laser (blue trace) with a sech^2 fit (dashed red line).	39

List of Figures

3.5	Overall scheme of the fully-stabilized Yb:CALGO GHz frequency comb.	41
3.6	Full octave-spanning SC spectrum measured at the output of the PCF.	42
3.7	f -to- $2f$ interferometer for f_{CEO} detection.	43
3.8	Radio frequency (RF) spectrum of the signal at the output of the f -to- $2f$ interferometer	43
3.9	Amplitude and phase transfer functions of the f_{rep} , f_{CEO} , and of pump optical power for pump current modulation, insets: static tuning curves of f_{rep} and f_{CEO}	45
3.10	Stabilization scheme of f_{rep} and f_{CEO}	47
3.11	Picture of the RC filter.	48
3.12	Comparison of the RIN of the pump diode measured without and with the RC filter placed between the high current source and the pump diode.	49
3.13	FN-PSD pf the f_{CEO} and f_{rep} free running and fully-stabilized GHz comb	51
3.14	FN-PSD pf the f_{CEO} and f_{rep} free running and fully-stabilized GHz comb with mechanical damping of the laser breadboard and a derivative filter added to the repetition rate feedback loop . . .	52
3.15	a) FN-PSD measured for the free-running f_{CEO} (yellow) compared with the contributions of the current noise of the pump diode driver (red) and of the pump RIN, b) Comparison of the RIN of the pump diode measured with the water cooling chiller on and off.	54

3.16 Frequency stability of the fully-stabilized GHz comb: overlapped Allan deviation of f_{CEO} (a) and relative (overlapped) Allan deviation of f_{rep} (b).	55
3.17 Schematic principle of the measurement setup implemented to characterize one optical line of the GHz comb with respect to an ultrastable laser at 1.56 μm	57
3.18 a) Comparison of the FN-PSD of the repetition rate assessed from the direct measurement of f_{rep} in the RF domain and from the optical CEO-free virtual beat $f_{\text{virt.beat2}}^{\text{CEO-free}}$ and of the reference synthesizer up-scaled by N^2 . b) FN-PSD of an optical mode of the fully-stabilized GHz comb, c) FWHM linewidth of the optical comb line calculated from the FN-PSD as a function of the low cut-off frequency	60
4.1 Noise of Rohde & Schwarz SMF100.	66
4.2 Comparison of Rohde & Schwarz SMF100 up-scaled noise and optical reference noise.	67
4.3 Experimental setup for the measurement of the fiber link noise. Yellow and black lines represent singlemode fibers and electrical connections respectively, PD: photodiode; AOM: acousto optic modulator.	68
4.4 Noise of the fiber link.	69
4.5 Transfer functions of the mirror mounts with acoustic vibrations.	71
4.6 FN-PSD of the repetition rate optimization.	72
4.7 Schematic of the stabilization of the GHz comb to an optical reference.	74

List of Figures

4.8	FN-PSD of the optical comb line of the GHz comb when stabilized with RF and optical reference.	75
4.9	FN-PSD of the repetition rate of the GHz comb when stabilized with RF and optical reference.	77
5.1	FN-PSD of f_{CEO} for the 1-GHz and 96-MHz Yb:CALGO laser.	80
5.2	Nonlinear reflectivity of the SESAM vs laser fluence.	81
5.3	Experimental setup of the OOM-SESAM stabilization of the CEO frequency.	84
5.4	SESAM structure used for OOM.	85
5.5	TFs of the CEO with gain and OOM modulation.	86
5.6	Phase response of f_{CEO} to a 10 Hz modulation of the SESAM-OOM pump power as a function of the average optical power P_{av} incident onto the SESAM.	87
5.7	FN-PSD of CEO frequency when stabilized with gain and SESAM-OOM method.	89
5.8	RF spectrum of the CEO beat in free-running mode, stabilized with gain modulation and with SESAM-OOM.	90

Publications

Parts of this thesis are published in the following journal papers and conference proceedings.

Journal publications

1. **S. Hakobyan**, V. J. Wittwer, K. Gürel, A. S. Mayer, S. Schilt, and T. Südmeyer, “*Carrier-envelope offset stabilization of a GHz repetition rate femtosecond laser using opto-optical modulation of a SESAM*”, Opt. Letters, Vol. 42, No. 22, 4651-4654 (2017).
2. **S. Hakobyan**, V. J. Wittwer, P. Brochard, K. Gürel, S. Schilt, A. S. Mayer, U. Keller, and T. Südmeyer, “*Full stabilization and characterization of an optical frequency comb from a diode-pumped solid-state laser with GHz repetition rate*”, Opt. Express 25, No. 17, 20437-20453 (2017).
3. **S. Hakobyan**, V. J. Wittwer, K. Hasse, C. Kränkel, T. Südmeyer, and T. Calmano, “*Highly efficient Q-switched Yb:YAG channel waveguide laser with 5.6 W of average output power*”, Opt. Letters 41, No. 20, 4715-4718 (2016).
4. K. Gürel, **S. Hakobyan**, V. J. Wittwer, S. Schilt, T. Südmeyer, “*Frequency comb stabilization of ultrafast lasers by opto-optical modulation of semiconductors*”, IEEE Journal of Selected Topics in Quantum Electronics (in press),

DOI 10.1109/JSTQE.2018.2814783 (2018).

5. K. Gürel, V. J. Wittwer, **S. Hakobyan**, S. Schilt, T. Südmeyer, “*Carrier Envelope Offset Frequency detection and stabilization of a diode-pumped mode-locked Ti:Sapphire laser*”, Opt. Letters 42, No. 6, 1035-1038 (2017).
6. N. Jornod, K. Gürel, V. J. Wittwer, P. Brochard, **S. Hakobyan**, S. Schilt, D. Waldburger, U. Keller, T. Südmeyer, “*Carrier-envelope offset frequency stabilization of a gigahertz semiconductor disk laser*”, Optica 4, No. 12, 1482-1487 (2017).
7. P. Brochard, N. Jornod, S. Schilt, V. J. Wittwer, **S. Hakobyan**, D. Waldburger, S. M. Link, C. G. E. Alfieri, M. Golling, L. Devenoges, J. Morel, U. Keller, and T. Südmeyer, “*First investigation of the noise and modulation properties of the carrier-envelope offset in a modelocked semiconductor laser*”, Opt. Letters 41, No. 14, 3165-3168 (2016).
8. K. Gürel, V. J. Wittwer, M. Hoffmann, C. J. Saraceno, **S. Hakobyan**, B. Resan, A. Rohrbacher, K. Weingarten, S. Schilt, T. Südmeyer, “*Green-diode-pumped femtosecond Ti:Sapphire laser with up to 450 mW average power*”, Opt. Express 23, No. 23, 30043-30048 (2015).

Conference presentations

1. **S. Hakobyan**, P. Brochard, V. J. Wittwer, K. Gürel, S. Schilt and T. Südmeyer, “*Compact GHz Frequency Comb from an Ultrafast Solid-State Laser with Cost-Efficient 3D-Printed Plastic Cavity Base*”, CLEO, San Jose, USA; May 13-18, 2018, poster.
2. **S. Hakobyan**, V. J. Wittwer, K. Gürel, P. Brochard, S. Schilt, A.S. Mayer, U. Keller and T. Südmeyer, “*Opto-Optical modulation for Carrier-*

-
- Envelope-Offset Stabilization in a GHz Diode-Pumped Solid-State Laser*”,
ASSL, Nagoya, Japan; October 01-05, 2017, AW1A.4.
3. **S. Hakobyan**, V. J. Wittwer, P. Brochard, K. Gürel, S. Schilt, A.S. Mayer, U. Keller and T. Südmeyer, “*Fully-Stabilized 1-GHz Optical Frequency Comb from a Diode-Pumped Solid-State Laser*”, *EFTF*, Besançon, France; July 9-13, 2017, D1L-A.
 4. **S. Hakobyan**, V. J. Wittwer, K. Gürel, P. Brochard, S. Schilt, A.S. Mayer, U. Keller and T. Südmeyer, “*Opto-Optical modulation for CEO Control and Stabilization in an Yb:CALGO GHz Diode-Pumped Solid-State Laser*”, CLEO-EU, Munich, Germany; June 25-29, 2017, CF-1.1.
 5. **S. Hakobyan**, V. J. Wittwer, P. Brochard, K. Gürel, S. Schilt, A.S. Mayer, U. Keller and T. Südmeyer, “*Fully-Stabilized Optical Frequency Comb from a Diode-Pumped Solid-State Laser with GHz Repetition Rate*”, CLEO, San Jose, USA; May 14-19, 2017, SF1C.1.
 6. **S. Hakobyan**, V. J. Wittwer, K. Hasse, C. Kränkel, T. Südmeyer and T. Calmano, “*5.3 W average output power MHz Q-switched Yb:YAG channel waveguide laser delivering 1 μ J pulse energy*”, CLEO, San Jose, USA; June 5-10, 2016, SM4M.3.
 7. K. Gürel, **S. Hakobyan**, V. J. Wittwer, N. Jornod, S. Schilt, T. Südmeyer, “*CEO frequency stabilization of an ultrafast fiber laser by opto-optical modulation (OOM) of a semiconductor absorber*”, UFO, Jackson Hole, WY, USA, October 8-13, 2017, We9.4.
 8. K. Gürel, V. J. Wittwer, **S. Hakobyan**, N. Jornod, S. Schilt, T. Südmeyer, “*Novel techniques for stabilizing fiber laser frequency combs*”, SPIE LASE Photonics West Conference, San Francisco, USA, January 27 - February 1, 2018, oral 10512-58.

9. N. Jornod, K. Gürel, V. J. Wittwer, P. Brochard, **S. Hakobyan**, S. Schilt, D. Waldburger, U. Keller, T. Südmeyer, “*Carrier-envelope offset frequency stabilization of an ultrafast semiconductor laser*”, SPIE LASE Photonics West Conference, San Francisco, USA, January 27 - February 1, 2018, oral 10515-18.
10. N. Jornod, K. Gürel, V. J. Wittwer, P. Brochard, **S. Hakobyan**, S. Schilt, D. Waldburger, U. Keller, T. Südmeyer, “*Carrier-envelope offset frequency stabilization of a mode-locked semiconductor disk laser*”, ASSL, Nagoya, Japan, October 01-05, 2017, AW1A.6.
11. N. Jornod, K. Gürel, V. J. Wittwer, P. Brochard, **S. Hakobyan**, S. Schilt, D. Waldburger, U. Keller, T. Südmeyer, “*Towards Self-Referencing of a VECSEL Frequency Comb*”, CLEO-EU, Munich, Germany; June 25-29, 2017, CF-1.4.
12. N. Jornod, P. Brochard, V. J. Wittwer, S. Schilt, **S. Hakobyan**, D. Waldburger, S.M. Link, C.G.E. Alfieri, M. Golling, L. Devenoges, J. Morel, U. Keller and T. Sdmeyer, “*First Investigation of the Noise and Modulation Properties of the Carrier Envelope Offset Frequency in a Modelocked Semiconductor Laser*”, CLEO, San Jose, USA, June 5-10, 2016, SM3I.4
13. K. Gürel, V. J. Wittwer, M. Hoffmann, **S. Hakobyan**, S. Schilt, T. Südmeyer, “*First Detection and Stabilization of the Carrier Envelope Offset Frequency of a Diode-Pumped Mode-Locked Ti:Sapphire Laser*”, ASSL, Boston, USA, 30 October-3 November, 2016, ATu1A.
14. K. Gürel, V. J. Wittwer, M. Hoffmann, **S. Hakobyan**, S. Schilt, T. Südmeyer, “*First Detection and Stabilization of the Carrier Envelope Offset of a Diode-Pumped Mode-Locked Ti:Sapphire Laser*”, Europhoton, Vienna, Austria, August 21-26, 2016, SSL-1 15.5.

-
15. K. Gürel, V. J. Wittwer, M. Hoffmann, C. Saraceno, **S. Hakobyan**, B. Resan, A. Rohrbacher, K. Weingarten, S. Schilt, T. Südmeyer, “*Noise Analysis of a Diode-Pumped Femtosecond Ti:Sapphire Laser*”, CLEO-EU, Munich, Germany; June 21-25, 2015, CA-6.1.
 16. K. Gürel, M. Hoffmann, C. Saraceno, V. J. Wittwer, **S. Hakobyan**, B. Resan, A. Rohrbacher, K. Weingarten, S. Schilt, T. Südmeyer, “*Ultrafast Diode-Pumped Ti:Sapphire Laser Generating 200-mW Average Power in 68-fs Pulses*”, CLEO, San Jose, CA, USA, May 10-15, 2015, STu1O.3.
 17. K. Gürel, V. J. Wittwer, M. Hoffmann, C. Saraceno, **S. Hakobyan**, B. Resan, A. Rohrbacher, K. Weingarten, S. Schilt, T. Südmeyer, “*Noise Analysis of a Diode-Pumped Femtosecond Ti:Sapphire Laser*”, IFCS-EFTF, Denver, CO, USA, April 12-16, 2015, B4P-J-5392.

Chapter 1

Introduction and motivation

Most measurements in physics rely on comparison with a reference value, similar to the use of a ruler for length measurements. Without a reference value or a ruler, the concept of measurement and comparison becomes difficult. Frequencies constitute the physical quantity that can be measured the most accurately among all possible physical quantities. Cesium primary frequency standards (atomic clocks) are capable of realizing the second, the unit of time of the international system of units (SI), with a relative accuracy at the 10^{-15} level [1], and optical atomic clocks have recently even achieved relative stabilities down to 10^{-18} [2]. One severe challenge for the operation of an optical clock is the precise counting of the extremely high optical frequencies of several hundreds of THz. Electrical and microwave frequencies up to a ten of GHz are directly measurable with electronic frequency counters. However, higher frequencies cannot be directly measured, as no device is fast enough to detect such ultra-rapid oscillations (in the order of 10^{14} per second). The only way to measure the frequency of light is to phase-coherently down-convert it to a radio-frequency (RF) that can be electronically measured, or alternatively to up-convert the primary cesium frequency standard at 9'192'631'770 Hz up to the optical domain. The first at-

tempts of such RF-to-optical links were a heroic effort that was realized only in a very few specialized institutes by means of a harmonic frequency chain [3]. The absolute measurement of optical frequencies, i.e., by comparison to a microwave frequency standard, has been enormously simplified with the invention of the optical frequency comb in 1999 [4–6]. An optical frequency comb typically relies on a modelocked laser that emits ultra-short pulses, usually in the sub-100-fs range. The optical spectrum corresponding to this train of ultrafast pulses is a frequency grid made of equally-spaced optical lines separated by the repetition rate of the laser as a result of the Fourier transform relationship between the time and frequency domains. However, in contrast to the simple picture of a ruler for length measurements, the frequency grid of a frequency comb is not only characterized by a single parameter that is the spacing between the grid lines, but the entire grid generally has a global offset, i.e., the first line of the ruler is shifted from the zero frequency. The invention of the nonlinear f -to- $2f$ interferometry method [7] to detect and stabilize this offset frequency (the so-called carrier-envelop offset (CEO) frequency) was a major contribution to the 2005 Nobel Prize in Physics awarded to T.W. Hänsch and J.L. Hall for the discovery of the frequency comb [8, 9]. The fact that this prize was awarded so shortly after the invention of the comb recognizes the importance of this new technology. The measurement of absolute optical frequencies is one of the key applications of frequency combs. However, frequency combs are being used nowadays in a wide field of applications like fundamental science, optical clocks, spectroscopy, astrophysics, metrology and many more.

Today's most frequency comb systems used in applications are based on modelocked lasers. Other approaches to generate frequency combs are based on cascaded parametric processes in nonlinear media, such as a variety of microresonators [10–12]. In the following we introduce the basics of fs-laser based combs. We start by introducing basic elements of lasers (Section 1.1) and frequency combs (Section 1.2), followed by a brief overview about their frequency-

stabilization (Section 1.3).

1.1 Lasers

Laser stands for Light Amplification by Stimulated Emission of Radiation. The main principle, as expressed in the abbreviation, is the coherent amplification of stimulated emission.

1.1.1 Continuous wave lasers

Continuous wave (CW) lasers typically consist of an optical cavity, a gain medium, and a pumping scheme, as schematized in Fig. 1.1(b). In order to

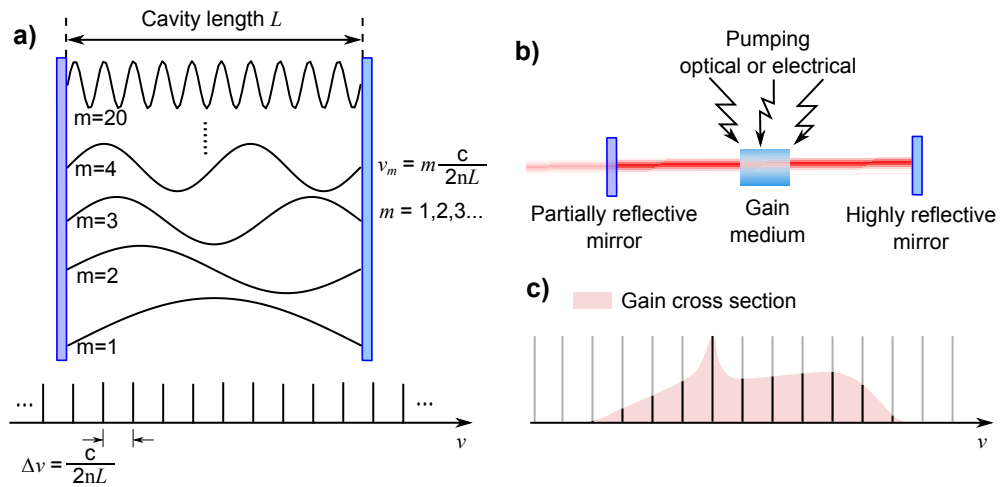


Figure 1.1: a) Fabry-Perot cavity with its supported modes $m = 1, 2, 3, 4,$ and 20 as examples. b) Schematic representation of a laser. Red and pink lines represent intra-cavity and output laser beams. c) Cavity supported modes superimposed to a gain cross section of an active medium showing the only allowed lasing modes (black lines).

provide amplification, the gain medium must be pumped to reach inversion population [13]. Pumping the gain medium is usually done either electrically (for gas lasers and most semiconductor lasers), or optically (for solid-state lasers, fiber lasers, thin-disk lasers, and some semiconductor lasers). One of the cavity mirrors usually has a partial reflectivity and its leakage provides the laser output beam; this mirror is called the output coupler (OC) [Fig. 1.1(b)].

The modes supported by the cavity are determined by the boundary conditions of the electric field circulating inside the cavity, and depend on the length between the mirrors and on the refractive index in the cavity (thus, on the optical length). For simplicity, we restrict this introductory discussions to the simplest case of the Fabry-Perot cavity, and neglect transverse mode effects and dispersion. The modes of a cavity with a length L and a refractive index n are described by the formula displayed in Fig. 1.1(a), where c is the speed of light in vacuum. If the cavity is in vacuum (refractive index $n = 1$), the cavity modes are equally-spaced in frequency [Fig. 1.1(a)]. However, lasing is possible only where the gain medium supports amplification, which depends on the energy levels of electrons in the medium and is quantified by the emission cross-section [13]. Hence, lasing takes place only at modes where the gain medium provides net gain [Fig. 1.1(c)]. Various gain media lase in different spectral regions, Fig. 1.2 shows an overview of some commonly used gain crystals in the wavelength range from the visible up to $\sim 2 \mu\text{m}$.

The most practical lasers used today can be sorted in the following main categories: gas lasers [14], solid-state lasers [15], fiber lasers [16], semiconductor lasers [17], and thin-disk lasers [18]. The most relevant types of lasers for this thesis are briefly described below.

Solid-state lasers consist of a cavity with discrete optical elements, and a doped crystal or a glass material acting as the active medium (see the list of some commonly used gain media in Fig. 1.2). This type of lasers is today

1.1. Lasers

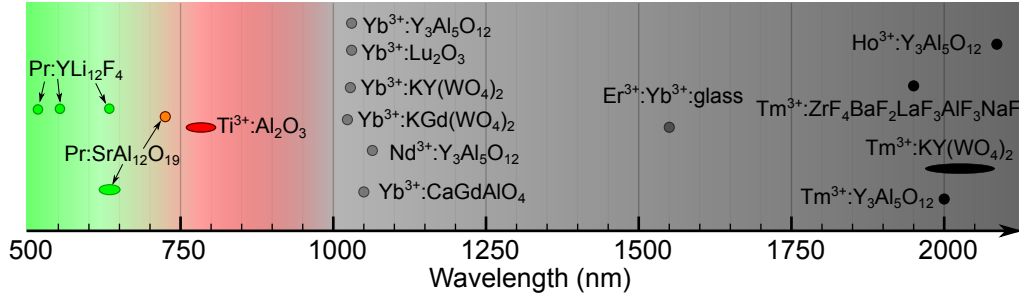


Figure 1.2: Overview of the center emission wavelengths of some commonly used laser gain crystals or glasses.

usually optically pumped using another pump laser, generally a CW laser, often a semiconductor laser diode. The cavity length can be varied in a large range, correspondingly to a mode spacing extending from few MHz up to few tens of GHz. Moreover, these lasers can operate in a large wavelengths range from the visible up to the mid-infrared (IR) owing to a wide choice of gain media (see Fig. 1.2). The drawback of these lasers is that they are not easily power scalable at high transverse mode quality due to potential damage and thermal issues arising in the gain medium. This is a challenge for modelocked operation at high power levels that will be discussed in the next Section 1.1.2, because the presence of different transversal modes usually prevents stable modelocking (due to the different frequencies of higher order modes).

Fiber lasers are one of the most long-term reliable and compact laser sources for applications. It is possible to build fiber lasers with an entire fibered cavity, such that the laser beam is confined inside the core of the fiber and is much less sensitive to external environmental perturbations than for solid-state lasers. The gain medium is the core of the fiber, typically a glass doped with different ions depending on the lasing wavelength. These lasers are usually also optically-pumped with another pump laser, typically a semiconductor pump diode. The drawback of this type of lasers is that they are not easily power scalable, since

the optical power is always localized inside the small core of the fiber. However, this issue can be improved by using fibers with a special geometry that have a significantly larger core diameter [19,20]. Another disadvantage of fiber lasers is that they usually operate in a regime of high gain, that leads to a higher quantum noise compared to the other types of lasers. They are also not appropriate for high repetition rates (in the GHz range) as targeted in this thesis.

Semiconductor lasers are the most common lasers used in everyday applications like telecommunications or CD/DVD players. They are also commonly used as pump lasers for the aforementioned types of lasers. They can lase at nearly any wavelength between the ultra-violet and more than 2 μm in the standard diode configuration (inter-band transition), and even in the mid-infrared range up to more than 10 μm for intra-band quantum cascade lasers, depending on the design of the semiconductor structure. They are usually electrically-pumped, however in some lasers optical pumping is used (for instance in vertical external-cavity surface-emitting laser (VECSEL) [21]). The optical resonator is either a simple Fabry-Perot made by the facets of a semiconductor gain medium chip (e.g., in edge-emitting diodes), or using additional mirrors in an external cavity configuration in the case of VECSELs. This latter geometry resembles the cavity of solid-state lasers, with the notable difference that the gain medium is a semiconductor chip. Edge-emitting semiconductor lasers in CW operation can be power scaled to hundreds of Watts output power at the cost of severely reduced transverse beam quality.

Thin-disk lasers are a successful solution to overcome the thermal and damage limitations of bulk lasers. The gain media is cut and polished such that the thickness is less than half a millimeter (typically $\sim 200 \mu\text{m}$), making it possible for efficient heat removal from the back side of the gain material with water cooling. However, the small pump absorption and low gain per single pass on the thin disk crystal requires a multi-pass geometry to recycle the unabsorbed

pump photons. The gain materials and lasing wavelengths are nearly the same as for solid-state lasers, and thin-disk lasers are also optically-pumped, typically by a stack of semiconductor lasers (for high power).

1.1.2 Modelocked lasers

In the simplest picture of a modelocked lasers, many longitudinal modes lase simultaneously with a constant phase relation with respect to each other. In the spectral domain, this implies that many equidistant cavity modes lase simultaneously and interfere with each other (constructively or destructively depending on time and position) since they are all phase coherent. This is illustrated in Fig. 1.3, where many cavity modes interfere constructively at one point in time where an intense lasing pulse forms. Due to the cavity mode determination, the time delay in-between the pulses matches exactly the cavity round-trip time, meaning that a single pulse travels back and forth in the cavity (we do not consider here for simplicity the case of harmonic modelocking where more than a pulse simultaneously circulate in the cavity). To achieve modelocking, a special component is required in the laser resonator to excite and phase-link the modes. The operation of this component can be pictured either in the time- or frequency-domain.

Modelocking is usually triggered by loss modulation in the laser resonator, at a repetition period normally equal to the cavity round-trip time (for our interest, we consider only fundamental modelocking here). When modulating the optical power of the laser at a frequency corresponding to the inverse of the round-trip time, sidebands are created at the exact same frequency as the neighboring cavity modes. Therefore, energy is transferred from a main mode to adjacent modes that start lasing coherently with respect to each other. In active modelocking, the loss modulator is actively controlled. In passive modelocking, an intra-cavity element introduces passive pulse formation, e.g. a saturable ab-

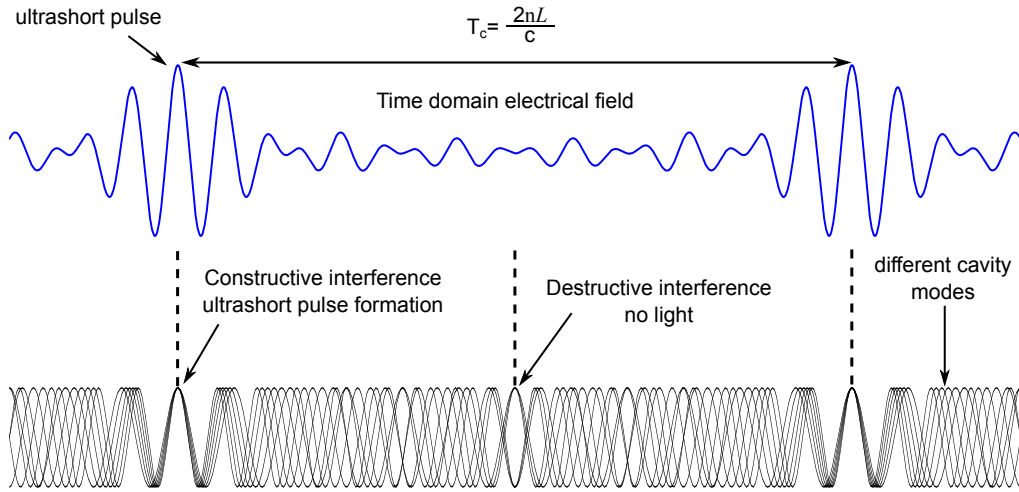


Figure 1.3: Cavity mode interference resulting in pulse formation in the time domain.

sorber. This thesis makes use of passive modelocking, hence, further discussions are presented only on that topic.

Passive modelocking relies on a passive intra-cavity loss modulator. Its operation should be self-starting and fast to lead to pulse formation. For this, a saturable loss modulator is required, meaning that its optical losses are reduced for higher peak power. The most common methods for passive modelocking include Kerr-lens modelocking (KLM) [22] and modelocking with semiconductor saturable absorber mirrors (SESAM) [23].

KLM is based on the self-focusing effect due to the transverse Kerr effect either in the gain medium or in an additional component used as a Kerr medium. Due to the Kerr lens effect, more intense light is differently focused than less intense light. Therefore, in combination with a suitable aperture, the transverse Kerr effect can act as a loss modulator. For KLM, the laser cavity is typically aligned to have larger losses when operating in CW. When Kerr lens focusing results in a better overlap between the pump beam and the laser mode,

the method is called soft aperture KLM. When a hard aperture is used to induce higher losses for less intense pulses via the Kerr effect, it is referred to as hard aperture KLM.

A SESAM is a semiconductor mirror that has a nonlinear reflectivity depending on the fluence of the incident laser light, meaning that more intense light pulses see lower losses than less intense light pulses. A SESAM consists of a distributed Bragg reflector (DBR) structure and a saturable absorber layer, which usually consists of quantum dot or quantum well layers, grown on top of a DBR. SESAMs can be carefully designed and grown with desired parameters, such as the recombination time, the modulation depth, and the saturation fluence. The SESAMs used in this thesis consists of quarter-wave layers of gallium arsenide (GaAs) and aluminum arsenide (AlAs) pairs for the DBR structure, and an indium-gallium-arsenide (InGaAs) quantum well for the saturable absorber. The quantum well is embedded in a layer in order to place it in an antinode of the standing wave of the electric field.

1.2 Frequency combs

As already discussed in the previous section, in the simplest picture of a mode-locked lasers many longitudinal modes lase simultaneously with a constant phase relation. The optical spectrum of such a laser is a series of equidistant lines (their distance corresponds to the inverse of the cavity round trip time), which resembles a comb. Three parameters are sufficient to determine the exact frequency of any comb line: the mode spacing that corresponds to the repetition rate frequency (f_{rep}) of the laser pulses (inverse of the cavity round trip time), the offset frequency of the entire comb spectrum from the origin and the mode number N . The offset frequency corresponds to the carrier-envelope offset (f_{CEO}) of the laser. It results from the difference between the phase and group velocities of the

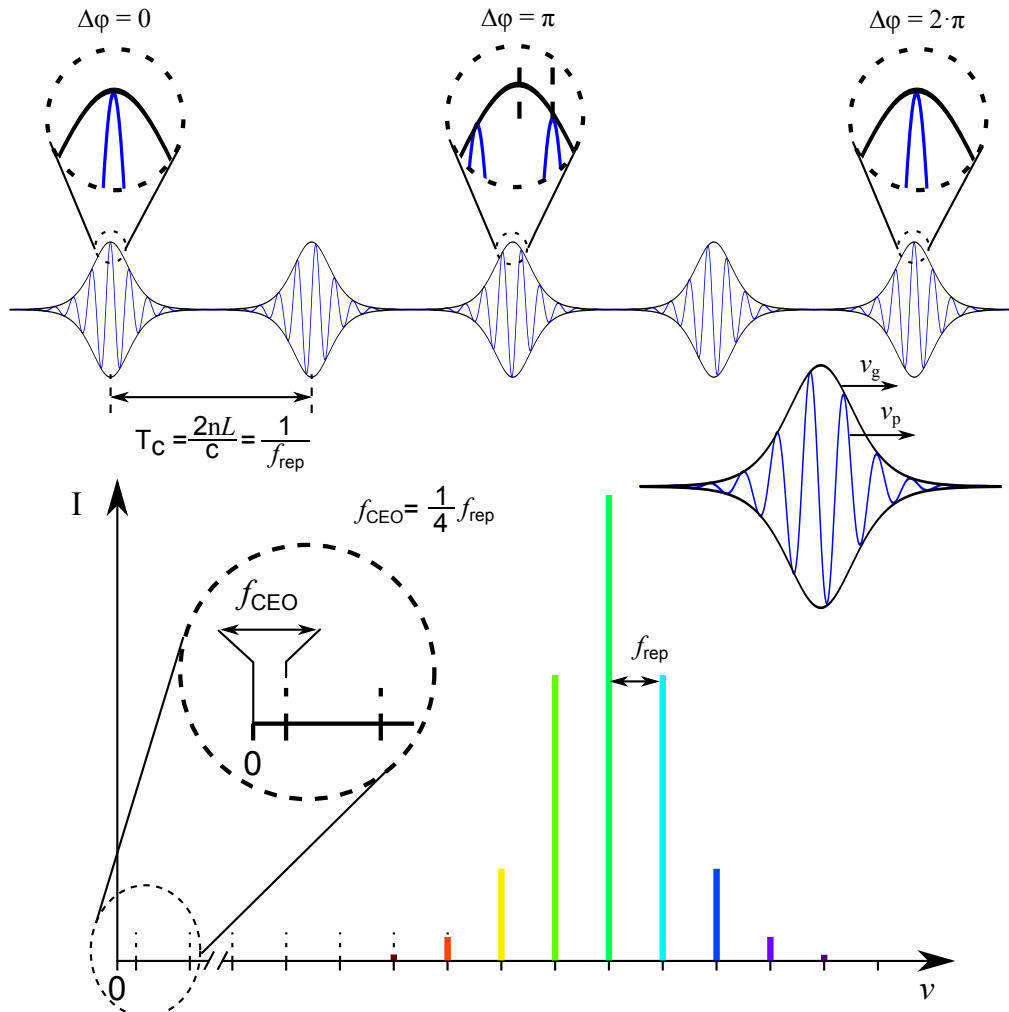


Figure 1.4: Time domain representation (top) and corresponding optical spectrum (bottom) of a modelocked laser frequency comb. In this particular example, the carrier-envelope phase $\Delta\varphi$ changes by $\pi/2$ from pulse to pulse, resulting in a CEO frequency of one fourth of the repetition rate.

pulses in the cavity (due to the dispersion). Between two consecutive pulses, the oscillating electrical field shifts with respect to the pulse envelope, leading to an offset frequency f_{CEO} of the comb spectrum as a result of the properties of the

Fourier transformation between the time- and frequency-domain (see Fig. 1.4). The frequency of any optical line ν_N with a mode number N within the comb spectrum is given by the simple comb equation:

$$\nu_N = N \cdot f_{\text{rep}} + f_{\text{CEO}} \quad (1.1)$$

This equation clearly shows that the knowledge of the comb frequencies f_{rep} and f_{CEO} is required in order to determine the frequency of each optical line.

The repetition rate frequency is determined by the cavity length and can be easily detected using a fast photodiode at the output of the laser, while the CEO frequency is not directly detectable as it is not in the optical bandwidth of the laser (see Fig. 1.4). The detection of f_{CEO} is described in the next section.

1.2.1 Carrier Envelope Offset frequency detection

The CEO frequency of a modelocked laser cannot be straightforwardly detected as it lies outside of the optical bandwidth of the laser, close to zero frequency. The standard method to detect f_{CEO} is based on nonlinear interferometry and is referred to as comb self-referencing (as it does not require any external laser for the determination of f_{CEO}) [7].

If the optical spectrum of a comb is coherent and covers a frequency octave, a long wavelength spectral component of the comb can be frequency-doubled and heterodyned with a low frequency component in an interferometer. As a result, the beat signal, which corresponds to the difference between the two optical frequencies, directly corresponds to the CEO frequency as can be seen in the formula highlighted in red in Fig. 1.5. This method is referred as f -to- $2f$ interferometry or self-referencing.

The main challenge of the method is the generation of an octave-spanning coherent optical spectrum from a modelocked laser. That is usually

realized by launching the laser light into a highly nonlinear fiber [24]. Since nonlinear processes are highly dependent on the peak power of the laser pulses, the supercontinuum spectrum (SC) generation is more challenging for high repetition rate lasers (because of their low corresponding peak power). Thus, high average laser output powers and high nonlinearity fibers with well controlled dispersion are necessary for CEO beat detection of high repetition rate frequency combs. If, however, a full octave coherent SC generation is not achievable, the CEO beat can still be detected by using only 2/3 of a full octave SC spectrum and a $2f$ -to- $3f$ interferometer [25]. In this case, the low frequency part of the SC spectrum is frequency-tripled and the high frequency part of the spectrum is doubled, then these signals are heterodyned in an interferometer, resulting in a beat component at f_{CEO} .

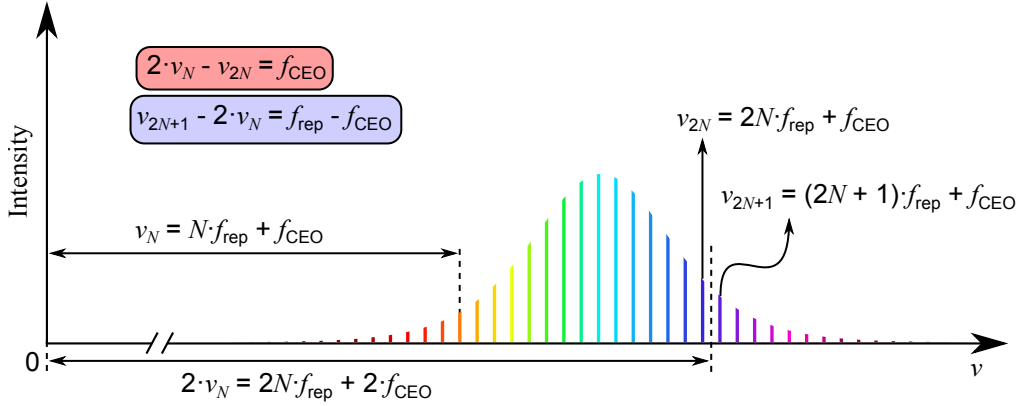


Figure 1.5: Measurement principle of the self-referenced f -to- $2f$ interferometry, method for CEO frequency detection, showing the resulting generated beat signals at f_{CEO} and $f_{\text{rep}} - f_{\text{CEO}}$ (formulas highlighted in red and blue, respectively).

1.3 Stabilization of frequency combs

The comb formula displayed in Eq. 1.1 clearly shows that achieving precise and stable optical comb line frequencies requires a frequency-stabilization of the two comb parameters f_{rep} and f_{CEO} . Since f_{rep} directly depends on the cavity length its stabilization is generally straightforwardly achieved by controlling the optical length of the cavity e.g., by using an optical element mounted on a piezo-electrical transducer (PZT) in the cavity, or using an electro-optic modulator (EOM), which can provide a high stabilization bandwidth (typically a few hundreds of kHz) [26]. CEO frequency stabilization, however, is usually much more challenging. Since f_{CEO} is determined by the difference in group and phase velocities of the optical pulses, it can be stabilized by acting on any parameter of the laser that influences group and/or phase velocities. The most commonly used stabilization method is by a feedback to the pump power of the laser. This method is reliable and can be directly implemented by modulating the current of the pump laser when it is electrically-driven, which is the case of semiconductor laser diodes. The drawback of the method is that its bandwidth is limited by the laser cavity dynamics (see more details in Section 5.1). Several other approaches to overcome this bandwidth limitation have been developed in the past years. For example, a reflective graphene EOM [27] can serve as fast intra-cavity loss modulator. More recently, CEO frequency stabilization was demonstrated in a fiber laser using feedback to a specially designed intra-cavity EOM [28] used to modulate the group velocity of the pulses. Another method to stabilize the CEO frequency was suggested and first demonstrated in University of Neuchâtel, the opto-optical modulation (OOM). The main idea is to use a SESAM not only for modelocking, but also as a fast loss modulator by shining a laser light onto it in order to control its nonlinear reflectivity. We have used this method and demonstrated first CEO stabilization of a GHz diod-pumped solid-state laser (DPSSL) with the OOM method, that will be discussed in Chapter 5. CEO stabiliza-

tion has also been demonstrated using a feed-forward loop to an acousto-optic frequency shifter (AOFS) that is placed in the laser beam outside the laser cavity [29]. The zeroth order diffracted beam of the AOFS has no effect on the CEO frequency, so this beam is used to detect f_{CEO} . The first order diffracted beam shifts down the frequency comb by the RF applied to the AOFS. Hence, when the CEO frequency is applied to the AOFS the diffracted beam results in a frequency comb with subtracted CEO frequency. Using this method, f_{CEO} can be set to any arbitrary frequency, including zero, which is not possible with the standard feedback loop.

Finally, active stabilization of the CEO frequency can be eluded by passively generating a CEO-free comb by difference frequency generation (DFG) between two spectral parts of the broad SC spectrum of a frequency comb [30]. As a result of the difference frequency process, the CEO frequency that is common to the two mixed optical signals cancels out as illustrated in Eq. 1.2.

$$\nu_{\text{DFG}} = (N \cdot f_{\text{rep}} + f_{\text{CEO}}) - (M \cdot f_{\text{rep}} + f_{\text{CEO}}) = (M - N) \cdot f_{\text{rep}} \quad (1.2)$$

1.4 Outline of the thesis

The work presented in this thesis covers various aspects of the development, characterization and stabilization of high repetition rate optical frequency combs. In addition, a compact Yb-doped channel waveguide laser operating in CW and Q-switched regimes has also been developed as a first step towards waveguide-based comb systems. The organization of this thesis is as follows:

Chapter 2 presents an Yb channel waveguide laser that achieved a record-high CW output power of 5.7 W. Pulsed operation was investigated using SESAMs. In Q-switched regime, 5.3-W average output power was achieved in 11-ns pulses, which is the highest power level ever demonstrated for channel

waveguides operating in this regime. This work is a first step towards future modelocking of such devices.

Chapter 3 describes the development of a 1-GHz Yb:CALGO mode-locked DPSSL and the full phase-stabilization of the corresponding frequency comb. A detailed noise analysis of the frequency comb is presented with the identification of the main noise sources.

Chapter 4 concentrates on further noise reduction in the GHz Yb:CALGO frequency comb, first by improving the passive stability of the laser resonator, then by investigating the stabilization of the comb to an optical frequency reference, which is an ultra-stable laser. The resulting noise properties of the repetition rate are analyzed and the improvement compared to the stabilization of the comb to an RF reference is shown.

Chapter 5 presents an alternative stabilization method for self-referenced CEO stabilization of the GHz Yb:CALGO laser by opto-optical modulation of the SESAM used to modelock the laser. This method enables an enlarged modulation bandwidth of the CEO frequency and a better CEO lock compared to the traditional method of pump current modulation.

Chapter 6 finally concludes the thesis by summarizing the most important outcomes and discussing future perspectives.

Chapter 2

High-power Yb:YAG waveguide lasers

2.1 Introduction

Dielectric channel waveguide (WG) lasers are among the most promising technologies for compact and reliable laser sources, which combine multiwatt power with a high level of integration [31]. Major breakthroughs in this field were achieved as a result of high progress in waveguide fabrication methods such as ion-exchange [32], liquid-phase epitaxy [33], and femtosecond-laser (fs-laser) inscription [34–36]. Waveguide-based lasers offer the possibility to achieve efficient laser operation with a minimum amount of cavity components. They also have the advantage to basically circumvent the cavity alignment step that is a very crucial, necessary and not a simple step for solid-state bulk lasers. This laser technology also offers the possibility to integrate the laser into a chip-based system that combines compactness, reliability and cost-efficiency. There are numerous waveguide fabrication methods, each of them with its own advantages and drawbacks. In Section 2.2 an overview of the most commonly used tech-

nologies is first presented. Then Section 2.3 reports on the development and achieved performance of Yb:YAG channel waveguide laser operating in CW and Q-switched regimes with nearly one order of magnitude higher average output power than the state-of-the-art channel waveguide lasers.

2.2 Dielectric waveguide fabrication methods

2.2.1 Ion-exchange

The ion-exchange method is widely used to fabricate glass-based waveguide structures and various integrated optics devices such as wavelength multiplexers [37], optical amplifiers [38], waveguide lasers [39] and many more. In order to achieve waveguiding on a chip, the refractive index of the material has to be locally increased to create the core of the waveguide. The refractive index of glass is determined by its composition. Therefore, it can be modified by locally substituting a fraction of one chemical element by a different one, hence making the waveguiding possible. This is the basic principle of the ion-exchange method. It is realized by doping the glass with alkali ions, which are weakly connected to the glass matrix and can be replaced by other ions when the system is heated. The manufacturing process consists of three steps (Fig. 2.1). The first one is the wafer preparation, the second is mask deposition with photolithography to define the areas of ion-exchange, and the final step is the ion-exchange that is realized by immersing the waveguide chip with its mask into the liquid ion composition. Phosphate glass is commonly used as the matrix, and the active ions are mainly Yb for 1- μm and Er:Yb for 1.5- μm lasing operation, with typical emission and absorption cross sections of about $5.4 \cdot 10^{-21} \text{ cm}^2$ (at 1030 nm) and $14.5 \cdot 10^{-21} \text{ cm}^2$ (at 974.6 nm), respectively [40]. Waveguides can be fabricated

2.2. Dielectric waveguide fabrication methods

with mode field diameters ranging from 1 to 20 μm , and propagation losses down to 0.3 dB/cm are achievable [41]. Transverse single mode lasing operation in the 1- μm wavelength range usually requires a mode field diameter of 5 to 10 μm .

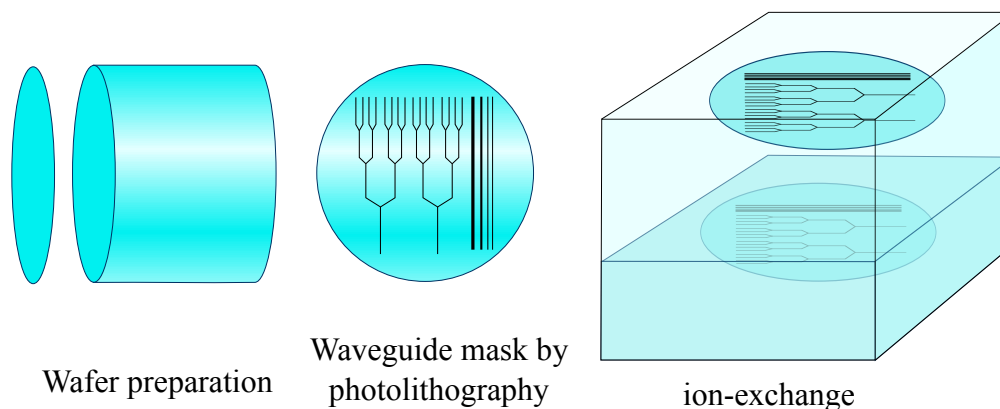


Figure 2.1: The main steps of the fabrication process of glass integrated channel waveguides by ion-exchange.

2.2.2 Liquid-phase epitaxy

Liquid-phase epitaxy is a reliable method to deposit crystalline layers of molten solutions onto a crystalline substrate. To make the channel waveguide, an active crystalline layer is first grown onto an undoped crystalline substrate. Then, photolithography and etching are used to define the waveguide. Finally, an undoped crystalline layer is grown on top of the active layer to bury the waveguide. As a result, very confined waveguide structures can be realized with waveguide dimensions of only a few microns [Fig. 2.2(a)]. This method is widely used in potassium double tungstates waveguide structures such as $\text{KY}(\text{WO}_4)_2$ (KYW), $\text{KGd}(\text{WO}_4)_2$ (KGdW) and $\text{KLu}(\text{WO}_4)_2$ (KLuW) where the Yb^{3+} doped active layer is also co-doped with optically inert rare atoms such as Gd^{3+} and/or Lu^{3+}

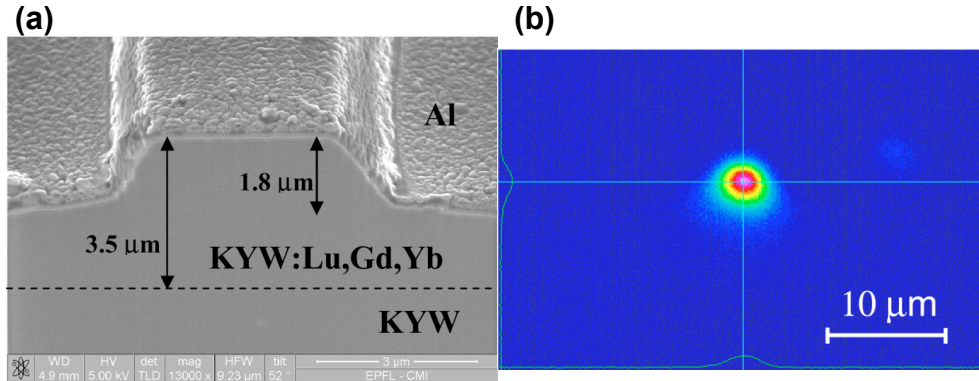


Figure 2.2: Images of a waveguide fabricated by liquid-phase epitaxy, (a) Scanning electron microscope image of a 5- μm wide, 1.8- μm high rib waveguide etched in a 3.5- μm thick layer of $\text{KLu}_{0.253}\text{Gd}_{0.13}\text{Yb}_{0.017}\text{Y}_{0.6}\text{W}$. An aluminum top layer is used to reduce charging effects. (b) Measured intensity distribution of the Yb^{3+} fluorescence guided in the 5- μm wide rib [42].

to achieve a strong refractive index contrast. These crystals with Yb^{3+} doping provide the highest emission and absorption cross sections for Yb-doped crystalline materials, with values as high as $3 \cdot 10^{-20} \text{ cm}^2$ at 1030 nm and $1.33 \cdot 10^{-19} \text{ cm}^2$ at 980.6 nm [43, 44]. Typical waveguides can achieve propagation losses as low as 0.34 dB/cm [44], and lasing operation at 1 μm or at 2 μm for Yb and Tm doping, respectively.

2.2.3 Femtosecond laser inscription

Refractive index change has been realized in dielectric materials by focusing femtosecond laser pulses in order to make passive and active micro-optical devices such as directional couplers [45], beam splitters [46], amplifiers [47], and waveguide lasers [48]. Due to the nonlinear absorption processes occurring in the material (and the resulting material deformations), the refractive index can

be changed and a waveguide can thus be realized. Careful adjustment of the pulse intensity, repetition rate, and writing velocity of the incident fs laser is required to achieve the desired result, since different writing parameters can lead to either an increase or a decrease of the refractive index. There are three types of femtosecond writing techniques, which are summarized in Fig. 2.3. Type-1 waveguiding is achieved when the material is irradiated along a single track with femtosecond pulses of an intensity comparable to the damage threshold of the material. As a result, the refractive index at the center of the damaged track is slightly increased compared to the surrounding areas, allowing waveguiding to occur within the track. Type-2 waveguides are made by two parallel damage tracks written with fs-laser irradiation with intensities higher than the damage threshold. As a result, the material gets damaged in the tracks, which reduces the refractive index at these locations and induces a stress on the surrounding areas. Waveguiding is thus allowed in the surrounding of the tracks. However, the most efficient waveguide is achieved in-between the two tracks where the refractive index contrast is the highest [Fig. 2.3(b)]. Finally, type-3 waveguides are achieved by inscribing many damaged tracks at different depths in the substrate. The cross section of the tracks gives the shape of the waveguide end facet [Fig. 2.3(c)], where the refractive index of the undamaged central part is higher than in the damaged surrounding areas, hence forming a waveguide in the inner region. This type of waveguides can have significantly larger dimensions compared to the previous ones, which leads to multimode (transverse) operation. This method can be used to realize waveguides in some special materials where types 1 and 2 fabrication methods are not applicable. There are numerous different materials that are being used for fs-written waveguides in a wide range of emission wavelengths, spanning from the visible up to 2 μm . The typical dielectric materials are Pr:SrAl₁₂O₁₉ and Pr:YLiF₄ for visible emission, Yb:YAG and Yb:CALGO for 1- μm emission, and ZrF₄-BaF₂-LaF₃-AlF₃-NaF (ZBLAN) for 2- μm emission. Waveguides with optical losses down to 0.5 dB/cm [49] are

possible with emission cross sections of up to $2.2 \cdot 10^{-20} \text{ cm}^2$ at 1030 nm and absorption cross section of $0.75 \cdot 10^{-20} \text{ cm}^2$ at 940 nm for Yb:YAG [50].

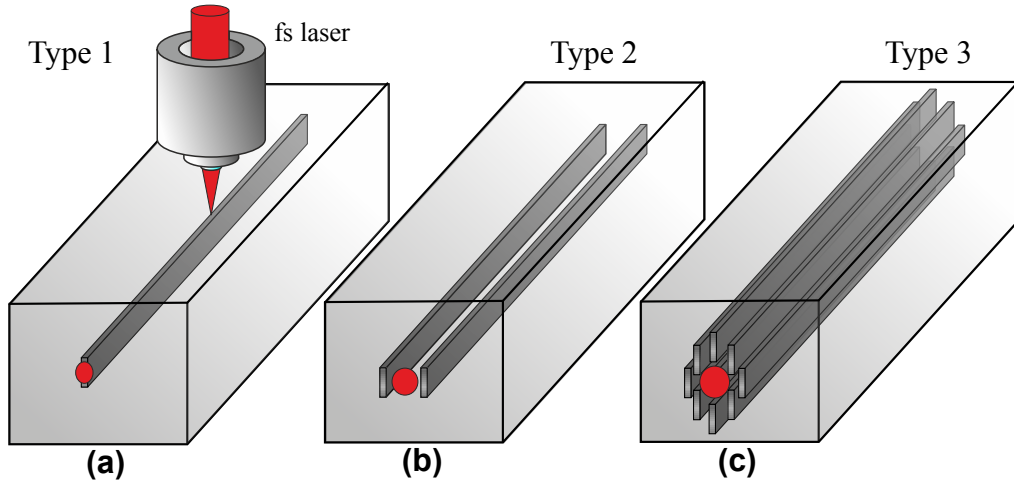


Figure 2.3: Femtosecond laser inscription of a waveguide.

2.3 Yb:YAG waveguide lasers

As previously mentioned, dielectric waveguide lasers are a promising solution for efficient high power compact lasers. In CW operation, power levels of up to 5.1 W and slope efficiencies up to 73% have been reported for fs-laser-inscribed channel waveguide lasers [35]. Several Q-switched and CW modelocked dielectric channel waveguide lasers have been demonstrated, and pulse durations down to 285 fs have been realized [51, 52]. Q-switched operation was demonstrated with average output power levels of up to 680 mW [53]. In this section, the combination of femtosecond laser-written crystalline channel waveguides with semiconductor saturable absorber mirrors (SESAMs) is demonstrated for the realization of a high-power Q-switched channel WG laser. The first Q-switched channel WG laser with multiwatt average output power is presented, achieving

pulse energies of up to 1 μJ .

2.3.1 Fabrication

Our waveguides were fabricated at the Institute of Laser Physics in Hamburg by fs-inscription into a $\text{Y}_3\text{Al}_5\text{O}_{12}$ (Yb:YAG) crystal doped with 7% Yb^{3+} . They consist of two parallel tracks, which were inscribed by a linear translation of the sample perpendicular to the incident fs-laser beam. These tracks are separated by a distance between 22 and 30 μm . Owing to a stress-induced refractive index change, the core of the waveguide is located between the two tracks. Such waveguides are referred to as type-2 waveguides (see section 2.2.3). Here, we superimposed a sine oscillation with an amplitude of 2 to 4 μm and a frequency of 70 Hz to the linear translation of the sample performed at a velocity of 25 $\mu\text{m}/\text{s}$ as schematized in Fig 2.4. A larger refractive index change and a better confinement of the laser mode can be achieved with this modified writing scheme [35]. We adapted a previous WG writing scheme [35,36,48] by inserting a pinhole with a diameter of 600 μm into the beam of the fs-laser to improve its quality by mode cleaning. As a result of the large distance between the pinhole and the aspheric focusing lens ($f = 3.1$ mm, $\text{NA} = 0.68$) used for the laser inscription, only the 0th order of the resulting diffraction pattern was transmitted through the lens aperture. The position of the pinhole was adjusted such that the aperture of the lens was filled by the incident beam. For the experiments, we used WGs with a length of 10.4 mm. We experimentally confirmed with a transmission measurement performed at 633 nm that the modified writing parameters of the waveguide reduced optical transmission losses from 1.2 to 0.5 dB/cm.

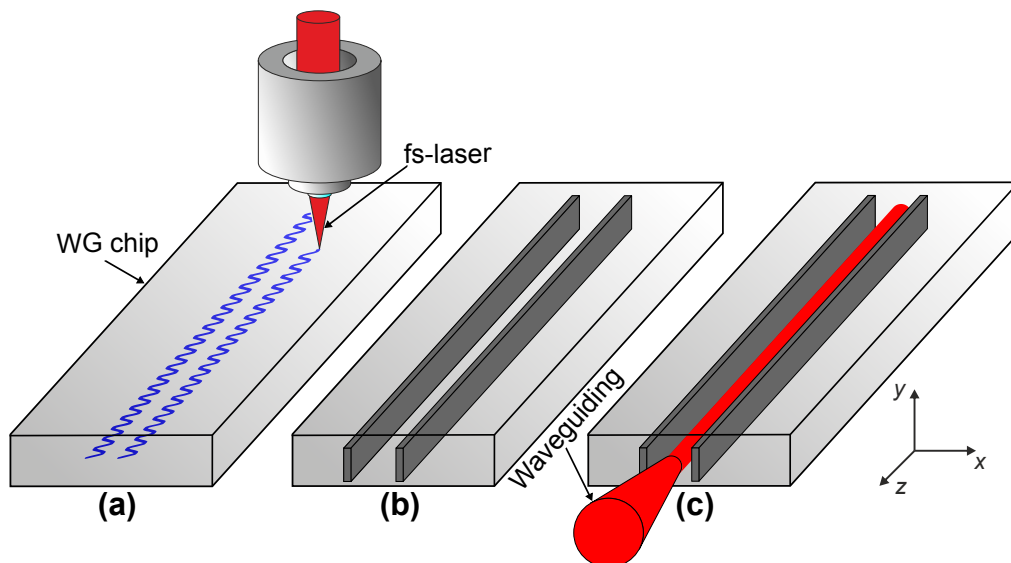


Figure 2.4: Schematic of the fs-laser writing mechanism. (a) fs-laser sinusoidal translation (along the x axis) superimposed to the linear translation (along the z axis), (b) pair of inscribed tracks (material modification in those areas), (c) resulting waveguiding in-between the tracks.

2.3.2 Experimental setup

The setup for the laser experiments is depicted in Fig. 2.5. The experiments shown here were performed using a WG with a track separation of $26\ \mu\text{m}$ and a superimposed oscillation with an amplitude of $2\ \mu\text{m}$. The Yb:YAG WG was pumped by an optically-pumped semiconductor laser (OPS), also referred to as a vertical external-cavity surface-emitting laser (VECSEL) or semiconductor disk laser [21], delivering up to 9 W of power at 969 nm with an $M^2 < 2$. The slightly elliptical collimated pump beam was focused onto the waveguide facet using a lens of 30-mm focal length. This resulted in a pump spot diameter of $23\ \mu\text{m} \times 19\ \mu\text{m}$. The waveguide mode field diameter is approximately $18\ \mu\text{m} \times 22\ \mu\text{m}$ at 969 nm. We estimated the coupling efficiency η_c by calculat-

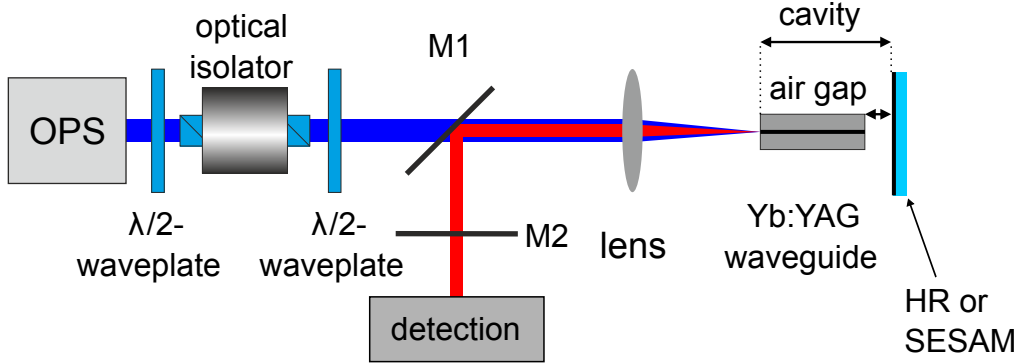


Figure 2.5: Experimental setup of the CW and Q-switched waveguide lasers. OPS laser at 969 nm as pump source; mirror M1, highly transparent (HT) at 969 nm, HR at 1030 nm; mirror M2, transparent at 1030 nm, HR at 969 nm.

ing the overlap integral [54] of the waveguide and pump modes to be $\eta_c = 97\%$. The laser cavity length is determined mainly by the length of the waveguide chip. The WG chip was pumped through the uncoated front facet, which also served as an output coupler for the WG cavity. The second cavity end mirror was either a highly reflective (HR) mirror for CW operation or a SESAM [23] for Q-switched operation. Each of them was placed close to the WG end facet, as illustrated in Fig. 2.6 for the waveguide laser in CW operation. Owing to the Fresnel reflection of 8.4% at 1030 nm at the front facet, the cavity exhibits a resulting total output coupling of 91.6%. The laser output light was separated from the pump light by a dichroic mirror M1, which was placed in front of the waveguide. An additional dichroic mirror (M2) was placed in front of the characterization setup to filter out residual pump light reflected on the front facet of the crystal. The SESAM was mounted on a Peltier-cooled holder for temperature control. During the entire experiment, the temperature of the SESAM was set to 17°C. However, no significant change of the pulsed laser operation has been observed when varying the SESAM temperature between 15°C and 35°C.

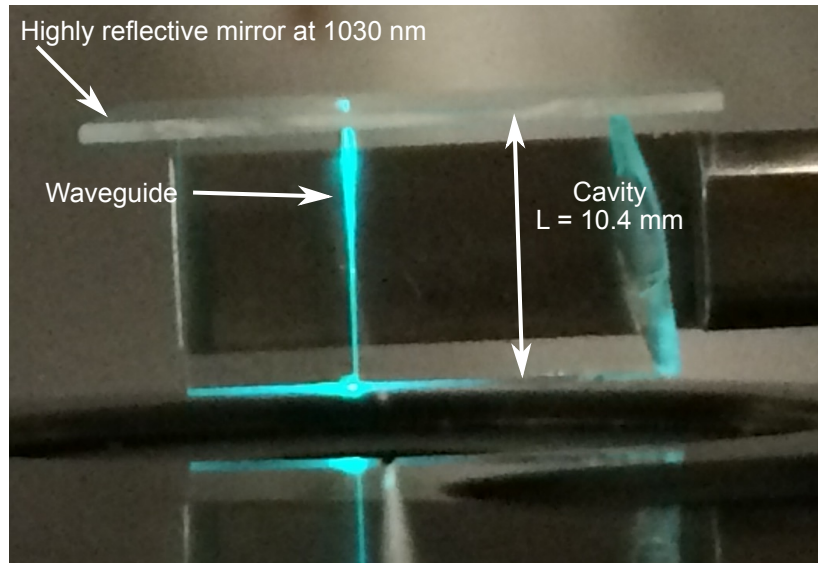


Figure 2.6: Picture of the waveguide laser in CW operation. The waveguide is made visible by parasitic fluorescence green light resulting from the optical pumping.

The SESAM has a saturation fluence of $57 \mu\text{J}/\text{cm}^2$, a modulation depth of 0.7%, and nonsaturable losses of 0.2%, when characterized with picosecond pulses at a wavelength of 1030 nm [55]. The recombination time of this SESAM was not measured, but is expected to be <100 ps, which is orders of magnitude shorter than the achieved pulse duration. Therefore, carrier recombination occurs during the presence of the pulse, whereas the states are immediately refilled leading to the bleaching of the absorber. No index matching fluid was applied between the SESAM and the waveguide end facet. Hence, a tiny airgap was left, which could be adjusted by a piezoelectric ring actuator placed on a mirror mount. During the entire experiment the air gap was kept between 10 and 100 μm . The pump power was measured after the mirror M1 in front of the focusing lens. In the following, we consider as pump power the measured pump power corrected by the transmission of the focusing lens (97.5%) and the Fresnel reflection of

the waveguide end facet (8.4%), and assuming the incoupling efficiency to be unity. It should be noted that this assumption leads to a minor underestimation of the actual efficiencies. The laser average output power was measured after the mirrors M1 and M2 and was corrected by their reflection and transmission coefficients, respectively. For the characterization of the Q-switched operation, a fraction of the laser power was sent to a high-speed InGaAs photodetector with 45-GHz bandwidth (Newport 1014), connected to an oscilloscope or an RF spectrum analyzer. Another fraction of the laser power was sent to an optical spectrum analyzer (Yokogawa AQ6370C) for wavelength characterization.

2.3.3 Laser results

For CW operation, the HR mirror was mounted on the piezo-controlled mount, as described above. In this configuration, laser operation started at 89 mW of pump power. A maximum output power of 5.7 W was achieved at a pump power of 7.5 W, corresponding to a slope efficiency of 78% (Fig. 2.7). These results outperformed earlier high power Yb:YAG waveguide lasers [35] and show that the writing parameters of the waveguide were considerably improved. For Q-switched operation the HR mirror was replaced by the SESAM. In this case, Q-switching started at the laser threshold corresponding to a pump power of 102 mW. During the entire experiment, no Q-switched modelocking was observed. A maximum average output power of 5.6 W was achieved at a pump power of 7.7 W. The low modulation depth and nonsaturable losses of the SESAM allowed for a high-power multiwatt Q-switched pulsed operation with an only slightly reduced slope efficiency of 74% [Fig. 2.8(a)]. The optical spectrum of both operation modes looks very similar, and is centered at 1030 nm with a full-width-half-maximum (FWHM) of ~ 0.5 nm. With increasing pump power the stability of the Q-switching decreased. However, it was possible to compensate for this effect by fine tuning the air gap between the SESAM and

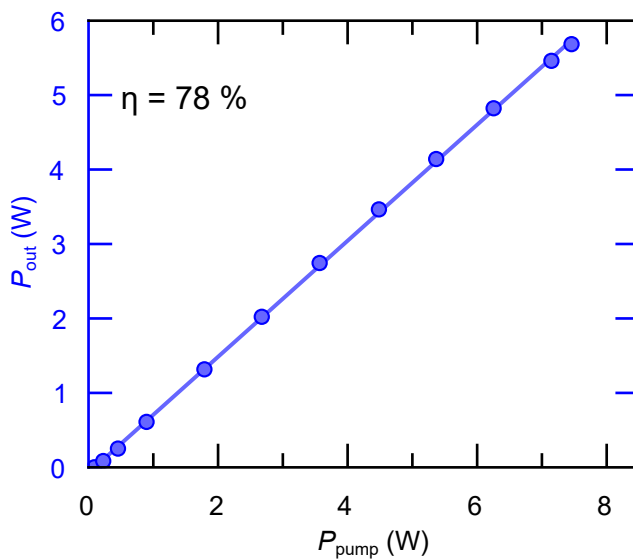


Figure 2.7: Output power (P_{out}) versus pump power (P_{pump}) for the CW laser configuration showing a slope efficiency η of 78%.

the waveguide chip. The resulting etalon effect significantly changed the coupling into the SESAM and thus its parameters [56]. By doing so, however, the slope efficiency was reduced by approximately 5% as depicted in Fig. 2.8(b). At the same time, the maximum average output power decreased to 5.3 W. In both cases, the maximum average output power was only limited by the available pump power. The pulse energy versus pump power is depicted in Figs. 2.8(a) and 2.8(b) (red curves). With increasing pump power the pulse energy increased and approached 1 μJ at the maximum average output power of 5.6 W. For the stable Q-switching configuration [Fig. 2.8(b)] the pulse energy varies approximately linearly with the pump power, while the dependence is distorted for the power-optimized (unstable) Q-switching configuration [Fig. 2.8(a)]. The dip observed in the pulse energy in Fig. 2.8(a) at a pump power of 5.4 W goes along with an abrupt increase of the repetition rate from 4.1 to 5.5 MHz. Figure 2.9 shows the oscilloscope trace of a fully modulated single pulse and the pulse train

(inset) of the Q-switched laser at 2.4 W (a) and 5.3 W (b) of average output power.

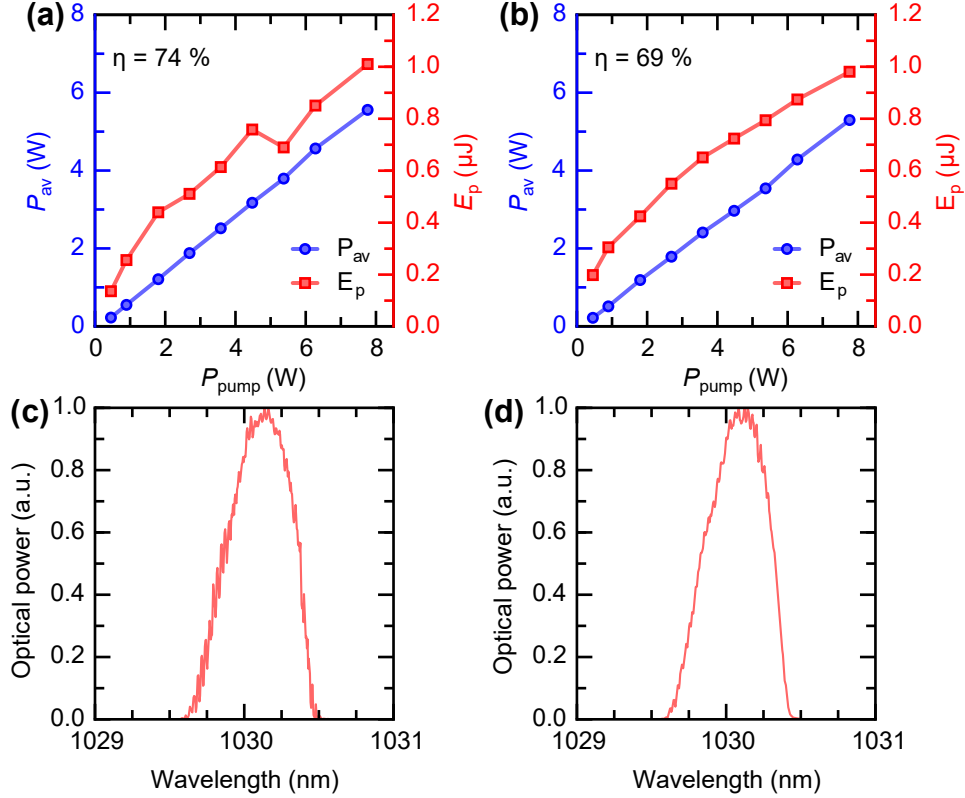


Figure 2.8: (a,b) Average output power P_{av} and pulse energy E_p versus pump power (P_{pump}) for the Q-switched laser configuration without (a) and with (b) adjustment of the airgap distance between the SESAM and the WG facet for the highest pulse stability. (c,d) Corresponding optical spectra [without (c) and with (d) adjustment of the SESAM-WG distance].

The Q-switching operation shown in Fig. 2.9(a) is stable with a maximum pulse peak power fluctuation of 18% (evaluated in a time span of 10 μs corresponding to 40 pulses). The average pulse period was evaluated to be 263 ns with an rms timing jitter of 12 ns, corresponding to a pulse repetition

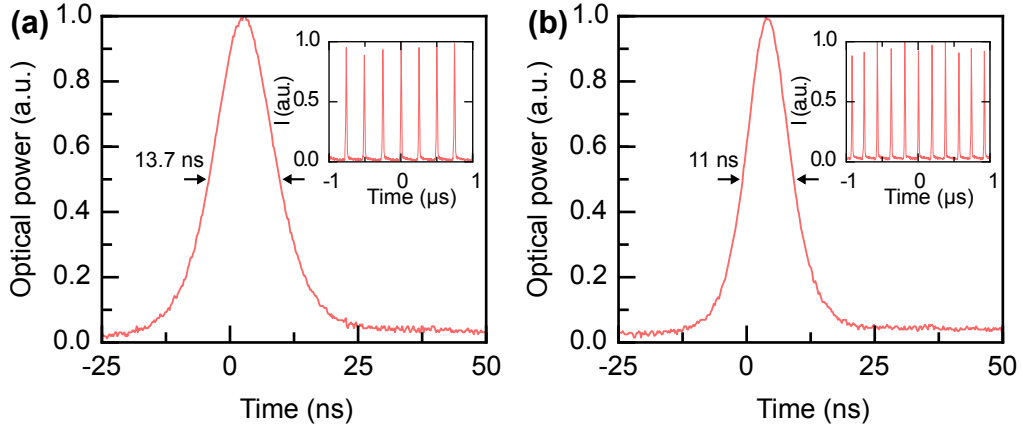


Figure 2.9: Single Q-switched pulse and Q-switched pulse train (inset) at 2.4 W (a) and 5.3 W (b) of average output power for the stable Q-switching operation.

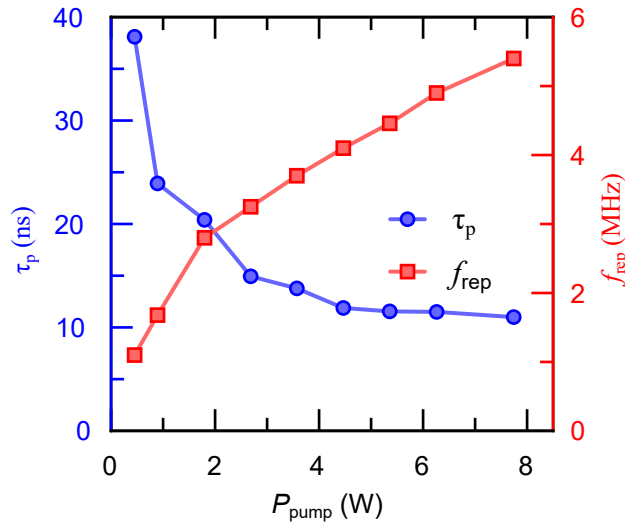


Figure 2.10: Pulse duration (τ_p) and repetition rate (f_{rep}) of the WG laser versus pump power (P_{pump}) for the stable Q-switching operation.

rate of 3.81 ± 0.19 MHz. The dependence of the pulse duration and repetition rate as a function of the pump power is depicted in Fig. 2.10. The pulse dura-

tion decreases from ~ 40 to 11 ns while the repetition rate increases from 1.0 to 5.4 MHz as the pump power is enhanced from 0.45 to 7.74 W.

2.3.4 Conclusion

A fs-laser-written Yb:YAG channel waveguide laser has been demonstrated with low losses of 0.5 dB/cm, high efficiency, and high output power. Using an HR mirror as a cavity end mirror, the CW laser has record high output power of 5.7 W and a slope efficiency of 78%. After exchanging the HR mirror by a SESAM, Q-switched operation was observed at all power levels. The maximum average output power amounts to 5.6 W with a slope efficiency of 74%. The Q-switched pulses have a pulse energy of up to 1 μ J at 11-ns pulse duration with a repetition rate of 5.4 MHz. These results are almost an order of magnitude higher in average output power than previously reported passively Q-switched channel waveguide lasers [31]. This is graphically shown in Fig. 2.11 where the present result displayed by a red star is compared to different previous results reported for pulsed waveguide lasers operating in Q-switched [35, 53, 57], Q-switch modelocked [51, 58, 59] and modelocked [39, 60, 61] regimes. This demonstrates the potential of fs-laser-inscribed waveguide lasers for highly efficient short pulse generation, allowing for compact integrated pulsed optical devices.

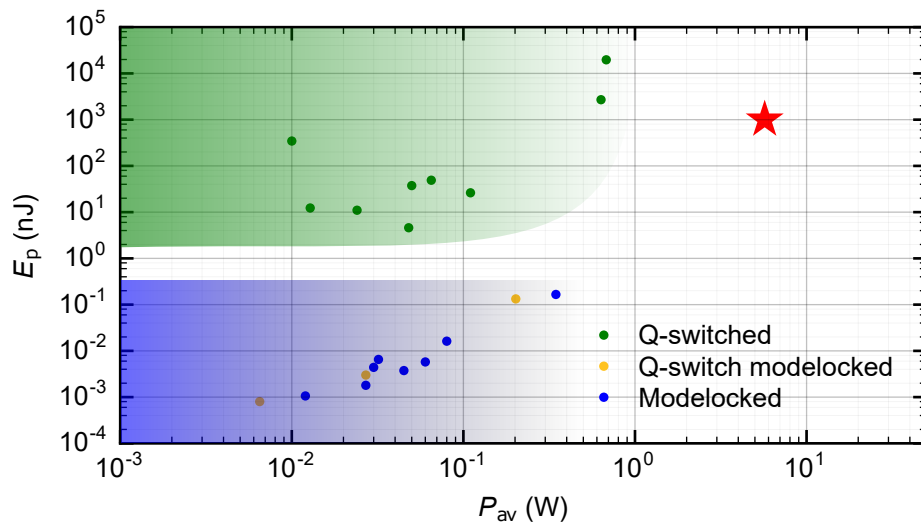


Figure 2.11: Overview of the reported results on Q-switched [35, 53, 57] (green), Q-switch modelocked [51, 58, 59] (grey) and modelocked [39, 60, 61] (blue) channel waveguide lasers in terms of output pulse energy (E_p) vs average output power (P_{av}). The red star displays the present result.

Chapter 3

GHz repetition rate

Yb:CALGO frequency comb

3.1 Introduction

Fully-stabilized optical frequency combs from modelocked lasers have revolutionized many fields in optics and physics by enabling ultra-precise measurements and by providing a direct and coherent link between the optical and microwave spectral domains [5–7]. Frequency combs constitute today a key component in various applications ranging from optical frequency metrology [8, 62] to ultra-high resolution broadband spectroscopy [63, 64] and optical atomic clocks [65, 66] that have become the most stable clocks existing today. Some of these applications, such as the calibration of astronomical spectrographs [67, 68] or the generation of ultra-low-noise microwave signals [69, 70] benefit from frequency combs with a high repetition rate, which provide a higher optical power per comb mode for a given average power and facilitate the spectral filtering of individual modes.

So far, modelocked frequency combs with GHz repetition rates have been demonstrated essentially from ultrafast Ti:Sapphire lasers, reaching up to a record-high repetition rate of 10 GHz for a self-referenced comb [71]. The most established comb technology today is based on modelocked fiber lasers [72, 73]. However, they are not well suited for high repetition rate operation due to the conjunction of high optical losses and limited gain per unit length of fiber cavities. Furthermore, fiber lasers generally suffer from a higher noise level than their solid-state resonator counterparts, which notably results from their lower cavity Q-factor. This makes the stabilization of the carrier-envelope offset (CEO) frequency in high repetition rate fiber lasers challenging, since the CEO noise typically scales with the repetition rate [74]. Modelocked DPSSL [75] are an excellent technology for GHz frequency combs, as they combine the advantages of simple diode pumping schemes with low loss optical resonators leading to suitable noise properties for comb stabilization. DPSSL combs can operate with various gain materials in different wavelength regions, for example Ti:Sapphire [76] around 780 nm, Ytterbium (Yb) doped materials around 1 μm [77–83] and Erbium (Er) around 1.5 μm [26, 84–86]. Self-referenced frequency combs from modelocked DPSSLs with a repetition rate in the GHz regime have been demonstrated from a few platforms like Yb:CALGO DPSSLs [80–82] or from a monolithic extremely low-noise Er:Yb:glass solid-state laser [87]. However, only the CEO frequency f_{CEO} was stabilized in these cases, and the second degree of freedom of the comb, i.e., the repetition rate frequency f_{rep} , was left free-running. On the other hand, a 15-GHz Yb:Y₂O₃ ceramic DPSSL was fully-stabilized by means of repetition rate locking on one side, and stabilization of one comb line to an ultra-stable laser using a feed-forward stabilization on the other side [77]. However, this comb was not self-referenced and suffered from the frequency drift of the reference laser in comparison to a CEO-stabilized comb. Detecting and stabilizing the CEO frequency represents a major challenge for lasers in the GHz regime and has often been the center of interest in past publications. Full control of the

comb, however, can only be achieved with additional repetition rate stabilization and the careful design of each feedback loop to avoid cross-talks is non-trivial. In addition, understanding the influence of both repetition rate and CEO control on the properties of individual optical comb lines is especially relevant for applications such as comb spectroscopy, where the noise and linewidth of the actual optical combs line matter.

In this chapter the first self-referenced full stabilization of a frequency comb from a modelocked DPSSL in the 1- μm spectral range with a GHz repetition rate is presented. The Yb:CALGO laser was phase-stabilized by feedback to the cavity length using a piezoelectric transducer (PZT) for f_{rep} and to the pump diode current for f_{CEO} . A thorough noise analysis of the resulting frequency comb is presented by individually characterizing the noise properties of f_{rep} , f_{CEO} and of an optical comb line obtained from the heterodyne beat with a narrow-linewidth continuous-wave laser. Finally, intensity noise of the pump diode and mechanical noise induced by its water cooling are shown to constitute the main contributions to the CEO phase noise.

3.2 1-GHz Yb:CALGO modelocked laser

3.2.1 Design

The modelocked laser is based on a previously reported design developed at ETH Zurich [80]. It consists of a 2-mm thick Yb:CALGO crystal with an asymmetric cut (a-cut) to prevent multi-polarization operation. The crystal, doped with 5% of Yb, is pumped by a commercial diode laser array (LIMO F100-DL980-EX1930) that can deliver an output power up to 60 W at a central wavelength of 980 nm out of a highly multimode fiber (core diameter of 100 μm , NA of 0.22). The laser pump diode array is driven by a commercially-available current source (Delta Elektronika SM 18-50) delivering a maximum current and voltage

of 50 A and 18 V, respectively. Figure 3.1(a) shows the linear variation of the output power of the pump diode as well as the voltage drop across the diode with respect to its driving current. In order to apply fast modulation of the pump diode optical power, a home-made voltage-to-current modulator has been developed that supports a modulation bandwidth as high as 1 MHz. However, the current range of this device is limited to around 1 A. Therefore, this modulation source is connected in parallel to the main current driver (see Fig. 3.2), and used when fast modulation of the pump power is needed, e.g for CEO frequency modulation and stabilization. The emission wavelength of the pump diode is stabilized by a volume holographic grating (VHG), resulting in lower relative intensity noise (RIN) of the diode and thus in a lower amplitude noise of the modelocked laser compared to the case of a non-wavelength stabilized pump diode [81]. The optical spectrum of the diode is centered at 980.9 nm with

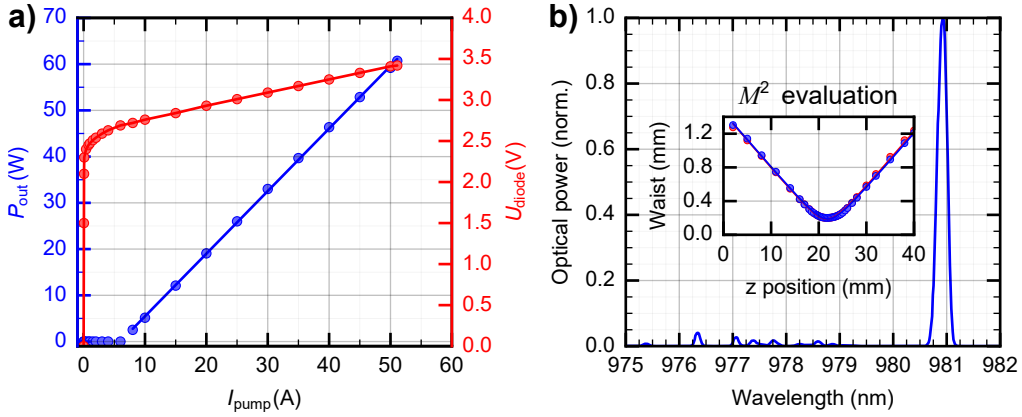


Figure 3.1: a) Output power P_{out} (left vertical axis) and voltage drop V_{diode} over the diode array (right vertical axis) vs the pump current I_{pump} . b) Optical spectrum of the diode array at an operation current of 17 A (0.1 nm resolution bandwidth); inset: M^2 measurement of the diode array at the output of the multimode fiber in the two transverse directions (red and blue dots: data; line: fit).

3.2. 1-GHz Yb:CALGO modelocked laser

a full-width at half-maximum (FWHM) of 0.2 nm [Fig. 3.1(b)]. There is some remaining parasitic emission in the 975 - 979 nm region. However, it is kept at a low level by the VHG stabilization. The inset of Fig. 3.1(b) depicts a M^2 measurement of the optical beam of the pump diode showing a nice fit by a Gaussian beam leading to M^2 values of $\sim 37.1 \times 37$ (horizontal and vertical directions). The pump diode is unpolarized, hence a polarizing beamsplitter (PBS) cube is used to select the s-polarization to pump the crystal (see the experimental scheme depicted in Fig. 3.2), resulting in only one half of the diode

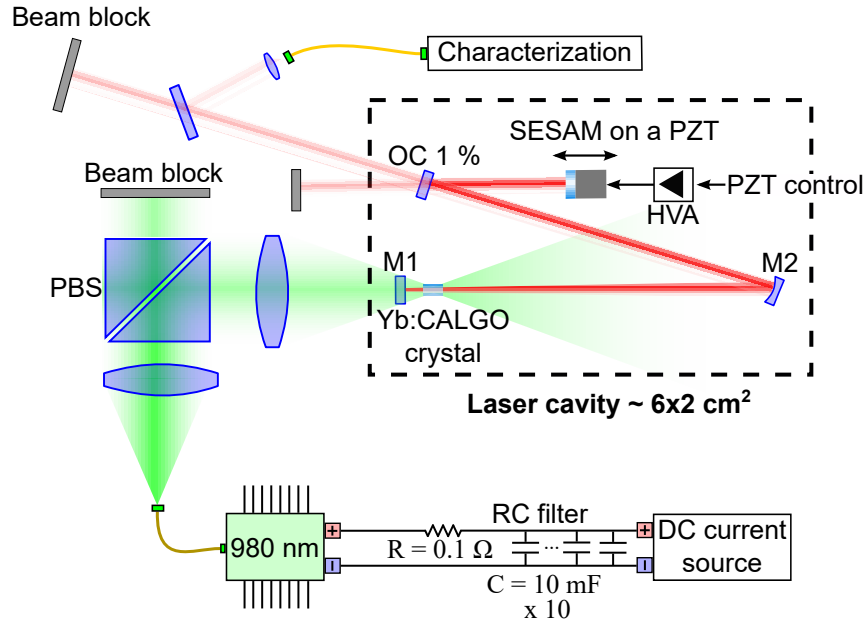


Figure 3.2: Scheme of the Yb:CALGO GHz laser. The laser cavity (center) is pumped by a 980-nm fiber-coupled diode array (left). The laser has two outputs, part of one of the output beams is used for characterization. The SESAM is mounted on a PZT driven by a high-voltage amplifier (HVA) for cavity length control. PBS: polarizing beam splitter cube. Yellow lines represent singlemode (SM) optical fiber connections, red, pink and green lines schematize free-space optical beams.

power effectively used to pump the laser. The cavity has a length of 14.2 cm, corresponding to a repetition rate of 1.05 GHz.

The cavity consists of a dichroic end mirror (M1) that is transmissive at the pump wavelength and highly reflective at the lasing wavelength. It is followed by a curved dispersive mirror (M2) with a radius of curvature of 75 mm, which provides a negative dispersion of 400 fs² per bounce. This mirror has a high transmission at the pump wavelength to remove residual pump light. An output coupler (OC) with 1% transmission is used as a folding mirror, resulting in two distinct output beams. A SESAM is mounted on a PZT driven by a high-voltage amplifier (HVA) for cavity length control (f_{rep} stabilization) and acts as the second cavity end mirror [see Fig. 3.2 and Fig. 3.3(a)]. The SESAM has a modulation depth of 1.15%, non-saturable losses of 0.07%, and a saturation fluence of 10.69 $\mu\text{J}/\text{cm}^2$.

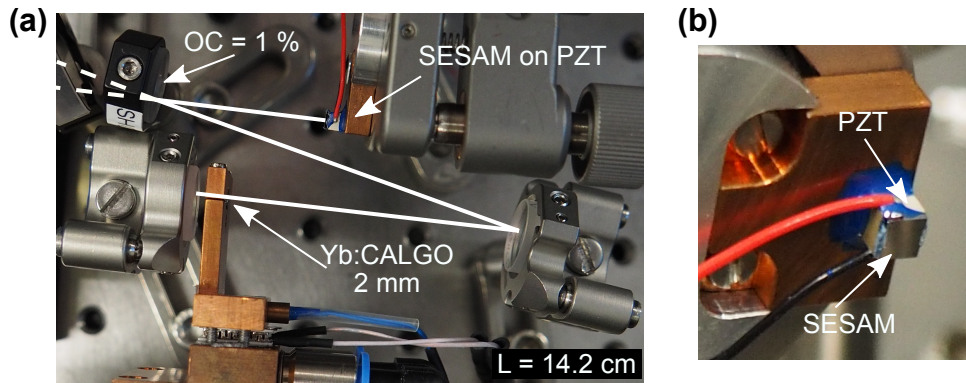


Figure 3.3: a) Picture of the overall Yb:CALGO laser cavity. f_{rep} is tuned or stabilized by cavity length control with a PZT. b) Zoom on the SESAM mounted onto the PZT.

3.2.2 Laser performance

The laser starts emitting in CW mode at a threshold pump power of 870 mW incident onto the dichroic mirror M1 and has a slope efficiency of 24.7% up to a pump power of ~ 4.8 W (corresponding to ~ 1 W of CW output power). Then, self-starting SESAM-modelocked operation occurs for pump powers ranging from ~ 4.8 W up to to the maximum used value of 7.7 W [Fig. 3.4(a)]. The maximum

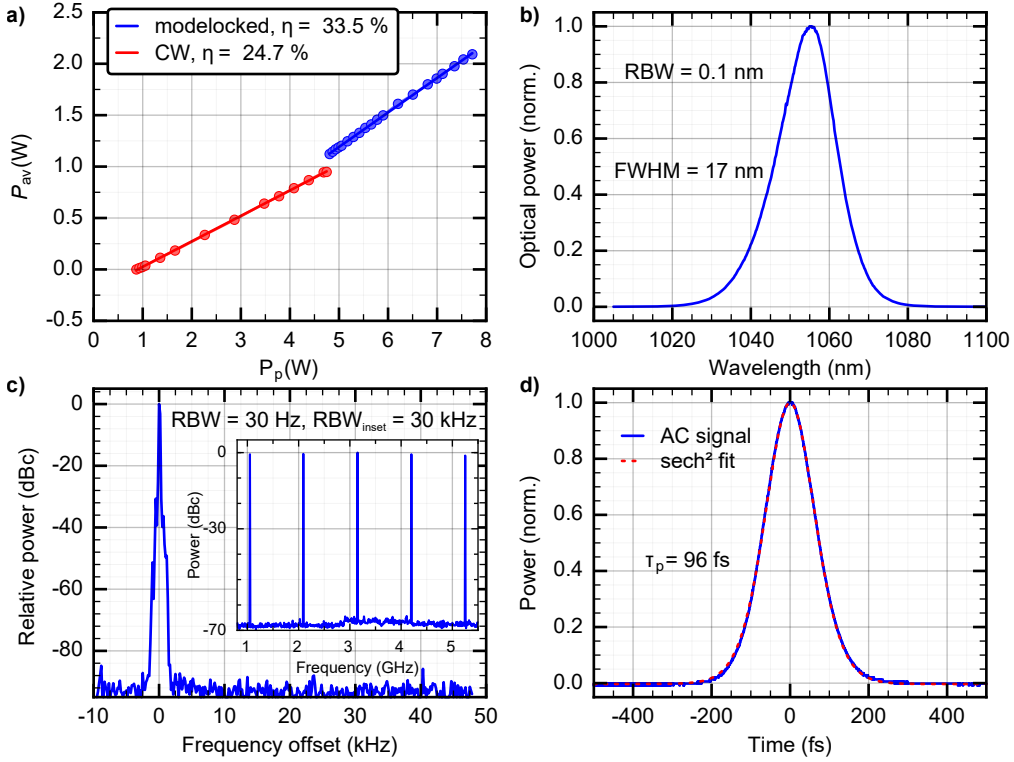


Figure 3.4: a) Average output power vs pump power for CW and modelocked (ML) operations. b) Optical spectrum of the laser in ML operation. c) Normalized radio-frequency (RF) spectrum of the laser in ML operation, offset from the fundamental $f_{rep} = 1.05$ GHz; inset c): first five harmonics of f_{rep} . d) Autocorrelation (AC) trace of an optical pulse of the laser (blue trace) with a sech^2 fit (dashed red line).

average output power of the laser is 2.1 W in modelocked operation with a slope efficiency of 33.5%. The laser emits an optical spectrum with a FWHM of 17 nm centered at 1055 nm [Fig. 3.4(b)], in 96-fs pulses [Fig. 3.4(d)] at a fundamental repetition rate of 1.05 GHz [Fig. 3.4(c)]. One of the laser output beams is used for f_{rep} stabilization and comb characterization, whereas the other one is used for supercontinuum (SC) spectrum generation, f_{CEO} detection and stabilization as depicted in Fig. 3.5.

3.3 CEO frequency detection

The overall scheme of the Yb:CALGO GHz frequency comb is depicted in Fig. 3.5, including the detection of the CEO frequency by nonlinear interferometry and the stabilization loops of f_{rep} and f_{CEO} . One of the two output beams of the laser is launched into a 1-m long photonic crystal fiber (PCF, NKT NL-3.2-945) with a zero dispersion wavelength of 945 nm for SC spectrum generation. The coupling efficiency is $\sim 80\%$, leading to an effective average power of 670 mW being coupled into the PCF. The SC spectrum measured at the output of the PCF spans over a full frequency octave ranging from ~ 650 nm to ~ 1420 nm at 35 dB from the maximum power at ~ 1350 nm (Fig. 3.6). This spectrum is then sent into a traditional f -to- $2f$ interferometer (see Fig. 3.7) for CEO detection [7]. The SC spectrum is separated at the input of the f -to- $2f$ interferometer into short and long wavelength components centered at 680 nm and 1360 nm, respectively, using a short-pass optical filter with a cut-off wavelength of ~ 1000 nm. The two beams propagate in two different optical paths, where they are reflected back by a mirror and are recombined using the same optical filter. A D-shaped mirror reflects the long and short wavelength components into a periodically-poled lithium niobate (PPLN) crystal with a poling period of 14.08 μm for second harmonic generation (SHG). A half-wave plate is used in the common path to align the polarization of the 1360-nm beam for efficient

3.3. CEO frequency detection

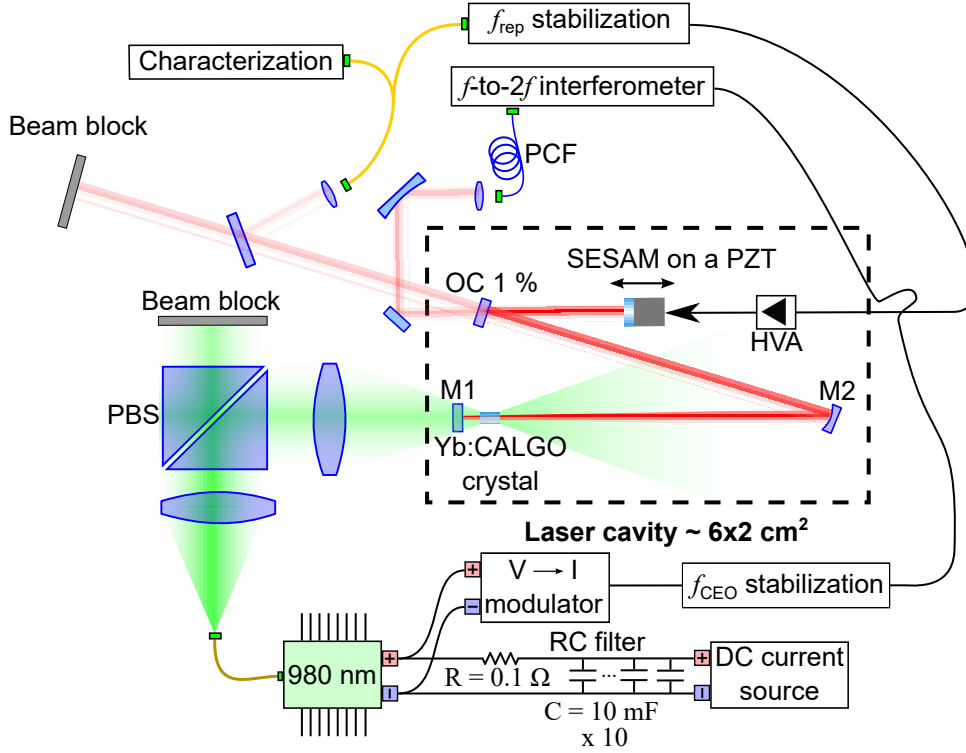


Figure 3.5: Overall scheme of the fully-stabilized Yb:CALGO GHz frequency comb. The laser cavity (center) is pumped by a 980-nm fiber-coupled diode array (left). One output beam of the laser is launched into a PCF for SC spectrum generation, followed by an f -to- $2f$ interferometer for CEO detection (top). The stabilization of f_{CEO} is implemented by a phase-lock loop with feedback applied to the pump diode current, whereas f_{rep} is stabilized by cavity length control with a PZT. PCF: photonic-crystal fiber; PBS: polarizing beamsplitter cube; HVA: high voltage amplifier. Yellow lines represent singlemode (SM) optical fiber connections, red, pink and green lines schematize free-space optical beams, and black lines are electrical connections.

SHG. Another waveplate in the 680-nm arm enables adjusting the polarization of this spectral component for optimized CEO beat generation. The PPLN is

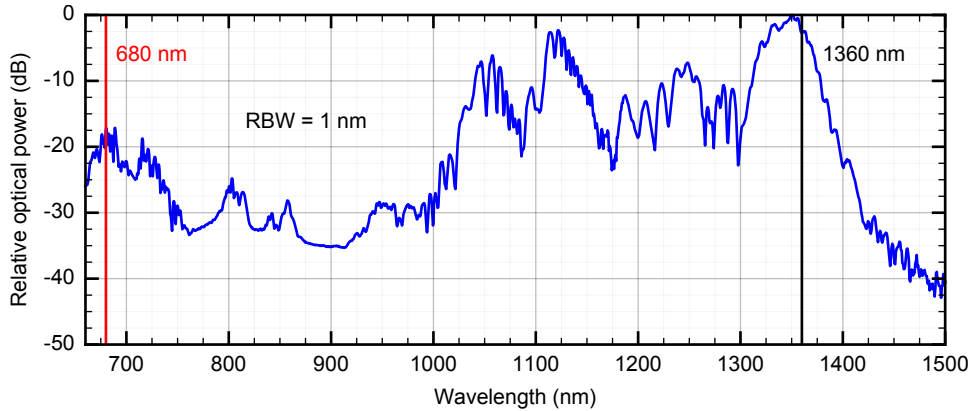


Figure 3.6: Full octave-spanning SC spectrum measured at the output of the PCF. The f and $2f$ frequency components used for CEO detection in the f -to- $2f$ interferometer are indicated by the black and red vertical lines, respectively. The spectrum is normalized with respect to the maximum spectral power achieved at 1350 nm; the total power at the output of the PCF is ~ 670 mW.

heated to 50°C for efficient SHG at 1360 nm. The 680-nm light at the output of the PPLN is focused onto a silicon avalanche photodiode for CEO beat detection (see Fig. 3.7). An adjustable delay line in the long-wavelength path enables adjusting the temporal overlap of the fundamental and frequency-doubled pulses on the photodiode. A CEO beat with a signal-to-noise ratio (SNR) of ~ 40 dB was detected in a resolution bandwidth (RBW) of 10 kHz (Fig. 3.8).

3.3. CEO frequency detection

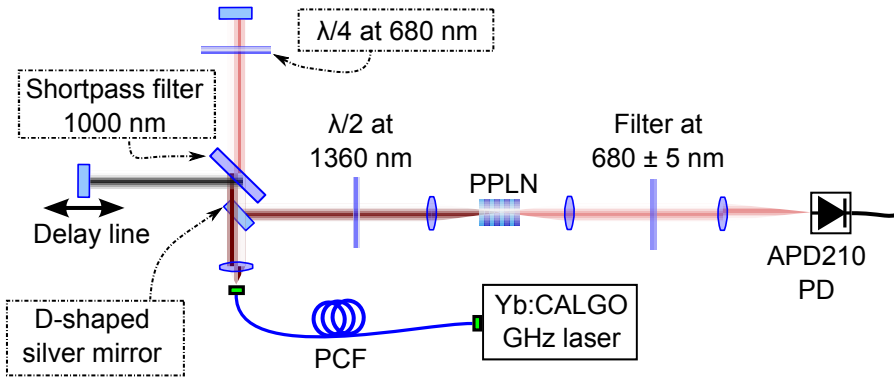


Figure 3.7: f -to- $2f$ interferometer for f_{CEO} detection. Colored lines represent the free space optical beams of the supercontinuum (dark red), long (black) and short (pink) wavelength components, respectively. PD: photodiode; PPLN: periodically-poled lithium niobate; PCF: photonic-crystal fiber.

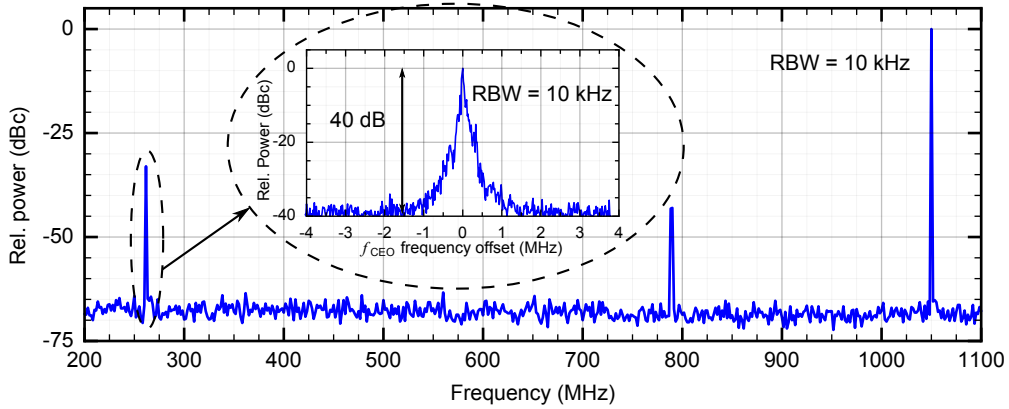


Figure 3.8: Radio frequency (RF) spectrum of the signal at the output of the f -to- $2f$ interferometer showing a CEO frequency of ~ 266 MHz. The inset displays a zoom on the CEO beat showing an SNR of 40 dB in a RBW of 10 kHz.

3.4 Full stabilization of the frequency comb

3.4.1 Static and dynamic comb control

Prior to the comb stabilization, the static and dynamic tuning rates of f_{rep} and f_{CEO} were measured as a function of the PZT voltage and pump current, respectively (Fig. 3.9). Whereas the static measurements aimed at determining the maximum span over which f_{rep} and f_{CEO} can be linearly shifted, the dynamic measurements provide useful information about the frequency-dependent amplitude and phase response of f_{rep} and f_{CEO} upon modulation, which are important parameters to assess the achievable locking bandwidth in a stabilization loop. The static curves displayed in the insets of Fig. 3.9(a) and 3.9(c) show a linear response with a tuning coefficient of 74.2 Hz/V over a span of ~ 12 kHz for f_{rep} as a function of the voltage at the output of the HVA, and 205 kHz/mW over a span of ~ 150 MHz for f_{CEO} as a function of the pump power, respectively. These tuning ranges are limited by the 150-V driving voltage of the PZT for f_{rep} , and by the range of detectable CEO beat for f_{CEO} . However, both tuning ranges are largely sufficient for precise adjustment and stabilization of these frequencies. For the dynamic curves, we modulated either the voltage at the input of the HVA or at the input of the home-made voltage-to-current converter with a sine waveform, corresponding typically to a peak-to-peak modulation of 80 V applied to the PZT or of 150 mW of the pump power. The resulting frequency modulation was measured in amplitude and phase by demodulating the repetition rate or CEO beat using a frequency discriminator [88], followed by a lock-in amplifier (HF2LI from Zurich Instruments) set to the applied modulation frequency. The measured transfer function of f_{rep} displayed in Fig. 3.9(a) shows a flat response in amplitude up to more than 50 kHz, followed by a narrow resonance peak at ~ 80 kHz. The amplitude of the transfer function of ~ 72.1 Hz/V observed at low modulation frequency is in excellent agreement with the aforementioned static

3.4. Full stabilization of the frequency comb

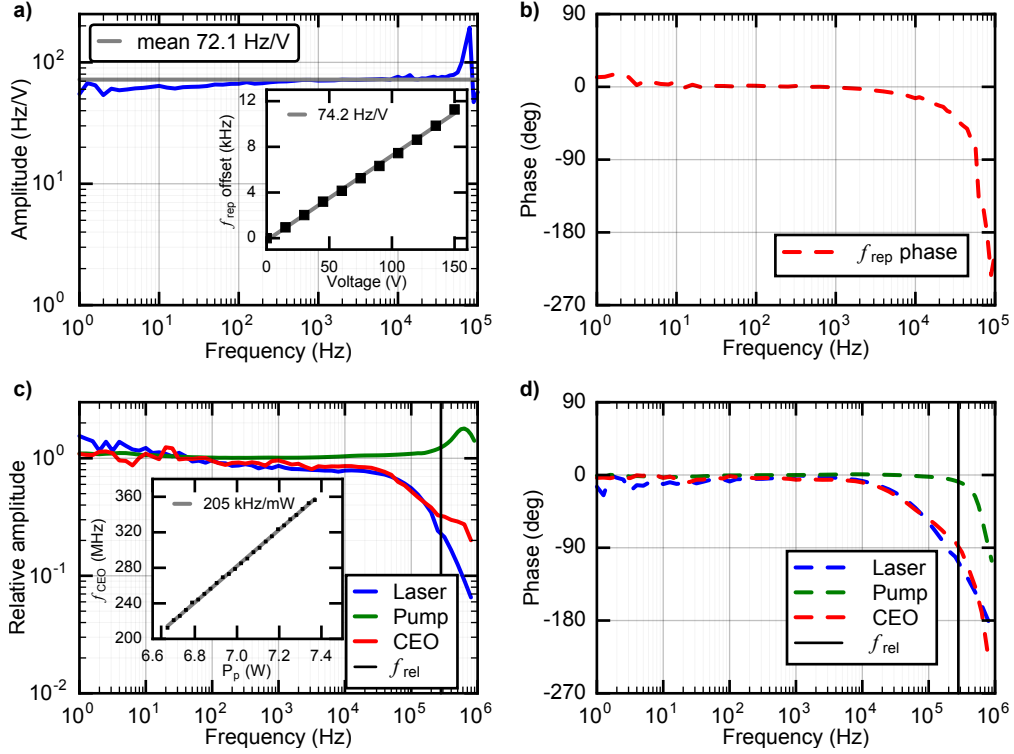


Figure 3.9: a) Amplitude of the transfer function of f_{rep} for PZT modulation (blue) and calculated mean value (gray); inset: static tuning of f_{rep} as a function of the PZT voltage. b) Phase of the transfer function of f_{rep} for PZT modulation (dashed red). c) Relative amplitude of the transfer functions of f_{CEO} (red), of the laser output power (blue), and of the pump optical power (green) for pump current modulation, and calculated relaxation frequency (f_{rel}) of the laser (straight black line); inset: static tuning of f_{CEO} as a function of pump current. d) Phase of the transfer functions of f_{CEO} (red), of the laser output power (blue), and of the pump optical power (green) for pump current modulation, and calculated relaxation frequency (f_{rel}) of the laser (straight black line).

value that was separately measured using an RF spectrum analyzer. The phase

of the transfer function remains close to zero for frequencies up to 10 kHz and a phase shift of 90° is reached at ~ 60 kHz [Fig. 3.9(b)]. For f_{CEO} , the measured transfer function behaves like a low-pass filter with a 3-dB cut-off frequency of ~ 100 kHz [Fig. 3.9(c)] and a 90° phase shift reached at a modulation frequency of ~ 280 kHz [Fig. 3.9(d)]. For comparison, the transfer function of the output power of the pump diode modulated by our home-made driver was also measured by detecting a small fraction of the pump power on a photodiode and performing similar lock-in detection. The achieved modulation bandwidth of the pump power was larger than 1 MHz in amplitude (with the presence of a small overshoot at ~ 700 kHz). Therefore, the observed modulation bandwidth of f_{CEO} in our modelocked laser is not limited by the pump response, but by the laser relaxation oscillation that accounts in particular for the upper state lifetime of the gain medium and the cavity dynamics. A relaxation oscillation of ~ 280 kHz was calculated for our laser [straight black lines in Fig. 3.9(c) and 3.9(d)] based on the formula given by Schlatter *et al* [89]. This value is in good agreement with the 90° phase shift of the CEO transfer function observed at ~ 280 kHz. For cross-check, we also measured the transfer function of the output power of the modelocked laser, which is influenced by the same dynamics and usually shows a very similar behavior as f_{CEO} [90], which is indeed the case in the present modelocked laser as shown in Fig. 3.9(c) and 3.9(d).

3.4.2 Stabilization schemes

The stabilization schemes implemented to phase-lock f_{rep} and f_{CEO} to reference frequencies are depicted in the correspondingly labeled frames in Fig. 3.10. For repetition rate stabilization, the 8th harmonic of f_{rep} at ~ 8.4 GHz was chosen to enhance the phase noise sensitivity compared to the fundamental component. It was detected using a high-bandwidth photodiode (New Focus 1434) with a small fraction of one of the laser output beams. The signal was filtered, am-

3.4. Full stabilization of the frequency comb

plified and frequency down-converted to ~ 25 MHz by mixing it with the signal of a reference synthesizer (Rohde-Schwarz SMF-100A). This is done in order to be able to measure the long term stability of the stabilized f_{rep} (see details in Section. 3.5.3). The down-converted signal was compared in a second double-

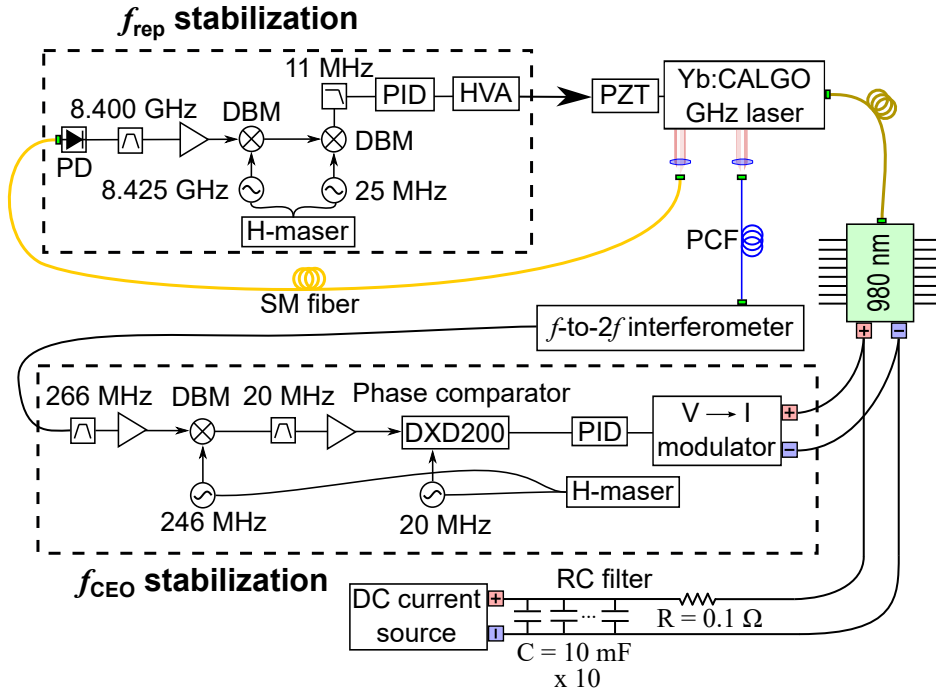


Figure 3.10: The stabilization of f_{CEO} is implemented by a phase-lock loop with feedback applied to the pump diode current through a home-built voltage-to-current ($U \rightarrow I$) modulator (bottom dashed frame), whereas f_{rep} is stabilized to an H-maser (through frequency synthesizers) by cavity length control with a PZT (top). PCF: photonic-crystal fiber; PD: photodiode; PID: proportional-integral-derivative controller; DBM: double-balanced mixer; HVA: high-voltage amplifier. Yellow lines represent singlemode (SM) optical fiber connections, pink lines schematize free-space optical beams, the blue line is the PCF, and black lines are electrical connections.

balanced mixer (DBM) to the reference signal from a second signal synthesizer (SRS DS345). To ensure stable long-term operation of the comb, both synthesizers were referenced to an H-maser. The resulting phase error signal was low-pass filtered and processed by a servo-controller to produce the correction signal to control the cavity length of the laser. This signal was amplified by a high-voltage amplifier (gain of 15) and applied to the PZT holding the SESAM in the cavity. For f_{CEO} stabilization, the CEO beat detected at the output of the f -to- $2f$ interferometer at ~ 266 MHz was low-pass filtered, amplified and frequency down-converted to ~ 20 MHz using a synthesizer and a DBM. The down-converted CEO beat signal was band-pass filtered, amplified to ~ 0 dBm and compared in a digital phase detector (DXD200 from Menlo Systems) to a ~ 20 -MHz reference signal. All frequency references were referenced to the same H-maser as used for f_{rep} stabilization. The phase error signal was processed by a proportional-integral-derivative (PID) controller (Vescent D2-125) and the resulting feedback signal was applied to the current of the pump diode. To achieve

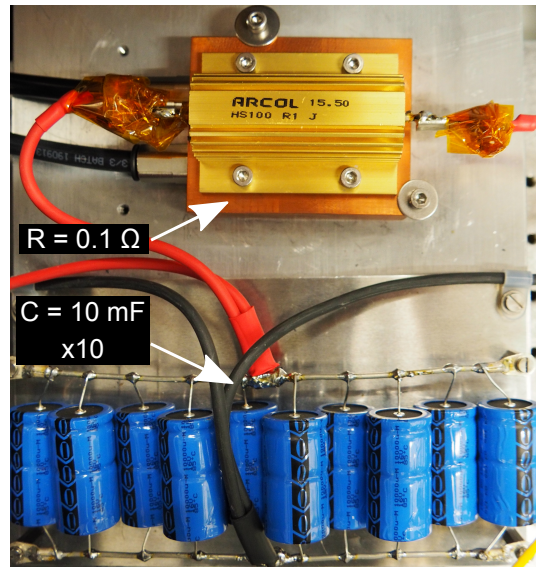


Figure 3.11: Picture of the RC filter.

3.4. Full stabilization of the frequency comb

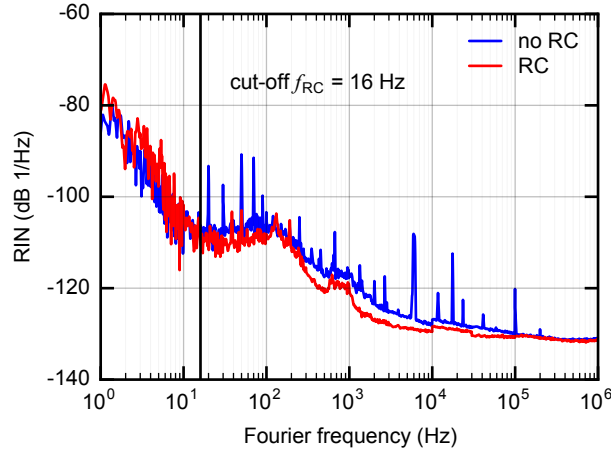


Figure 3.12: Comparison of the RIN of the pump diode measured without (blue) and with (red) the RC filter placed between the high current source and the pump diode. The cut-off frequency of the RC filter of ~ 16 Hz is indicated by the straight vertical line. The RC filter efficiently suppresses the discrete noise peaks of electrical origin located between 10 and 100 Hz, and in the range of 1 kHz to 100 kHz. The broadband excess noise present at $f > 10$ Hz is not affected by the filter as it arises from a different origin that is discussed in detail in Section 3.5.2

the fast pump modulation that is required for CEO stabilization, our home-made voltage-to-current converter with a modulation bandwidth of ~ 1 MHz and a gain of 120 mA/V was used to drive the pump diode in parallel with the high current source delivering the typical pump current of 17.7 A for the diode. A low-pass RC filter made of a resistor of 0.1 Ω and 10 capacitors of 10 mF connected in parallel (see Fig. 3.11), resulting in a nominal cut-off frequency of ~ 16 Hz, was placed between the current source and the pump diode for a double purpose. First, it reduced the current noise of the DC source coupled to the diode, thus decreasing its RIN, especially by effectively filtering out some strong spurious noise peaks occurring at 50 Hz and other discrete frequencies (see Fig. 3.12).

Secondly, it ensured that the modulation signal from the fast current modulator was properly applied to the pump diode, avoiding any cross-coupling to the DC source.

3.5 Characterization of the fully stabilized comb

3.5.1 Frequency noise of the phase-locked comb parameters

The noise properties of the GHz comb have been characterized, both in free-running and fully-stabilized conditions, by measuring the frequency noise power spectral density (FN-PSD) of the repetition rate and CEO beat using a phase noise analyzer (Rohde & Schwarz FSWP26). In a first step, we aimed at optimizing the CEO stabilization loop to minimize its residual integrated phase noise. Figure 3.13(a) shows the measured FN-PSD for the free-running and locked CEO beats. A locking bandwidth of ~ 150 kHz assessed from the position of the servo bump in the FN-PSD was achieved using our home-made diode current modulator. The FN-PSD of the CEO beat was entirely reduced below the β -separation line [91], indicating the achievement of a tight lock that is characterized by the presence of a coherent peak in the CEO RF spectrum. The observed coherent peak is shown in the inset of Fig. 3.13(a), with an SNR of 50 dB in a resolution bandwidth of 1 Hz. The integrated phase noise of the stabilized CEO beat was 680 mrad [1 Hz - 1 MHz]. In this first configuration, the stabilization loop for f_{rep} was implemented only with a PI (proportional-integral) servo-controller (Newport LB1005). The resulting FN-PSD of f_{rep} is shown in Fig. 3.13(b), together with the noise spectrum of the free-running repetition rate. With this stabilization loop, the noise of f_{rep} was reduced to the

3.5. Characterization of the fully stabilized comb

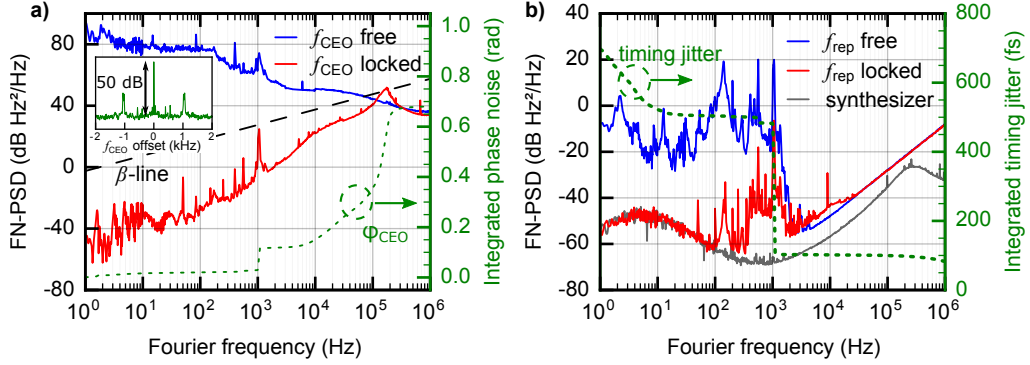


Figure 3.13: Noise performance of the fully-stabilized GHz comb obtained using a PID controller for the CEO feedback loop and a PI controller for the repetition rate. a) Frequency noise power spectral density (FN-PSD) of the CEO beat in free-running (blue) and stabilized (red) conditions, and corresponding integrated phase noise as a function of the upper cut-off frequency (right vertical axis); inset: RF spectrum of the CEO beat showing a coherent peak with an SNR of 50 dB at a RBW of 1 Hz. b) FN-PSD of the free-running (blue) and phase-locked (red) repetition rate stabilized using a PI servo gain. The FN-PSD of the reference synthesizer is also shown for comparison (gray). Right vertical axis: integrated timing jitter as a function of the low cut-off frequency.

level of the reference synthesizer at Fourier frequencies up to ~ 100 Hz. The integrated timing jitter was 520 fs in this case (integrated from 10 Hz to 1 MHz). We found that the noise peaks occurring in the FN-PSD of f_{rep} in the range of ~ 100 Hz to ~ 2 kHz [Fig. 3.13(b)] were originating from mechanical noise (see also further investigations presented in Section 4.2). To damp these peaks, we isolated the laser breadboard from the optical table by using damping foam rubber, and we also isolated the water tubes of the pump diode cooling circuit that could transfer some mechanical noise to the optical table. With these changes,

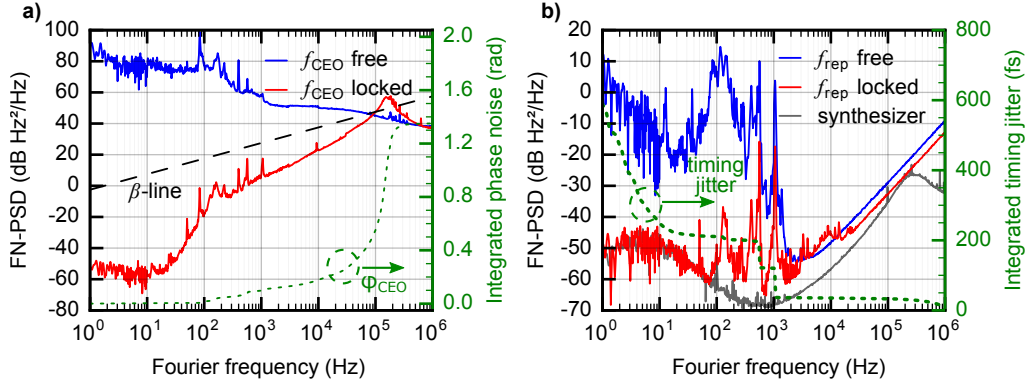


Figure 3.14: Noise performance of the fully-stabilized GHz comb obtained with the same CEO feedback loop as in Fig. 3.13, but with mechanical damping of the laser breadboard and a derivative filter added to the repetition rate feedback loop. a) FN-PSD of the CEO beat in free-running (blue) and stabilized (red) conditions, and corresponding integrated phase noise as a function of the upper cut-off frequency (right vertical axis). b) FN-PSD of the free-running (blue) and phase-locked (red) repetition rate stabilized using a PID servo controller. The FN-PSD of the reference synthesizer is also shown for comparison (gray). Right vertical axis: integrated timing jitter as a function of the low cut-off frequency.

the noise peaks at ~ 100 Hz and ~ 600 Hz in the FN-PSD of f_{rep} were reduced by approximately one order of magnitude, while the peak at 1 kHz was reduced by nearly two orders of magnitude [compare the blue curves in Fig. 3.13(b) and Fig. 3.14(b)]. To be able to extend the stabilization bandwidth of f_{rep} and further reduce its noise, we used a different servo controller (Vescent D2-125) providing a derivative filter, as well as a second integrator, in addition to the PI gain previously used. With this, the detrimental noise peaks occurring in the FN-PSD of the repetition rate in the frequency range of 100 Hz to 1 kHz have been reduced as shown in Fig. 3.14(b), leading to an improved timing jitter

of 250 fs [10 Hz - 1 MHz]. However, this increased stabilization bandwidth for f_{rep} produced a negative side effect by increasing the noise of the free-running CEO beat as a result of a possible cross-effect of the PZT modulation to the CEO frequency as previously observed in an Er: fiber comb [92]. As a result, the noise of the stabilized CEO beat slightly increased around the servo-bump, clearly exceeding the β -separation line. The corresponding integrated phase noise increased to 1.34 rad.

3.5.2 CEO noise source analysis

A further analysis was performed to investigate the dominant noise sources of the CEO beat. First, the RIN of the pump diode was measured and its contribution to the CEO FN-PSD was calculated using the measured transfer function of f_{CEO} for pump current modulation [Fig. 3.9(a)]. Figure 3.15(a) shows an excellent overlap between the contribution of the pump RIN to the CEO frequency noise and the actual CEO noise. This demonstrates that the pump RIN is essentially responsible for the CEO frequency noise, except for some narrow noise peaks at ~ 80 Hz, ~ 160 Hz, ~ 240 Hz and at ~ 400 Hz, that are likely of mechanical origin in the laser cavity. To further investigate the origin of the pump RIN, we also measured the current noise of the DC source used to drive the pump diode, and converted it into an equivalent CEO frequency noise. This was realized by taking into account the drive-current-to-output-power response of the pump diode and the pump-power-to-CEO-frequency transfer function of the modelocked laser previously shown in Fig. 3.9. One can observe in Fig. 3.15(a) that the current noise of the pump diode driver is responsible for the CEO frequency noise at low Fourier frequencies (< 10 Hz). However, another source of excess noise is dominant at higher frequencies.

To identify the origin of this excess noise, we measured the RIN of the pump diode with its water cooling circuit switched on and off. A significant

difference in the pump RIN was observed in these two cases as displayed in Fig. 3.15(b). The RIN of the pump diode is larger at low Fourier frequencies without the water cooling due to a thermal drift resulting in a linear shift of its optical output power. However, the noise is significantly larger at higher frequencies (above ~ 30 Hz) when the water cooling is activated, and the RIN presents the same noise pattern as the CEO beat. Therefore, the water cooling circuit has a strong contribution to the excess RIN of the pump diode. The fact that the water-cooled plate has internal micro-channels supports the idea that the cooling circuit can induce mechanical vibrations and noise. This effect could be significantly reduced by replacing the water cooling of the pump diode by a thermo-electrical cooler.

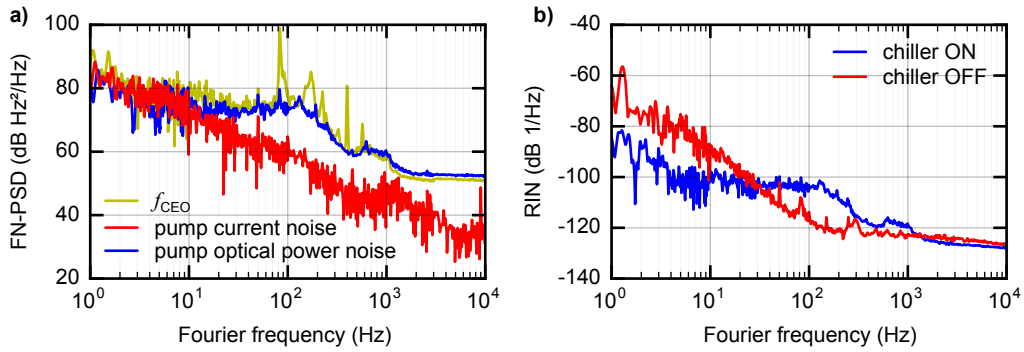


Figure 3.15: a) FN-PSD measured for the free-running f_{CEO} (yellow) compared with the contributions of the current noise of the pump diode driver (red) and of the pump RIN (blue). The last two curves were obtained by converting the measured current noise and RIN into an equivalent frequency noise of the CEO by taking into account the slope efficiency of the pump diode and its pump-power-to-CEO-frequency transfer function. The water cooling chiller was in operation in this measurement. b) Comparison of the RIN of the pump diode measured with the water cooling chiller on (blue) and off (red).

3.5.3 Frequency stability

Whereas the frequency noise analysis presented before allows for the characterization of high-frequency noise components, a time-domain analysis reveals useful information about the long-term behavior of a frequency comb. For this purpose, we simultaneously recorded the time series of f_{rep} and f_{CEO} using a multi-channel II-type frequency counter without dead-time (FXM-50 from K-K Messtechnik) with 1-s gate time. The 8th harmonic of f_{rep} , which was mixed down to a frequency of ~ 25 MHz in the measurement range of the counter, has been used in this measurement. This allowed us to ensure that the recorded frequency was not limited by the 1-mHz counter resolution (which corresponds to a relative frequency resolution of $1.3 \cdot 10^{-13}$ with respect to a 8-GHz signal).

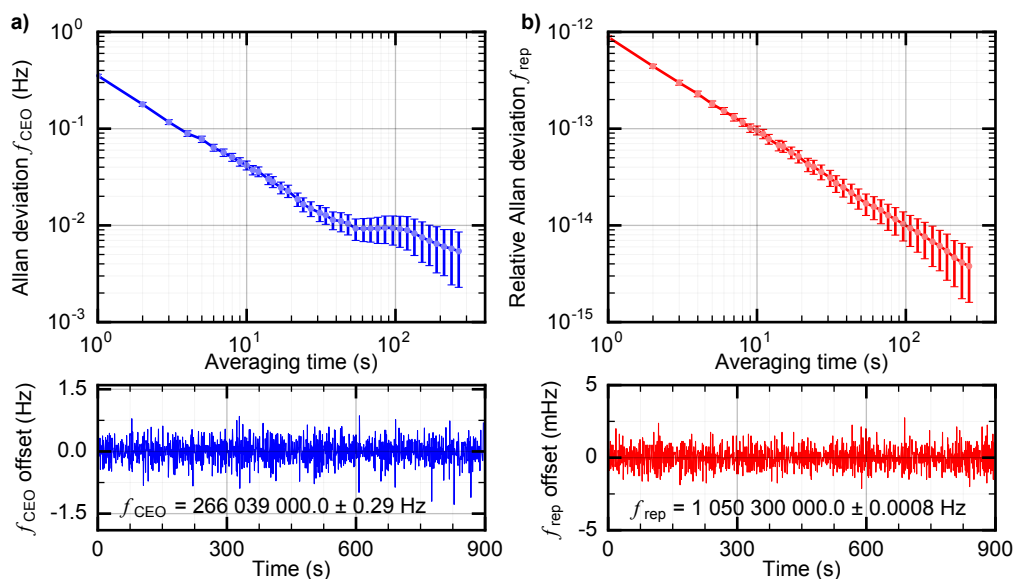


Figure 3.16: Frequency stability of the fully-stabilized GHz comb: overlapped Allan deviation of f_{CEO} (a) and relative (overlapped) Allan deviation of f_{rep} (b) calculated from the recorded time series displayed in the bottom of the figure. The mean values and standard deviations of f_{CEO} and f_{rep} are also indicated on the plots.

Figure 3.16 shows a time series of 900 s simultaneously recorded for f_{rep} and f_{CEO} with the frequency counter and the corresponding calculated overlapped Allan deviation [93]. The relative frequency stability of f_{rep} in the range of 10^{-12} at 1-s averaging time is limited by the reference synthesizer used in the stabilization loop. The sub-Hz Allan deviation observed for f_{CEO} at an integration time of 1 s contributes at the level of 10^{-15} only to the relative frequency instability of an optical comb line at 1 μm (≈ 300 THz), which is negligible in comparison to the frequency instability arising from the repetition rate. Even if the comb was locked to an ultra-stable optical reference, the contribution of the CEO frequency instability to an optical comb line would not be dominant.

3.5.4 Characterization of an optical comb mode

Furthermore, we investigated the noise properties of an individual line of the fully-stabilized comb by implementing a heterodyne beat with a narrow-linewidth CW laser. Due to the lack of a suitable low-noise laser in the emission spectrum of our GHz comb, we developed a dedicated experimental setup to measure the noise of a comb line in comparison to an ultra-stable laser at 1557 nm (see Fig. 3.17). This laser was stabilized to an ultra-low thermal expansion (ULE) optical cavity by the Pound-Drever-Hall locking technique [94], enabling a linewidth at the Hz level to be achieved. To link this laser to the 1- μm GHz comb, a fully-stabilized Er:fiber frequency comb (FC1500 from Menlo Systems) with 250-MHz repetition rate and centered at 1.55 μm was used as a transfer oscillator. For this purpose, an additional SC spectrum extending down to the 1- μm range was generated from the modelocked Er:fiber oscillator using a highly non-linear fiber as schematized in Fig. 3.17. A first virtual beat $f_{\text{virt.beat1}} = \nu_{1030}^{\text{GHz}} - \nu_{1030}^{\text{Er}}$ between one line of the SC spectrum generated from the Er:fiber comb (at frequency ν_{1030}^{Er}) and of the GHz comb (frequency ν_{1030}^{GHz}) was detected at 1030 nm by combining (mixing) the beat signals between each comb

3.5. Characterization of the fully stabilized comb

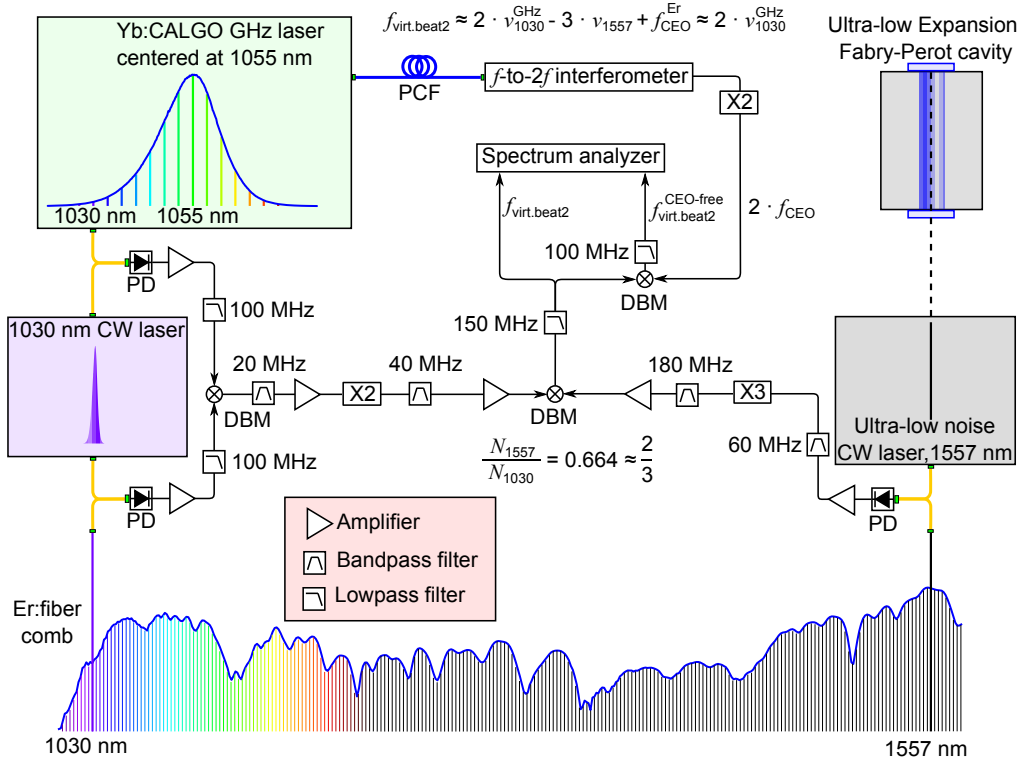


Figure 3.17: Schematic principle of the measurement setup implemented to characterize one optical line of the GHz comb with respect to an ultrastable laser at 1.56 μm using an Er:fiber comb as a transfer oscillator (bottom). PD: photodiode, DBM: double-balanced mixer, PCF: photonic-crystal fiber, X2: frequency doubler, X3: frequency tripler, yellow lines represent singlemode (SM) optical fiber connections, the blue line is the PCF, and black lines are electrical connections.

and a distributed feedback (DFB) laser (Eagleyard DFB-1030-00100-BFW01-0002). The DFB laser was too noisy with a typical linewidth of $\sim 1\text{-}2$ MHz to enable a direct characterization of the GHz comb line. However, its noise cancelled out in the virtual beat as it was common to the two signals. The beat signal between the GHz comb and the DFB laser was realized after propagating the output of the Yb:CALGO oscillator in a few meters of singlemode fiber in

order to slightly broaden its spectrum to reach the DFB laser wavelength of 1030 nm. As the noise spectrum of the virtual beat $f_{\text{virt.beat1}}$ between the two combs was partially limited in some spectral regions by the Er:fiber comb, an additional virtual beat $f_{\text{virt.beat2}}$ was realized between this signal and the 1557-nm ultra-stable laser, using the Er:fiber comb as a transfer oscillator. This was implemented by beating the Er:fiber comb, optically band-pass filtered at 1557 nm, with the cavity-stabilized narrow-linewidth laser, and by mixing this signal with the first virtual beat $f_{\text{virt.beat1}}$. As these two beat signals contained a different noise contribution of the Er:fiber comb (due to the different upscaling factor of the dominant repetition rate noise by the mode number N_{1030}^{Er} or N_{1557}^{Er} involved in the two beats), they had to be scaled by a factor $N_{1557}^{\text{Er}}:N_{1030}^{\text{Er}} \approx 0.66$ prior to be mixed following the principle of the transfer oscillator [95]. We did not implement here a perfect transfer oscillator with the exact factor $N_{1557}^{\text{Er}}:N_{1030}^{\text{Er}}$, but we approximated it by a value of 2:3 that was fully sufficient to suppress the noise contribution of the Er:fiber comb in the considered measurement. Therefore, the first virtual beat $f_{\text{virt.beat1}}$ and the heterodyne beat at 1557 nm have been frequency doubled and tripled, respectively, before being filtered, amplified, and mixed together. The CEO beat $f_{\text{CEO}}^{\text{Er}}$ the Er:fiber comb has not been removed from this virtual beat, but we have checked that its contribution to the measured noise spectrum was negligible. Finally, the virtual beat between the GHz comb line at 1030 nm (ν_{1030}^{GHz}) and the ultra-stable laser at 1557 nm (ν_{1557}) is given by:

$$\begin{aligned}
 f_{\text{virt.beat2}} &= | 2 \cdot (\nu_{1030}^{\text{GHz}} - N_{1030}^{\text{Er}} \cdot f_{\text{rep}}^{\text{Er}} - f_{\text{CEO}}^{\text{Er}}) - 3 \cdot (\nu_{1557} - N_{1557}^{\text{Er}} \cdot f_{\text{rep}}^{\text{Er}} - f_{\text{CEO}}^{\text{Er}}) | \\
 &\approx | 2 \cdot \nu_{1030}^{\text{GHz}} - 3 \cdot \nu_{1557} + f_{\text{CEO}}^{\text{Er}} |
 \end{aligned} \tag{3.1}$$

This virtual beat, in which the noise of the Er:fiber comb was canceled to a large extent in the condition $2 \cdot N_{1030}^{\text{Er}} \approx 3 \cdot N_{1557}^{\text{Er}}$, was finally analyzed. It contained two times the noise of the investigated line ν_{1030}^{GHz} of the GHz comb. A CEO-free virtual beat that contained only the noise contribution of $N \cdot f_{\text{rep}}$ of the GHz comb was finally obtained by mixing the virtual beat $f_{\text{virt.beat2}}$ with the

3.5. Characterization of the fully stabilized comb

frequency-doubled CEO beat of the GHz comb to cancel its noise contribution:

$$\begin{aligned} f_{\text{virt.beat2}}^{\text{CEO-free}} &\approx | 2 \cdot \nu_{1030}^{\text{GHz}} - 3 \cdot \nu_{1557} + f_{\text{CEO}}^{\text{Er}} | - 2 \cdot f_{\text{CEO}} \\ &\approx 2 \cdot N \cdot f_{\text{rep}} - 3 \cdot \nu_{1557} + f_{\text{CEO}}^{\text{Er}} \end{aligned} \quad (3.2)$$

The FN-PSD of the virtual beat $f_{\text{virt.beat2}}$ between one line of the GHz comb at 1030 nm and the ultra-stable laser at 1557 nm has been measured with the phase noise analyzer. Due to the negligible contribution of the ultra-stable laser (Hz level linewidth), this noise directly represents the noise of a comb line at around 1030 nm, i.e. $\nu_{\text{N}} = N \cdot f_{\text{rep}} + f_{\text{CEO}}$ with $N \approx 276'600$ [multiplied by a factor 4 in terms of PSD due to the factor 2 occurring in Eq. (3.1) or (3.2)]. The noise contribution of $N \cdot f_{\text{rep}}$ only was obtained from the CEO-free virtual beat $f_{\text{virt.beat2}}^{\text{CEO-free}}$ for comparison, without limitation by the instrumental noise floor occurring when directly measuring f_{rep} in the RF domain. Figure 3.18(a) shows a comparison of the noise spectrum measured directly at the fundamental repetition rate f_{rep} and up-scaled to the optical frequency $N \cdot f_{\text{rep}}$ on one side, and obtained from the CEO-free virtual beat signal $f_{\text{virt.beat2}}^{\text{CEO-free}}$ on the other side. The two curves overlap in the low frequency range up to ~ 10 kHz (they also coincide with the reference synthesizer below 100 Hz), and the optical measurement overcomes the noise floor limitation of the RF measurement occurring at frequencies higher than 10 kHz (corresponding to a white phase noise of 139 dBc/Hz).

In Fig. 3.18(b), the noise spectrum of the optical line is compared to the individual contributions of $N \cdot f_{\text{rep}}$ and f_{CEO} . At low Fourier frequencies (1 to 100 Hz), the noise of the optical line coincides with the noise of the reference synthesizer, up-scaled by the factor N^2 . In the frequency range of 100 Hz to 100 kHz, the noise of the optical line results from the excess noise of f_{rep} , whereas f_{CEO} has a negligible contribution. Furthermore, the FN-PSD of f_{CEO} is much lower than the β -separation line in this frequency range, indicating that

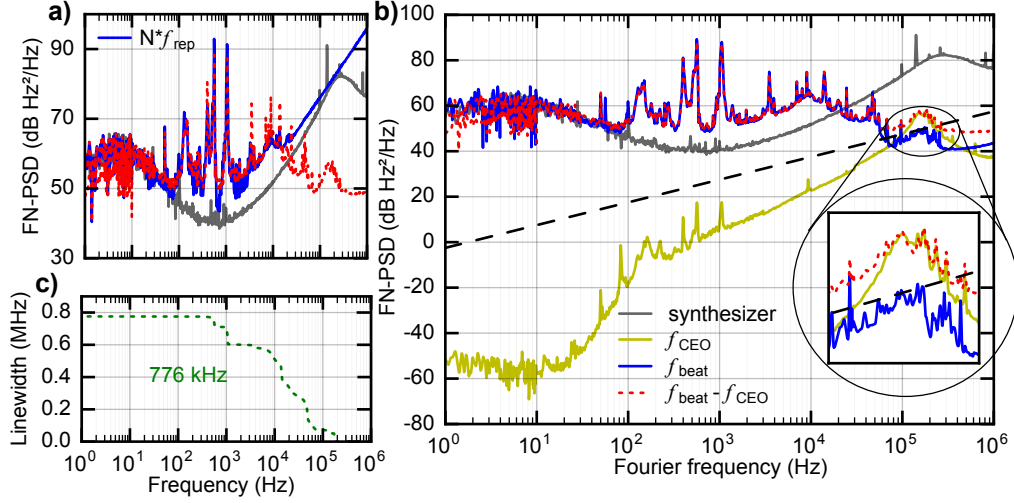


Figure 3.18: a) Comparison of the FN-PSD of the repetition rate assessed from the direct measurement of f_{rep} in the RF domain (solid blue curve) and from the optical CEO-free virtual beat $f_{\text{virt.beat2}}^{\text{CEO-free}}$ (dashed red curve), with a mode number $N \approx 276'600$, and of the reference synthesizer up-scaled by N^2 (gray). b) FN-PSD of an optical mode of the fully-stabilized GHz comb (blue), and comparison with the individual contribution of f_{CEO} (yellow), $N \cdot f_{\text{rep}}$ (red dashed) and of the reference synthesizer up-scaled by N^2 (gray). The inset shows a zoom in the frequency range of the CEO servo bump, where the noise of the optical comb line is lower than the individual contributions of f_{rep} and f_{CEO} . c) FWHM linewidth of the optical comb line calculated from the FN-PSD as a function of the low cut-off frequency (inverse of the integration time).

it does not contribute to the linewidth of the optical comb line [91]. In the frequency range around 150 kHz, where the CEO servo bump is located, this is no longer the case and the CEO noise may contribute to the optical linewidth. In this frequency range [see inset of Fig. 3.18(b)], the FN-PSD of $N \cdot f_{\text{rep}}$ is

very similar to the CEO noise, both in shape and amplitude (the two spectra overlap). However, the optical comb line has a noise lower than each of these individual contributions and lies underneath the β -separation line. The reason is that the noise in this spectral band mainly arises from the CEO servo-bump, which couples to the repetition rate as this degree of freedom of the comb is also affected by a modulation of the pump power, but with an opposite phase (anti-correlation). This anti-correlation combined with the similar amplitude of the noise of f_{rep} and f_{CEO} leads to a partial noise cancelation in the optical comb line $\nu_N = N \cdot f_{\text{rep}} + f_{\text{CEO}}$. A similar coupling of the CEO servo-bump in the frequency noise spectrum of f_{rep} and its partial compensation in the noise of an optical mode have been previously observed in an Er: fiber laser [92]. As a result, the servo-bump of f_{CEO} does not contribute to the optical linewidth of the comb mode, despite the fact that its integrated phase noise is not as low as in the first stabilization configuration of Fig. 3.13. From the measured FN-PSD of the comb line, its linewidth was calculated using the approximation of the β -separation line [91] and is displayed in Fig. 3.18(c) as a function of the low cut-off frequency of the FN-PSD (inverse of the integration time). An optical linewidth (FWHM) of ~ 800 kHz is obtained at 1-s integration time.

3.6 Conclusion

The first self-referenced fully-stabilized GHz frequency comb from a DPSSL has been demonstrated and a detailed characterization of its noise and frequency stability properties has been presented. Frequency combs with GHz repetition rates offer several benefits over standard fiber-based combs that typically operate at 50-250 MHz only. A GHz repetition rate provides a higher power per mode (at constant average power), an easier access to individual comb lines, and an easier filtering of the beat-note with a continuous wave laser. So far, self-referenced fully-stabilized GHz frequency combs have been demonstrated

only from Ti:Sapphire lasers. In comparison, DPSSL combs have the advantage of a simpler and cost-efficient diode pumping scheme, which enables direct high-bandwidth pump power modulation for CEO stabilization. In contrast, Ti:Sapphire combs have for a long time required an external acousto-optic modulator. Although a new green pump laser enabling direct and fast modulation was recently introduced in a commercial 1-GHz Ti:Sapphire comb [96], this pumping scheme is not as simple and cost-effective as the direct diode pumping of our Yb:CALGO laser. Furthermore, the fully-stabilized Yb:CALGO DPSSL reported here operates in the 1- μm wavelength range where low-noise narrow-linewidth continuous-wave lasers are easily available, opening attractive perspectives for future comb stabilization to an optical reference, instead of an RF reference as used in the results reported here. A first stabilization of an optical mode of this GHz Yb:CALGO DPSSL to an optical reference (low-noise laser) will be presented in Chapter 4.

The performed noise investigation of the GHz DPSSL comb included its two independent degrees of freedom, i.e., the repetition rate f_{rep} and the CEO frequency f_{CEO} , and additionally also an optical line at 1030 nm. This characterization was performed using a virtual heterodyne beat with an ultra-narrow linewidth CW laser at 1557 nm implemented with an auxiliary CW laser at 1030 nm and an Er:fiber comb used as a transfer oscillator. The Yb:CALGO DPSSL with a repetition rate of 1.05 GHz was pumped with a commercial laser diode array wavelength-stabilized at 980 nm with a VHG. The self-starting SESAM-modelocked laser delivers an average output power of 2.1 W in 96-fs pulses. These properties were fully sufficient to generate a coherent octave-spanning SC spectrum for CEO self-referencing in a PCF directly from one of the two output beams of the oscillator, without any external amplification or pulse compression. The detected CEO beat with an SNR of 40 dB (in a 10-kHz RBW) and a free-running FWHM linewidth of ~ 500 kHz (over an observation time of ~ 1 s) was phase-locked with a bandwidth of ~ 150 kHz to an external fre-

3.6. Conclusion

quency reference by feedback to the current of the pump diode using home-built fast modulation electronics. A tight lock of f_{CEO} was obtained with a residual integrated phase noise of 680 mrad [1 Hz - 1 MHz] in optimized stabilization conditions, corresponding to a fraction of more than 60% of the CEO power contained in the coherent peak.

The GHz repetition rate was phase-locked to a synthesizer referenced to an H-maser using a standard scheme of feedback to an intra-cavity PZT, resulting in an integrated timing jitter of 250 fs [10 Hz - 1 MHz]. This stabilization slightly affected the lock of f_{CEO} as a result of some cross-coupling effects, increasing the CEO integrated phase noise to 1.34 rad for an optimized lock of f_{rep} , but without any detrimental effect on the noise of an optical line. The presented noise analysis showed the respective contribution of f_{rep} and f_{CEO} to the optical line, from which a linewidth in the range of 800 kHz was assessed, dominated by the residual noise of the repetition rate. The long-term relative frequency stability of the comb was also measured, limited at the level of 10^{-12} at 1-s averaging time by the reference synthesizer used in the repetition rate stabilization, whereas the frequency instability of the locked CEO beat contributed only at the level of $10^{-15}/\text{s}$.

Further improvements of the pump diode RIN and thus also of the general comb noise performance are expected by replacing the current water cooling circuit by Peltier coolers. In addition, a better mechanical isolation of the laser cavity should reduce the influence of the mechanical noise that currently has a dominant effect on the noise of the repetition rate presented in this chapter. Finally, a stabilization of the comb CEO frequency with a larger bandwidth will be presented in Chapter 5 with the use of an opto-optical modulation of the intra-cavity SESAM, which will lead to improved CEO noise performance.

Chapter 4

GHz comb stabilization to an optical reference

4.1 Motivation

The noise investigation of the GHz frequency comb stabilized to an RF reference, presented in Section 3.5.4, showed that the main contribution to the frequency noise and linewidth of an optical comb line was originating from the noise of the repetition rate. There were two main contributions to the f_{rep} noise. The first one was mechanical noise that affected the cavity, resulting from acoustic noise and mechanical vibrations present in the laser environment. It induced noise on some cavity components that lead to significant noise peaks in the f_{rep} frequency noise (see Fig. 3.13). This type of noise can potentially be reduced by properly isolating the cavity from the environment and by using better mechanical mounts for the cavity components. A partial reduction of this spurious noise was shown in Section 3.5.1 in a first attempt (compare Fig. 3.13 and Fig. 3.14), in which particular noise peaks were damped. The second main contribution to the f_{rep} noise was the noise of the reference signal used in the stabilization.

In the results shown in Chapter 3, f_{rep} was stabilized to an RF reference (via synthesizers). The lowest noise synthesizer available in our lab in the GHz range is a Rohde & Schwarz SMF100 RF source. The phase noise PSD of an RF signal scales quadratically with its carrier frequency. Figure 4.1 shows the frequency noise of the SMF100 synthesizer at different carrier frequencies ranging from 1 to 15 GHz. When the 8th harmonics of f_{rep} was stabilized to this synthesizer at 8.4 GHz, the best achieved integrated timing jitter was 590 fs [1 Hz - 1 MHz] (see Fig. 3.14). This value was equivalently due to the spurious mechanical noise peaks at ~ 600 Hz and 1 kHz and to the low frequency noise limit of the reference synthesizer (below 10 Hz). As the noise PSD of the stabilized f_{rep} is multiplied

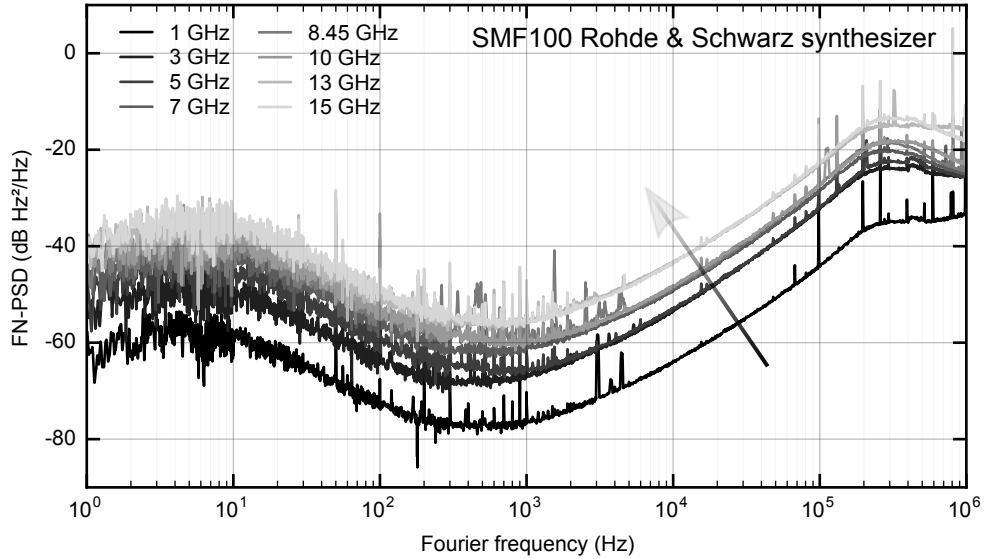


Figure 4.1: Frequency noise power spectral density of various signals from the Rohde & Schwarz SMF100 synthesizer at carrier frequencies from 1 GHz to 15 GHz.

by the huge scaling factor $N^2 \approx 10^{11}$ to an optical line at 1 μm , any residual noise contribution in f_{rep} has a detrimental influence on the linewidth of the optical lines. Even if the first noise source (mechanical) could be suppressed in

4.1. Motivation

the laser, the fundamental limitation to the frequency noise and linewidth of the stabilized comb line would arise from the upscaled noise of the RF reference. By considering the frequency noise of the current reference synthesizer used for f_{rep} stabilization in a frequency range corresponding to the PZT bandwidth of ~ 40 kHz, the narrowest linewidth that could be obtained for the optical lines of the GHz comb would be ~ 280 kHz when neglecting any additional mechanical noise (see Fig. 4.2).

In order to overcome this RF noise limitation, an alternative solution is to not stabilize f_{rep} directly to an RF reference, but to lock an optical line

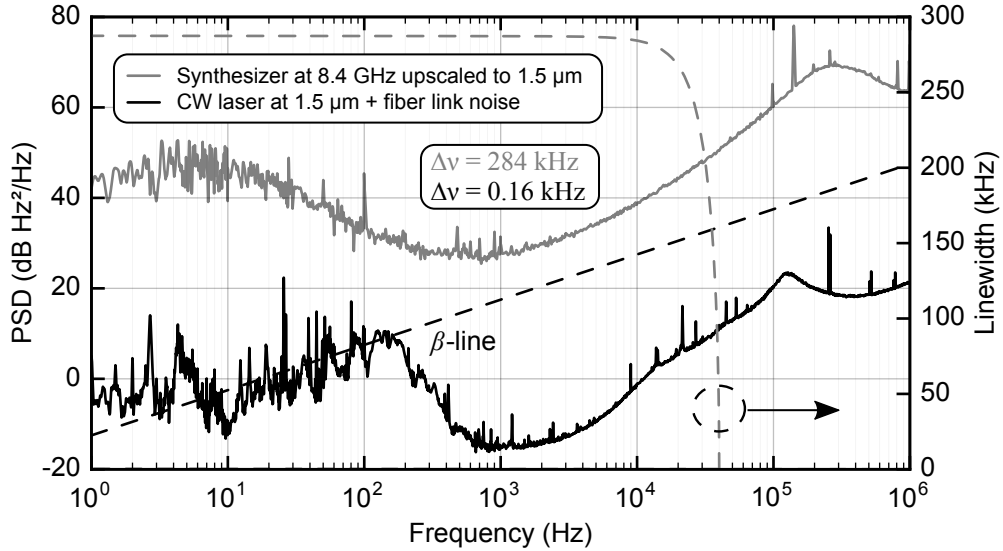


Figure 4.2: Frequency noise power spectral density of a 8.45-GHz signal from the Rohde & Schwarz SMF100 synthesizer up-scaled to 192 THz ($1.56 \mu\text{m}$) (grey), and of the CW $1.56\text{-}\mu\text{m}$ ultra-stable laser measured at the output of the 30-m fiber link (black). The right vertical axis displays the calculated linewidth of the signals obtained by integrating the FN-PSD from 1 Hz to 40 kHz (corresponding to the PZT modulation bandwidth).

of the frequency comb to an optical reference (ultra-stable CW laser). Such a laser can have a significantly lower frequency noise compared the up-scaled synthesizer noise. This method avoids the RF-to-optical noise multiplication since the stabilization is directly realized in the optical domain. This scheme benefits from ultralow noise CW lasers that are well established and widely used in different experimental systems [97]. They constitute in particular a key component of optical atomic clocks. At the LTF we have two 1.5- μm CW lasers stabilized to ULE Fabry-Perot cavities that provide Hz-linewidth optical signals. A comparison between the noise level of one of these lasers, measured at the output of a 30-m fiber link (see details after), and the synthesizer up-scaled to the optical frequency of ~ 190 THz (for 1.56 μm) shows a difference of several orders of magnitude (see Fig. 4.2). The estimated linewidth of the CW laser is ~ 1700 times narrower than for the up-scaled synthesizer noise. The 160-Hz linewidth considered here for the 1.5- μm CW laser is significantly broader than the expected Hz-level of this laser. The reason is that it was measured at the

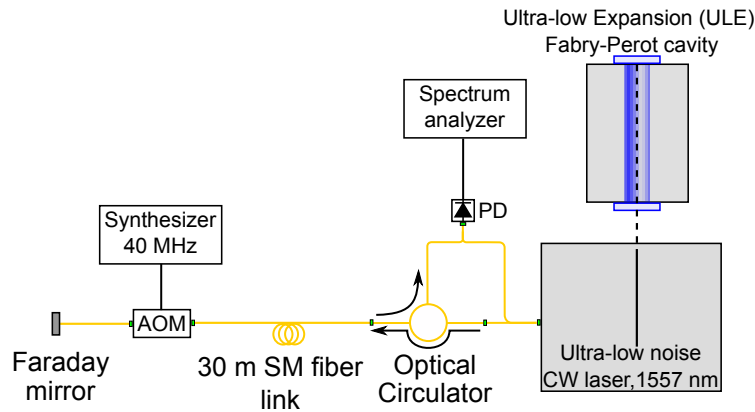


Figure 4.3: Experimental setup for the measurement of the fiber link noise. Yellow and black lines represent singlemode fibers and electrical connections respectively, PD: photodiode; AOM: acousto optic modulator.

4.1. Motivation

output of a 30-m optical fiber that links the respective laboratories of the GHz comb and of the ultra-low noise laser, and this fiber link adds phase noise to the transmitted CW laser signal. The noise contribution of the fiber link was assessed using the experimental setup shown in Fig. 4.3.

The light of the 1.56- μm CW laser was sent through a 30-m fiber that links two different labs at the LTF. At the fiber end an acousto-optic modulator (AOM) shifted the light frequency by 40 MHz and the signal was reflected back through the same fiber link by a Faraday mirror. At the local end the reflected signal was heterodyned with the laser light before the fiber link and the beat note at 80 MHz was measured (corresponding to a double path through the AOM). Figure 4.4 shows a comparison of the frequency noise of the 1.5- μm CW

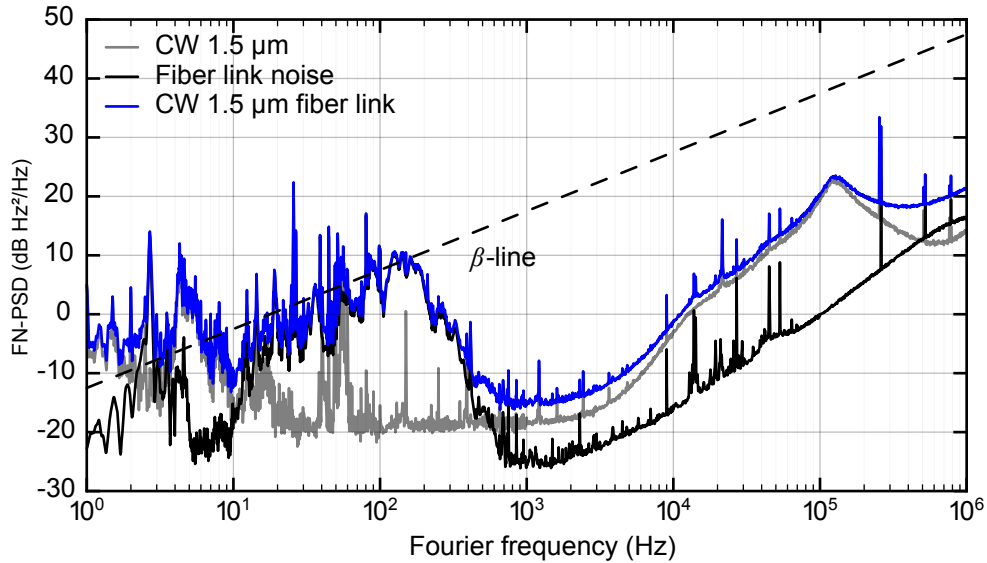


Figure 4.4: Frequency noise power spectral density of the CW 1.56- μm ultra-stable laser (grey) obtained from beat with 2nd ultrastable laser, of the fiber link (black), and the resulting noise of the CW laser after the fiber link that is obtained by summation of the two noises mentioned earlier.

laser (grey, assessed from the beat with a second similar laser) and assessed for the fiber link (black). The resulting noise of the ultra-stable laser at the output of the delivery fiber is the addition of these two (blue).

4.2 Further investigation on f_{rep} noise

As previously discussed in Section 3.5.1, the noise of the optical lines of our GHz comb is dominated by the noise of the repetition rate, which originates to a large extent from the effect of environmental acoustic and mechanical vibrations onto the laser cavity. Therefore, a further investigation of the repetition rate noise was performed and attempts to reduce it were investigated before trying to stabilize the comb to an optical reference. First, the origin of acoustic and mechanical noise was investigated by applying acoustic perturbations to the laser cavity and measuring the resulting effect on f_{rep} . This was realized by successively attaching a loud-speaker to each individual cavity component and by mechanically exciting it by a sine signal. A frequency discriminator (Miteq FMDM 21.4/4-2) followed by a lock-in amplifier was used to quantify the effect of the applied modulation onto the repetition rate frequency f_{rep} . By scanning the excitation frequency from 1 Hz to 10 kHz, the corresponding transfer function of f_{rep} upon the mechanical excitation was measured in amplitude and phase. This measurement was made for the three most critical components of the cavity that are the crystal (mounted on a 3-axis stage Newport M-462-XYZ), the curved mirror (mounted on a linear stage Thorlabs MT1), and the SESAM (mounted on a 3-axis stage Newport M-461-XYZ). The corresponding measured transfer functions are displayed in Fig. 4.5. They clearly show that the curved mirror and the SESAM are the most sensitive components to acoustic and/or mechanical noise. Whereas an adjustable mount is needed for the SESAM and cannot be removed (it must be able to adjust the three linear degrees of freedom), we tried to remove the linear translation stage initially used for the curved mirror and

4.2. Further investigation on f_{rep} noise

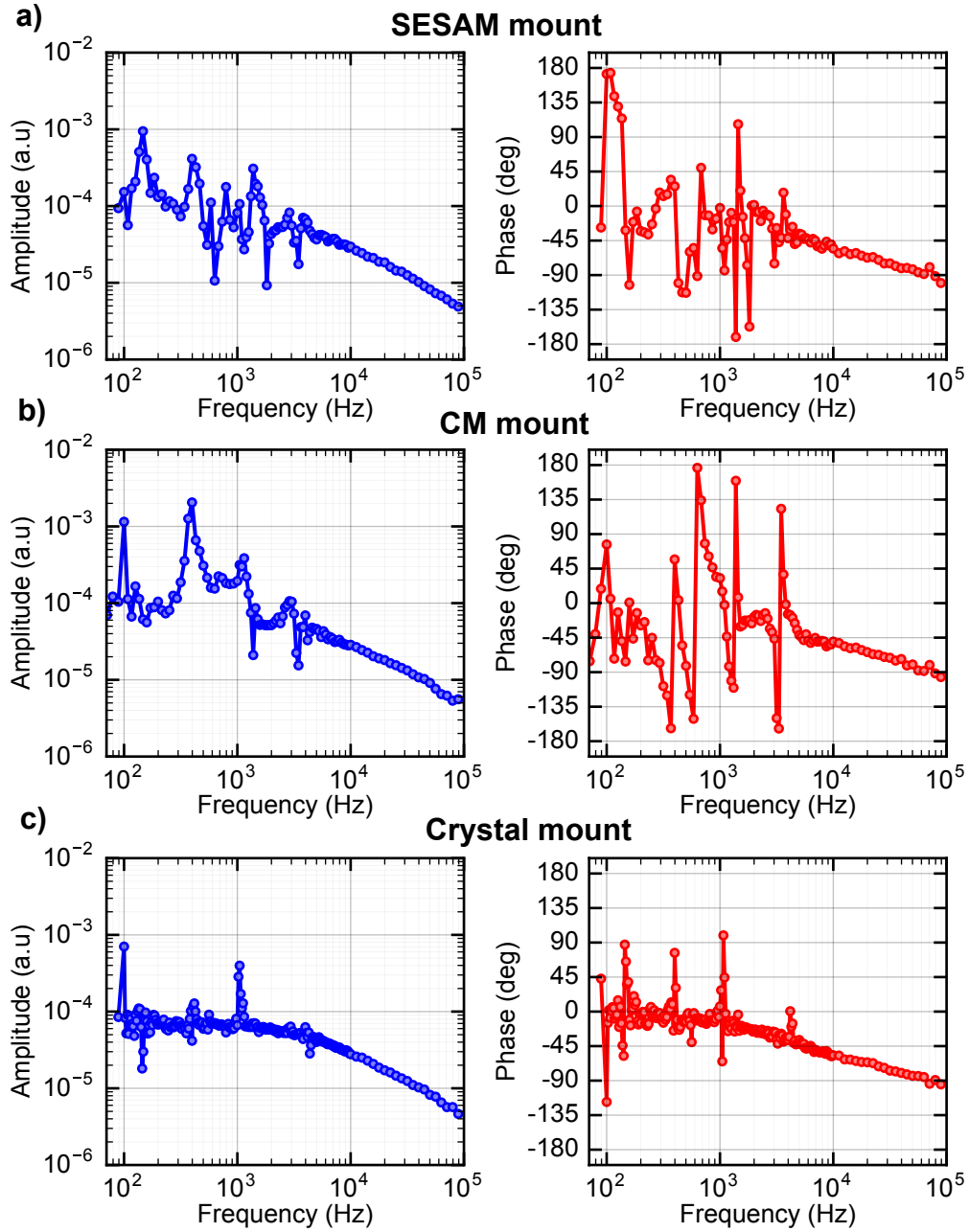


Figure 4.5: Amplitude (left) and phase (right) of the transfer functions of f_{rep} measured for an acoustic excitation applied to a) the SESAM mount, b) the curved mirror (CM) mount, and c) the crystal mount.

to replace it by a fixed mount. This resulted in a significant reduction of the frequency noise of f_{rep} in the frequency range of 400 Hz to 1 kHz (see Fig. 4.6). In addition, we also replaced the water cooling system of the gain crystal by Peltier cooling, which resulted in a clear reduction by a factor of 10 and 100 of the 1-kHz and ~ 600 -Hz noise peaks, respectively. This seems to indicate that the circulating water induces vibrations to the 3-axis stage of the crystal mount and excites some mechanical resonances at these frequencies, which is also visible on the transfer functions of f_{rep} when the acoustic perturbation was applied to the crystal mount [see Fig. 4.5(c)].

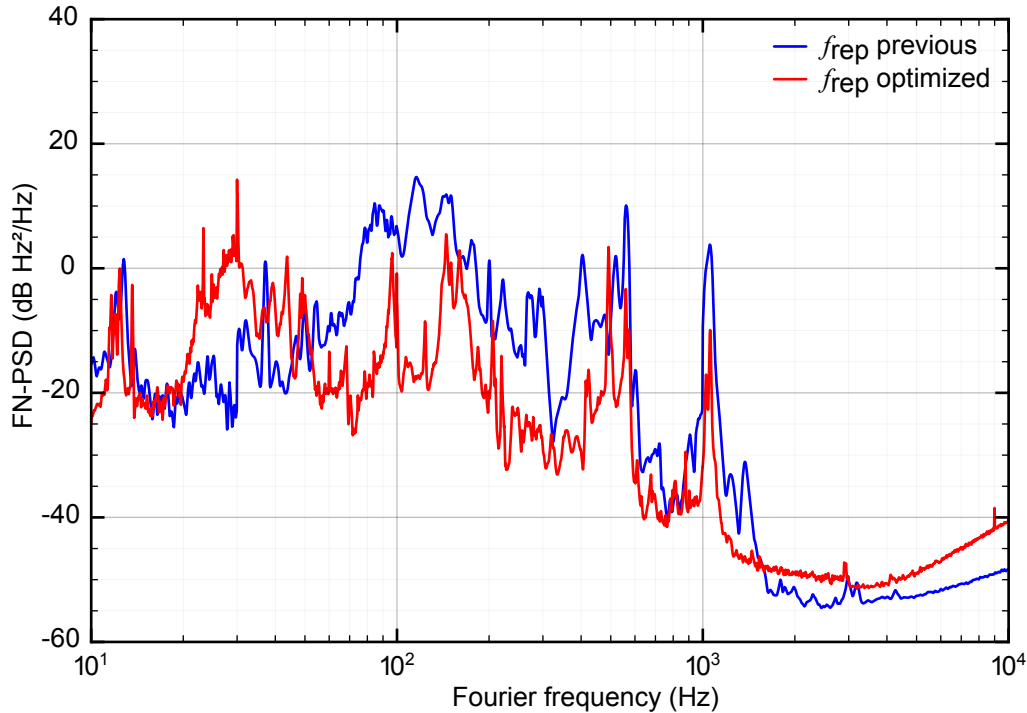


Figure 4.6: Frequency noise power spectral density of the repetition rate of the Yb:CALGO laser. Blue: previous result corresponding to the situation presented in Section 3.5.1; red: improved configuration with the translation stage of the curved mirror removed and the water cooling of the crystal replaced by Peltier cooling.

4.3 Comb stabilization to an optical reference

As the SC spectrum generated from the GHz laser used for CEO detection did not have any optical component at 1.56 μm (see Fig. 3.6), we used another special highly nonlinear PCF to generate light at 1.56 μm (NKT Photonics, model NL-PM-750), and heterodyned that light with the ultra-stable CW laser at the same wavelength. This PCF has a core diameter of 1.8 μm and has two zero dispersion wavelengths (ZDW) at 670 nm and 1260 nm, making the supercontinuum broadening even more efficient. One of the laser outputs was sent through a half-wave plate for polarization adjustment and a free-space optical isolator before being launched into the PCF (see Fig. 4.7). With $\sim 70\%$ coupling efficiency, a power of ~ 595 mW was coupled into the PCF, allowing us to achieve a supercontinuum spectrum spreading from ~ 400 nm (assessed from the observed blue light at the fiber end) to ~ 1600 nm. The SC was bandpass filtered at 1.56 μm , and combined with the CW laser on a photodiode (see Fig. 4.7). The beat note between the CW laser and an optical comb line at 1.56 μm was detected at ~ 300 MHz with an SNR of ~ 40 dB (at 100-kHz RBW). As the repetition rate was relatively noisy, it was not possible to directly stabilize the beat note since it was moving in a span of ~ 20 MHz. Therefore, we first frequency divided the beat note by a factor 15 using a frequency prescaler (RF Bay FPS-15-8). Then the phase fluctuations of this signal were compared to a reference synthesizer in a digital phase detector (DXD200 from Menlo Systems). The error signal was sent to a PID controller, and feedback signal was applied to the PZT in the laser cavity (see Fig. 4.7). The other output of the modelocked laser was used to generate the CEO as previously described in Section 3.3. The CEO frequency was self-referenced via feedback to the pump diode current (same scheme as in Subsection 3.4.2).

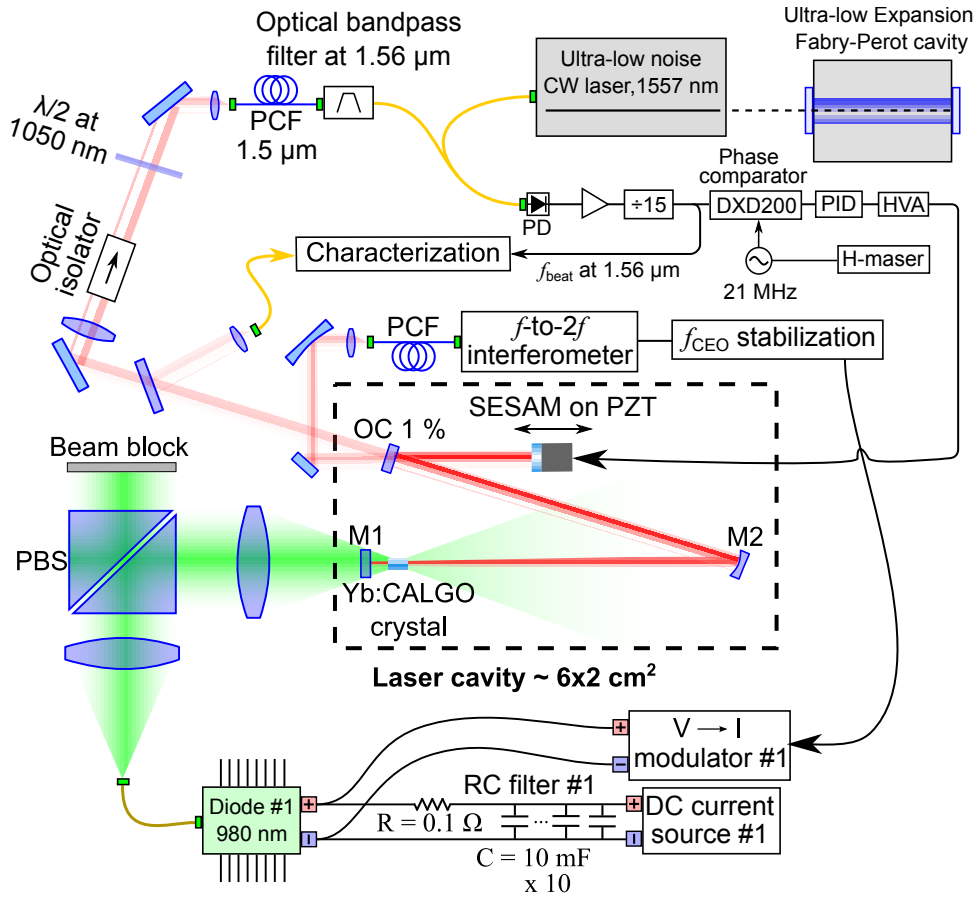


Figure 4.7: Schematic of the experimental setup for optical line stabilization of the GHz comb to an ultra-stable laser at $1.56\ \mu\text{m}$ stabilized to an ULE cavity. PCF: photonic-crystal fiber; PID: proportional-integral-derivative controller; DXD200: phase comparator; HVA: high-voltage amplifier. Yellow lines represent singlemode (SM) optical fibers, pink lines schematize free-space optical beams, blue lines are PCFs, and black lines are electrical connections.

The resulting noise of the stabilized comb line was measured in-loop (from the beat signal with the ultra-stable laser) and is shown in Fig. 4.8. For comparison, the frequency noise of the optical line is also displayed when f_{rep}

4.3. Comb stabilization to an optical reference

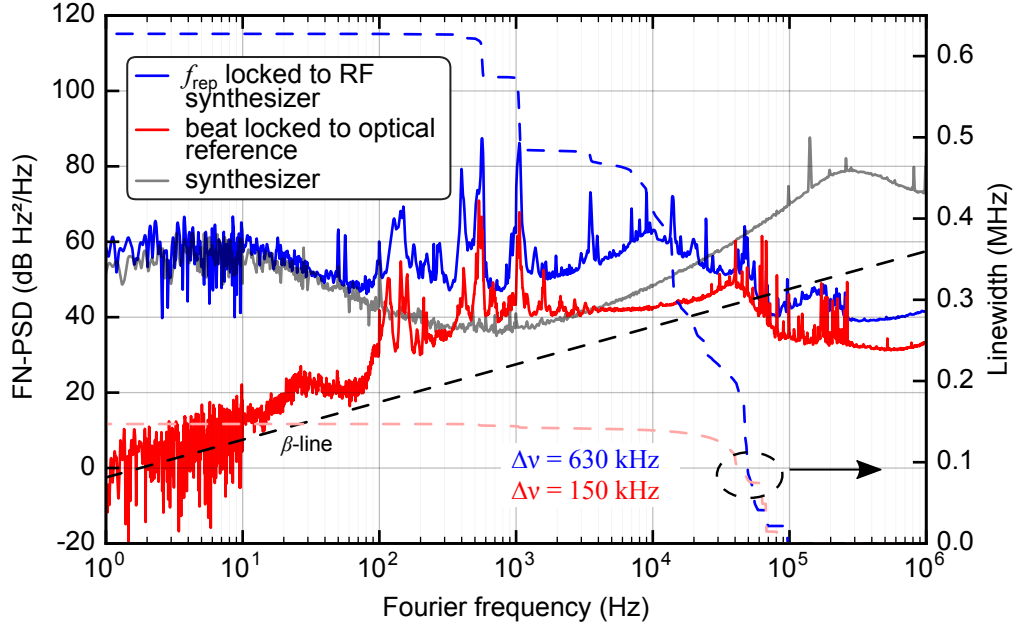


Figure 4.8: Frequency noise power spectral density of an optical line of the comb at 1.56 μm when stabilized to an RF reference as in Chapter 3 (blue), and to the optical reference (red). For the stabilization to the RF synthesizer, the noise was measured for an optical line at 1030 nm as described in Section 3.5.4 and was scaled to 1.56 μm . The noise of the reference synthesizer is also displayed (grey). The estimated linewidth of the frequency comb line is displayed on the right vertical axis.

was stabilized to the RF synthesizer. The stabilization to the optical reference overcomes the low-frequency noise limitation of the synthesizer and results in an improvement by more than four orders of magnitude of the FN-PSD at 10 Hz. The estimated linewidth of the comb line is reduced by more than factor of 4 reaching ~ 150 kHz at 1-s integration time.

In order to quantify the effect of the optical lock onto the frequency noise of f_{rep} , a cross-correlation method has been used. Measuring the phase or frequency noise of a signal requires comparing it in a phase detector to a

reference signal at the same frequency. The noise of the reference signal must be lower than the one of the signal under test in order to be able to observe this latter. All noise characterizations of our comb have been performed using the Rohde-Schwarz FSWP26 phase noise analyzer. This instrument incorporates a relatively good (low-noise) synthesizer as a reference. However, the 1-GHz repetition rate of the Yb:CALGO comb optically-locked to the ultra-stable laser has a lower phase noise than the internal reference oscillator of the phase noise analyzer, meaning that a standard phase noise measurement would be limited at the level of this oscillator. In order to measure phase noise levels lower than the available reference oscillators, a cross-correlation method can be used [98]. In the cross-correlation method the signal under test is splitted into two parts that are separately compared to two independent reference oscillators. In this case, the noise contributions from the two channels (oscillators, mixers, amplifiers) are assumed to be uncorrelated and the only noise common to the two signals originates from the signal under test. By processing the cross-spectrum between the two signals and averaging it, all the uncorrelated noise components average down leaving only the correlated noise, i.e., the noise of the signal under the test. Hence, the noise of this signal can be measured even if it is lower than the two used reference oscillators. As the noise floor of the measurement is reduced with the square root of the numbers of correlations, averaging longer leads to a lower noise floor. The only disadvantage of the method is that the cross-correlation significantly increases the measuring time.

The noise of the repetition rate stabilized to the ultra-stable laser and measured by cross-correlation using the Rohde-Schwarz FSWP26 phase noise analyzer is shown in Fig. 4.9. The previous spectrum obtained for stabilization to an RF synthesizer is also shown for comparison. One clearly observes a reduction of the noise in the low frequency range with the optical lock, resulting in an improvement by a factor of ~ 11 of the integrated timing jitter of the pulses, which reaches ~ 50 fs [1 Hz - 1 MHz]. The noise level observed in the range of

4.4. Conclusion

1 to ~ 100 Hz corresponds to the noise floor of the analyzer, which depends on the number of cross-correlations. One complete measurement shown here took ~ 20 minutes.

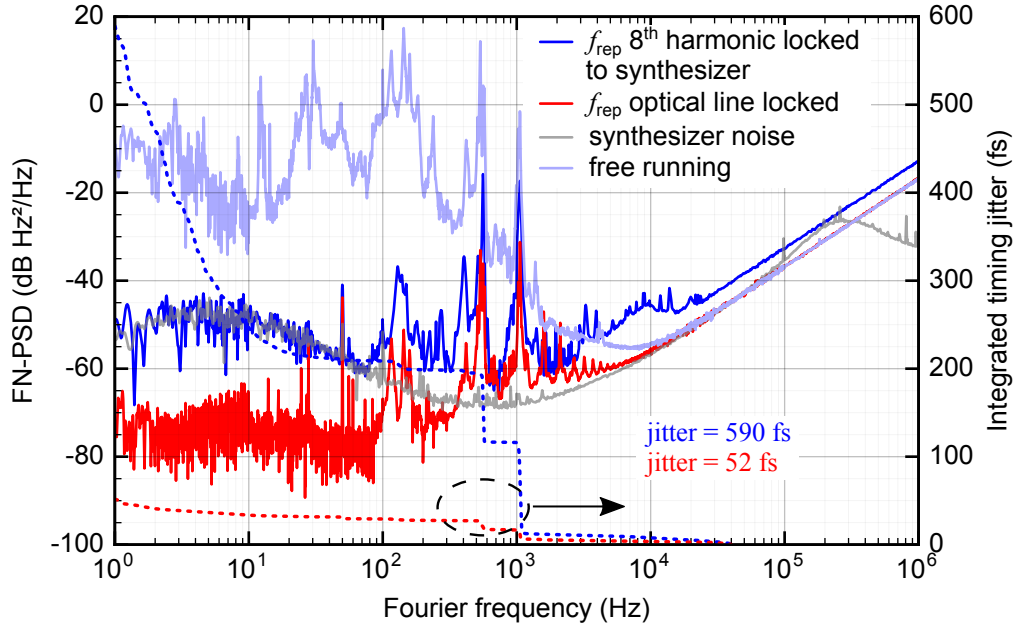


Figure 4.9: Frequency noise power spectral density of the fundamental repetition rate f_{rep} of the laser when free-running (light blue), previously stabilized to a microwave signal generator (same as in Fig. 3.14, dark blue), with the noise floor of the synthesizer also plotted (grey), and when stabilized to an ultra-stable laser at $1.56 \mu\text{m}$ (red). The second vertical axis shows the integrated timing jitter of the repetition rate signal.

4.4 Conclusion

A detailed investigation of the origin of the frequency noise of the repetition rate has been performed, showing the different contributions of various cavity

components. In particular, this analysis showed that the 3-axis stages holding the cavity components such as the curved mirror and the SESAM are crucial noise contributors, and the most sensitive in a wide frequency range. The 3-axis stage of the crystal mount, however, has a lower noise contribution, but it has a spurious resonance peak at ~ 1 kHz resulting in a high contribution to the f_{rep} noise when triggered by mechanical vibrations (partially from the water cooling tubes of the gain crystal) and acoustic noise. By exchanging the water-cooling system of the pump diode by Peltier cooling, and by replacing the linear stage of the curved mirror mount by a fixed mount, a significant reduction of the frequency noise of the free-running repetition rate has been achieved.

The stabilization of an optical line of the GHz frequency comb to an ultralow-noise CW laser has been demonstrated. This allowed overcoming the low-frequency noise floor limitation of the RF synthesizer used when directly locking f_{rep} and led to an improvement by a factor of $\sim 10^6$ of the FN-PSD of the optical comb line at a Fourier frequency of 1 Hz (Fig. 4.8).

These preliminary results show the attractiveness of this approach to achieve high repetition rate frequency comb with sub-kHz linewidth, as well as for the future generation of ultralow-noise microwave signals using a GHz frequency comb as an optical-to-microwave frequency divider. However, this would first require to improve the noise performance of the free-running repetition rate by designing a mechanically-stable cavity with optimized mechanical isolation.

Chapter 5

Opto-optical stabilization of f_{CEO}

5.1 Introduction

Most frequency comb applications require full comb stabilization, meaning that the two degrees of freedom, the repetition rate f_{rep} , and the CEO frequency f_{CEO} , need to be phase-coherently stabilized as demonstrated in Chapter 3. The phase-stabilization of the CEO beat is usually the most challenging part. Since the CEO noise intrinsically scales with the repetition rate [99], the challenge is particularly pronounced for GHz repetition rate lasers. This is illustrated in Fig. 5.1, which shows the CEO frequency noise of the Yb:CALGO laser with a repetition rate of 1 GHz, and for a similar laser with a much lower repetition rate of 100 MHz. The low frequency part of the noise spectra is very similar for the two lasers, as it arises from the transfer of the pump RIN, and the two lasers are pumped with the same diode. However, the noise at higher Fourier frequencies (>2 kHz) is significantly different and it extends to a broader range in the GHz laser. A good approximation of the necessary feedback bandwidth required to

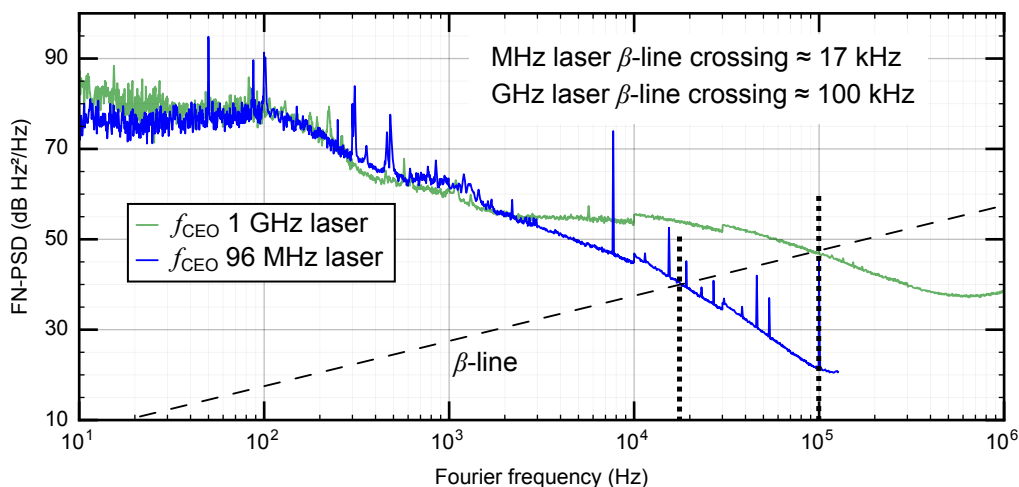


Figure 5.1: FN-PSD of the f_{CEO} for 1-GHz Yb:CALGO laser (green) and for a similar laser with 96-MHz repetition rate (blue), showing a very different requirement on the stabilization bandwidth needed to achieve a tight CEO.

achieve a tight CEO lock in a stabilization loop is given by the crossing point of the free-running FN-PSD of f_{CEO} with the β -separation line [91]. According to Fig. 5.1, this crossing point is ~ 100 kHz for the GHz laser while it is an order of magnitude smaller (~ 17 kHz) for 100-MHz laser.

Traditionally, CEO stabilization is achieved using a phase-locked loop with feedback applied to the pump power of the femtosecond laser, after detection of the CEO beat using non-linear f -to- $2f$ interferometry as described in Section 3.3. This method is particularly suitable for diode-pumped femtosecond lasers, such as fiber lasers or DPSSLs, for which the injection current of the pump diode can be directly modulated. This is the method previously implemented in Chapter 3. However, the stabilization bandwidth is fairly limited by the cavity dynamics. The latter is partially determined by the upper-state lifetime of the gain material, which is typically in the range of few μs to few

5.1. Introduction

ms for the most common crystals or glasses gain materials doped with erbium or ytterbium ions. Therefore, alternative stabilization methods have been proposed to overcome this limitation and enhance the stabilization bandwidth, thus improving the locking performance. Modulation of the stimulated emission in a co-doped Yb:Er:glass laser has been reported [100], where the gain material was additionally illuminated by modulated laser light at a wavelength within the gain bandwidth of the crystal, which enabled circumventing the low-pass filtering effect originating from the slow Yb³⁺ to Er³⁺ energy transfer mechanism. A different approach is based on the use of intra-cavity loss modulation, which was first demonstrated using a reflective graphene electro-optic modulator [27]. In 2013, the first CEO control by opto-optical modulation of a SESAM was demonstrated at the LTF. An Er:Yb:glass SESAM-modelocked DPSSL operating at a

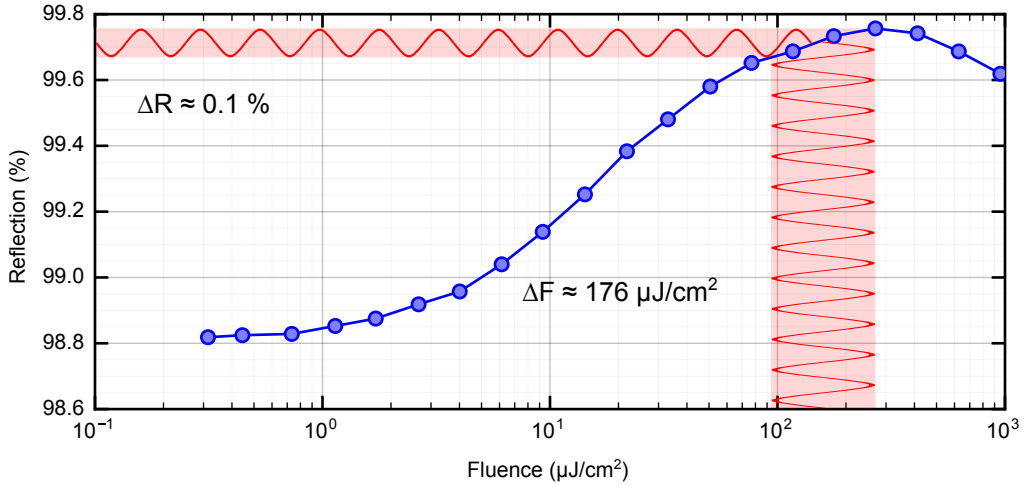


Figure 5.2: Nonlinear reflectivity of the SESAM used in the GHz laser vs laser fluence. Due to external pumping of the SESAM by an additional CW laser, the fluence can be changed resulting in slight reflectivity change. For our laser operation the maximum possible fluence change is $\Delta F \approx 176 \mu\text{J}/\text{cm}^2$, that would lead to a reflectivity change of $\Delta R \approx 0.1\%$.

wavelength of 1.5 μm with a repetition rate of 75 MHz was used in this first demonstration [101]. An additional continuous-wave beam from a diode laser was focused onto the SESAM, slightly changing its reflectivity as a function of the incident power, thus acting as a fast loss modulator for the intra-cavity pulses due to the short SESAM response time (see Fig. 5.2). In comparison to the traditional gain modulation, the OOM showed strong improvements in terms of CEO modulation bandwidth and residual integrated phase noise achieved for the locked CEO beat (65 mrad vs 720 mrad).

5.2 OOM-SESAM stabilization of f_{CEO} in the 1-GHz Yb:CALGO laser

Here the first CEO stabilization of a DPSSL with a GHz repetition rate is presented via OOM of a SESAM. In the previous OOM demonstration realized with a low repetition rate laser, the bandwidth necessary for a tight CEO lock amounted to a few kHz only. For the CEO-stabilization of the present GHz oscillator, the bandwidth requirement is more than an order of magnitude larger and thus represents a key test for the viability of the OOM method. A record high stabilization bandwidth of 500 kHz for a 1- μm Yb-based DPSSL is demonstrated. A tight locking of the CEO beat was achieved both for gain modulation and OOM, but more than 30% reduction of the residual integrated phase noise of the locked CEO beat was achieved with the OOM.

5.2.1 Experimental setup

The overall experimental setup shown in Fig. 5.3 makes use of the same laser as described in Chapter 3 and the CEO beat was also detected as previously explained. The error signal was sent to the same PID servo-controller as previ-

ously used (Vescent D2-125) and feedback was applied either to the laser pump diode (gain modulation, Diode #1 and channel #1 in Fig. 5.3) or to the SESAM pump power (SESAM-OOM, Diode #2 and channel #2 in Fig. 5.3).

The OOM was implemented by pumping the SESAM with an s-polarized 980.9-nm laser beam (Diode #2 in Fig. 5.3) focused onto the SESAM at an incidence angle of $\sim 45^\circ$. Here the same type of pump diode as for the laser crystal was used for convenience, but a standard low-cost low-power laser diode could be used as well (CEO stabilization is achieved for less than 200 mW output power). The present pump diode has a spectral width of ~ 0.2 nm. The OOM pump beam was aligned to overlap with the intra-cavity laser pulses onto the SESAM with a spot diameter of ~ 300 μm . From simulations of the electrical field propagation of the OOM pump light inside the SESAM structure, an absorption of only 1.3% was calculated in the InGaAs quantum well absorber. Another 1.3% is transmitted through the entire structure and eventually gets scattered at the unpolished back surface of the GaAs substrate. Finally, the remaining 97.4% is simply reflected on the Bragg mirror and does not play any role for the OOM (see Fig. 5.4). It is important to note that no material other than the quantum well notably absorbs the OOM pump laser light since the GaAs SESAM material is transparent at the 980-nm pump wavelength, which minimizes undesired temperature-induced effects. The SESAM has a saturation fluence of 10.69 $\mu\text{J}/\text{cm}^2$ and is operated at an intra-cavity laser fluence of 93.6 $\mu\text{J}/\text{cm}^2$ close to the maximum of its nonlinear reflectivity curve (Fig. 5.2). Hence, the maximum reflectivity change produced by the pump light can be at most 0.1% (Fig. 5.2). From the induced frequency change of f_{CEO} , the reflectivity change produced by the pump light is estimated to be much smaller, two orders of magnitude lower than the 1.15% SESAM modulation depth.

To enable fast modulation of the pump diodes (for gain or SESAM pumping, respectively), we used the same high-bandwidth voltage-to-current

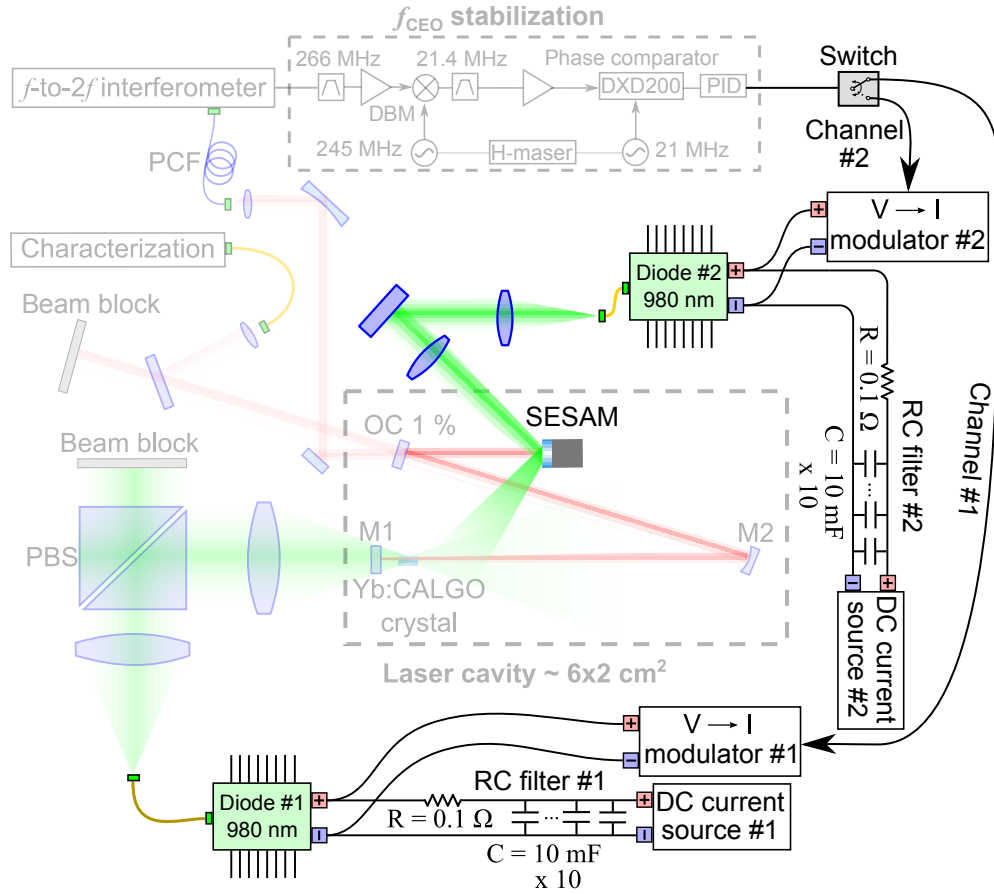


Figure 5.3: Experimental setup for CEO stabilization by SESAM OOM. The laser configuration and CEO beat detection are identical to the case presented in Chapter 3 (see Fig. 3.5). A pair of DC current sources, 980-nm pump diodes, RC filters and V-I modulators are used to pump the GHz laser crystal and SESAM, respectively, and to stabilize f_{CEO} via gain modulation (channel #1) or SESAM-OOM (channel #2). These elements are highlighted in the figure, whereas the other elements previously described in Chapter 3 are displayed in attenuated colors. DBM: double-balanced mixer; PCF: photonic crystal fiber; PID: proportional-integral-derivative servo-controller; green/red/light-red lines: free-space optical beams (pump/intra-cavity/outputs); yellow/blue lines: optical fibers (single-mode/PCF); black lines: electrical connections.

5.2. OOM-SESAM stabilization of f_{CEO} in the 1-GHz Yb:CALGO laser

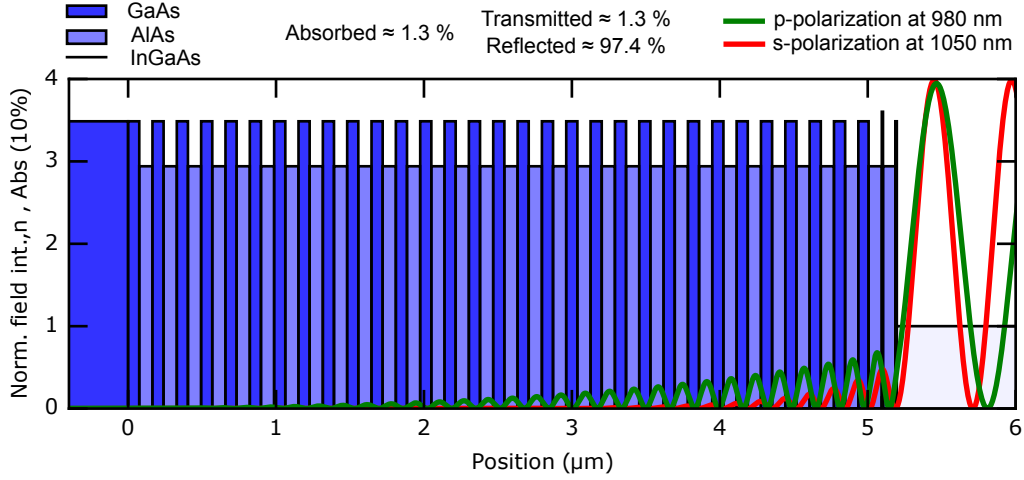


Figure 5.4: SESAM structure along with the propagation of 980-nm electrical field at 45° incidence angle.

(V-I) converters as previously described in Sections 3.1 and 3.4.2 (V-I modulator #1 and #2 in Fig. 5.3), with the same RC filter.

To characterize the OOM operation, the transfer function of f_{CEO} was first measured for a sine modulation with a peak-to-peak amplitude of 190 mW of the OOM pump power using a frequency discriminator (Miteq FMDM 21.4/4-2) [88] and a lock-in amplifier. This measurement was performed at two different OOM average pump power levels of 212 mW and 763 mW (dark and light red curves, respectively, in Fig. 5.5). For comparison, the figure also displays the measured transfer function of the pump power (black curve in Fig. 5.5) and of f_{CEO} for a modulation of the Yb:CALGO laser pump power (blue curves in Fig. 5.5). The OOM pump laser diode has a modulation bandwidth of ~ 800 kHz (defined by the 90° phase shift in the transfer function of the diode output power). The CEO bandwidth for gain modulation is limited to ~ 280 kHz by the dynamics of the modelocked laser cavity as previously described in Section 3.4. The OOM overcomes this limitation and achieves a CEO modulation bandwidth more than two times larger, with a 90° phase shift reached at ~ 630 kHz. At

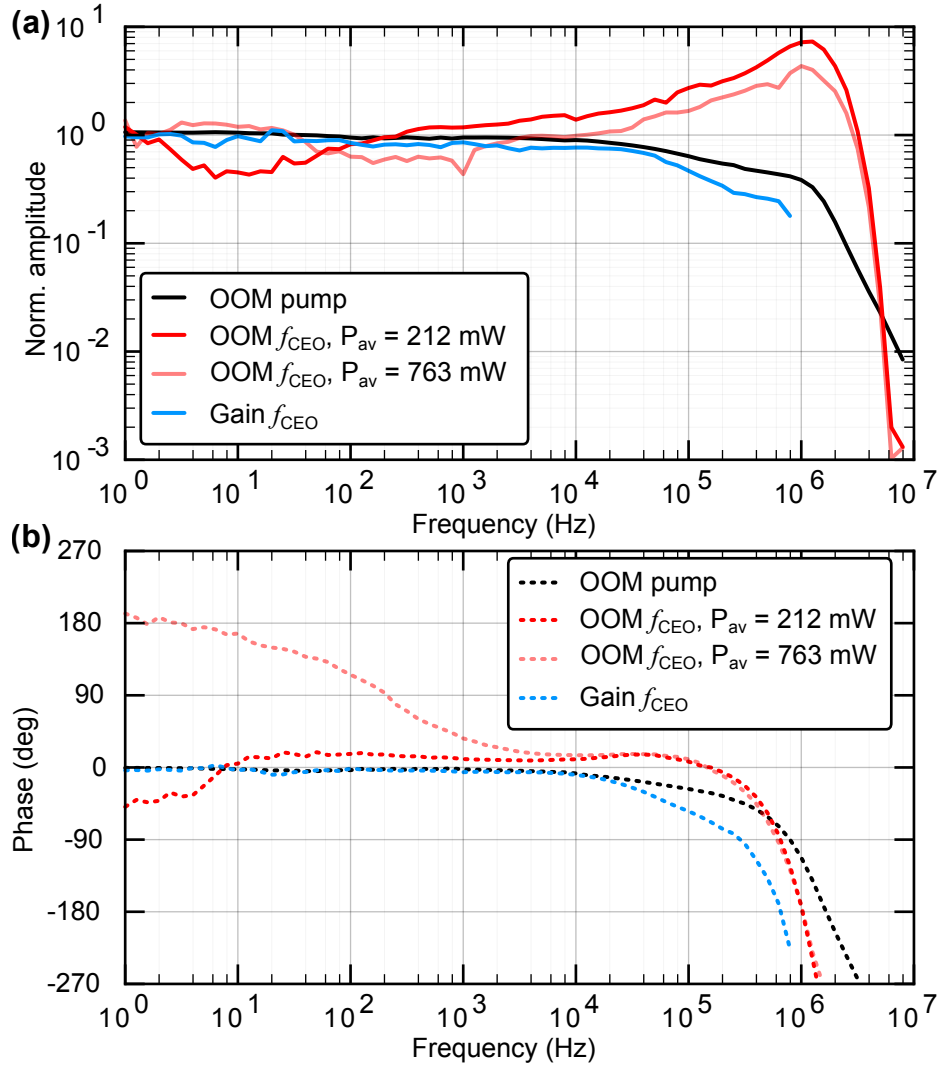


Figure 5.5: Relative amplitude (a) and phase (b) of the transfer function (TF) of f_{CEO} for a modulation of the OOM pump at two different average powers P_{av} incident onto the SESAM: 212 mW (red) and 763 mW (light red). The TFs of f_{CEO} for gain modulation (blue) and of the OOM pump laser power (black) are also shown for comparison.

high average pump power incident onto the SESAM, a phase reversal of 180° is observed at low frequency in the transfer function of f_{CEO} in comparison to

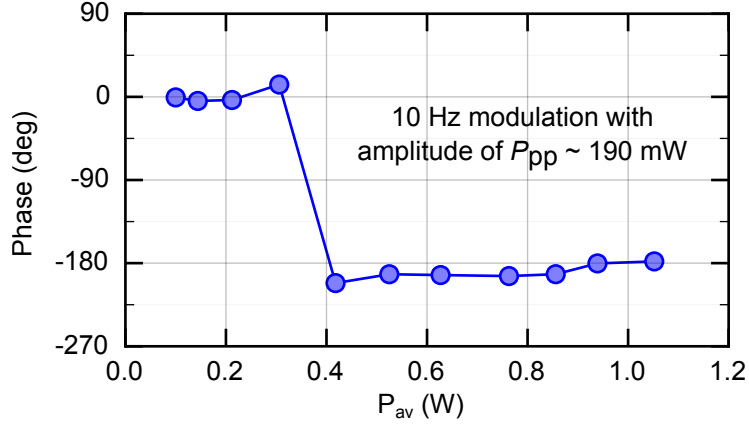


Figure 5.6: Phase of the response of f_{CEO} to a 10-Hz modulation of the SESAM-OOM pump power as a function of the average optical power P_{av} incident onto the SESAM, showing a phase reversal point at $P_{\text{av}} \approx 400$ mW. A constant modulation amplitude of 190 mW (peak-to-peak value) was used in all cases.

the low power case (compare the red and light red curves in Fig. 5.5(b) below 10 kHz), while above ~ 10 kHz the phase of the transfer function is equal in both cases. This behavior is believed to result from a dominant slow thermal effect resulting from spurious pump light absorption outside of the quantum well occurring at high average OOM pump power. In contrast, the desired optically-induced change in the SESAM reflectivity prevails at lower average power. The SESAM was neither cooled nor actively temperature-stabilized. To further investigate this phase reversal, we measured the phase of the change in f_{CEO} induced by a slow SESAM pump modulation of 10 Hz with a constant peak-to-peak amplitude of 190 mW at different average pump power levels ranging from ~ 0.1 W to 1.2 W. In Fig. 5.6, a clear phase reversal is observed at an average power of ~ 400 mW incident onto the SESAM.

The response of f_{CEO} with respect to the OOM pump power is in the range of 1 kHz/mW. This value is 200 times lower compared to the typical

tuning coefficient of f_{CEO} with the laser pump power (gain modulation) reported in Section 3.4.2. Nevertheless, the achievable CEO tuning was sufficient for f_{CEO} locking by means of the OOM only. It is important to remind that only 1.3 % of the incident pump power is absorbed in the quantum well, that leads to a relatively low response of the CEO frequency. The stabilization was successful for low average power incident onto the SESAM (typ. 210 mW). However, CEO stabilization was not possible at high average pump power incident onto the SESAM as a result of the inadequate CEO transfer function resulting from the low-frequency phase reversal, as previously observed in a 1.5- μm DPSSL affected by a similar CEO dynamics [102].

5.2.2 Stabilization results

The FN-PSD measured for the free-running (light green), gain-stabilized (blue), and OOM-stabilized (red) CEO beat is shown in Fig. 5.7. While the free-running CEO beat has a FWHM of ~ 500 kHz, the OOM stabilization leads to a tight lock characterized by a coherent peak with an SNR of ~ 60 dB at 1-Hz resolution bandwidth in the CEO beat measured in-loop [see Fig. 5.8(b)]. The residual integrated phase noise amounts to 430 mrad [10 Hz - 1 MHz] (Fig. 5.7, right axis), which is an improvement by more than 30% compared to stabilizing the CEO of this laser via gain modulation as reported in Chapter 3. A stabilization bandwidth of 500 kHz was obtained with the OOM, assessed from the servo bump in the CEO FN-PSD. This is two times higher than the ~ 250 kHz bandwidth of the gain-modulation stabilization. Higher stabilization bandwidths were even possible with the OOM, typically up to ~ 580 kHz, however the best noise properties were obtained with the 500-kHz stabilization bandwidth shown in Fig. 5.7. The RF spectra of the free-running and stabilized CEO beats are shown in Fig. 5.8. The side peaks present in the spectrum at around ± 310 kHz and ± 620 kHz are believed to be of electrical origin (they are also present in the CEO spectrum ob-

5.2. OOM-SESAM stabilization of f_{CEO} in the 1-GHz Yb:CALGO laser

tained by gain modulation) and have a negligible contribution to the integrated phase noise of the stabilized CEO beat.

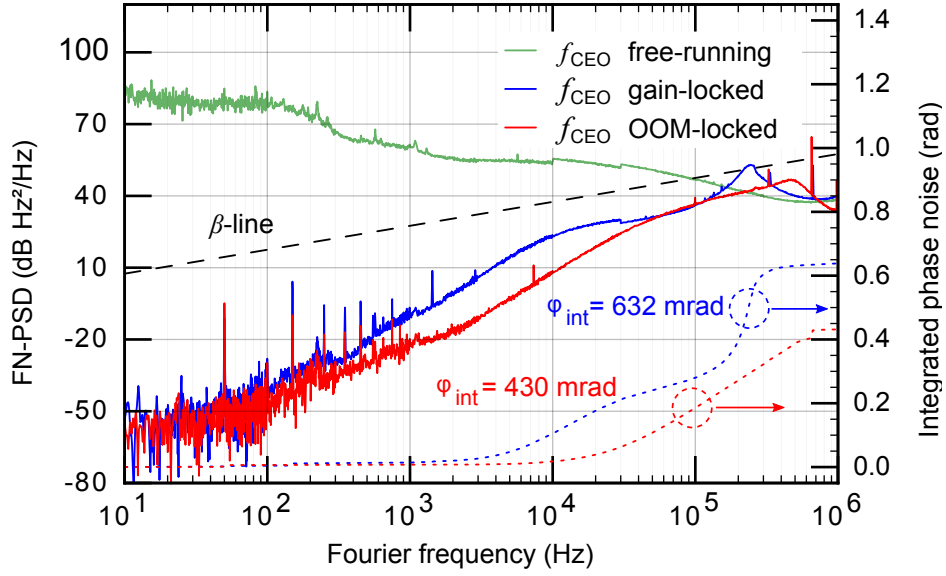


Figure 5.7: Frequency noise power spectral density (FN-PSD) of the CEO beat obtained in free-running conditions (green), and for the CEO beat stabilized by gain modulation (blue) and by SESAM-OOM (red). The corresponding integrated phase noise is shown as a function of the upper cut-off frequency (right vertical axis).

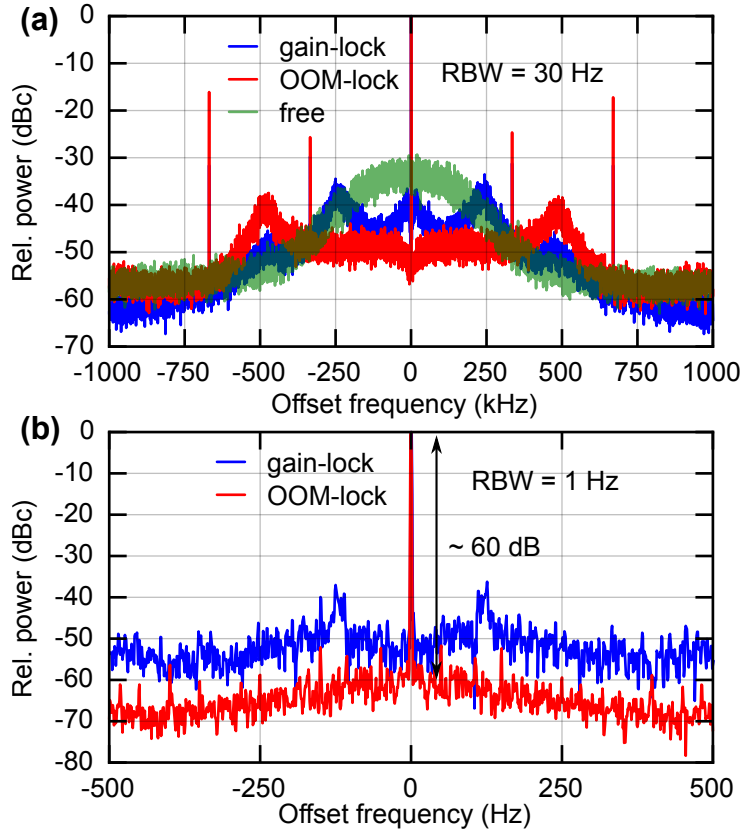


Figure 5.8: a) RF spectrum of the CEO beat in free-running mode (green), stabilized with gain modulation (blue) and with SESAM-OOM (red), showing a 2-fold enhancement of the stabilization bandwidth. b) Zoom on the coherent peak over a total span of 1 kHz showing an SNR of 60 dB (1-Hz resolution bandwidth) for OOM stabilization.

5.2.3 Conclusion

The first SESAM-OOM self-referenced stabilization of a GHz DPSSL has been demonstrated, overcoming the cavity dynamics limitation and extending the stabilization bandwidth by a factor of more than two compared to standard gain modulation. As a result, the CEO residual integrated phase noise was reduced by more than 30%. These results demonstrate that SESAMs are reliable components not only for modelocking, but can also serve as fast loss modulators for frequency comb stabilization which can overcome limitations of the standard gain modulation.

Chapter 6

Conclusion and outcomes

In this thesis, two main research areas have been addressed: (i) the demonstration of highly efficient channel waveguide lasers in CW and Q-switched operations and (ii) the development, phase-stabilization and characterization of a high repetition rate frequency combs from a DPSSL.

Channel waveguide lasers provide cost effective solutions with a compact and robust design allowing for stable systems in a simple arrangement. Previously, pulsed channel waveguide lasers were strongly limited in output power, which prevented their practical use in real world applications. The recent simultaneous progress in SESAMs and waveguides fabrication has opened up a large potential for novel solutions. In this thesis, we have shown that combining the advantages of SESAMs with compact and efficient waveguides allowed for μJ -level pulse energies and multi-watt power level operation of an Yb:YAG Q-switched channel waveguide laser. We have also presented CW operation of the same waveguide laser with record-high 5.7 W of average output power. These results clearly demonstrate that pulsed fs-laser-written channel waveguide modelocked lasers based on SESAMs have a great potential for the generation of pulses at high repetition rates and average output powers. This work paves

the way towards a new class of integrated waveguide lasers, which combine compactness, reliability and cost-efficiency. Moreover, it also opens the door towards future applications such as integrated lab-on-the-chip systems based on pulsed waveguide lasers. It is important to mention that further power scaling of the laser systems reported here was only limited by the available pump laser power. Recently, modelocking of such waveguide lasers was reported [60], opening a new potential towards chip-integrated high-power ultrashort pulse sources. This is a first step towards a possible future development of fully-integrated chip-based optical frequency combs.

The main part of this thesis was dedicated to the development of a high-power optical frequency comb with a high repetition rate in the GHz range generated from a modelocked DPSSL. The implementation and detailed study of various schemes for the phase-stabilization of the two comb parameters (f_{rep} and f_{CEO}) were also investigated, leading to the full stabilization of the frequency comb spectrum. Femtosecond DPSSLs are excellent laser sources for low-noise high repetition rate frequency combs with a high output power. However, DPSSL-based combs were limited in average output power so far, due to the lack of high-power single-mode pump laser diodes. We show that fully stabilized GHz combs are also achievable with a highly transverse multimode pumping scheme, which enables modelocked operation with a maximum average output power of up to 2.1 W, an efficiency of 33.5 %, and sub-100 fs pulse duration at GHz repetition rate.

The first full phase stabilization of a GHz frequency comb from a bulk laser was achieved using a SESAM mounted onto a PZT for repetition rate stabilization, and by self-referenced CEO stabilization with feedback to the current of the pump diode. A detailed noise analysis of the frequency comb has been performed, showing a linewidth of an optical mode below 800 kHz. The noise of the repetition rate was identified as the main contribution to the

frequency noise of the optical comb line. It originated both from the influence of environmental mechanical vibrations and from the low-frequency noise floor of the reference RF signal used for the stabilization of f_{rep} . The mechanical noise of the laser cavity was then partially damped by removing unnecessary translation stages in the laser resonator, and by an improved acoustic isolation of the laser cavity. The low-frequency limit imposed by the reference RF signal was strongly reduced by replacing the RF lock of the repetition rate by a stabilization of a comb line to an ultra-stable CW laser with an ultra-narrow linewidth at the Hz-level. In this way, the linewidth of the comb line was reduced to 150 kHz in a preliminary experiment.

A further improvement of the noise properties of the developed laser would first require reducing the impact of environmental acoustic and mechanical noise onto the laser resonator. This would require a redesign of the laser cavity which can be achieved by using more stable opto-mechanical components and/or a monolithic cavity design. A careful design of the cavity may also enable repetition rate scaling of the GHz comb as already reported in free-running unstabilized operation [103,104], which would be attractive for applications like ultra-low noise microwave signal generation. We did not observe severe thermal effects in the gain medium or damage of the intra-cavity components, moreover we only applied 25% of the available power of our pump diode. Therefore, we expect that higher output powers can be achieved in the future.

In the final part of this thesis, SESAM-OOM has been applied for the first time in a high repetition rate comb for the stabilization of the CEO frequency. A record-high modulation bandwidth of more than 600 kHz for the CEO frequency in a DPSSL has been demonstrated, twice higher than with traditional gain modulation. The modulation bandwidth of f_{CEO} is a very important parameter to achieve a tight CEO lock. This is particularly important for multi-GHz lasers, since the CEO frequency noise typically scales with the

repetition rate. The traditional gain modulation stabilization is limited by the cavity dynamics and the SESAM-OOM is an excellent solution to overcome this limitation, since the stabilization bandwidth is not limited by the SESAM and it does not require any additional intra-cavity component. The SESAM used in our experiments was not specifically designed for OOM operation, but it could be successfully used in this proof-of-principle demonstration. Next steps for this technology would consist in making a special design of the semiconductor structure in order to improve the current performance of the OOM and reduce unwanted effects (e.g., thermal effects). In the future, this method is also planned to be used in high-power thin-disk lasers where the cavity dynamics limits the stabilization bandwidth to a range of $\sim 10\text{-}20$ kHz resulting from their lower repetition rate. Therefore the use of a SESAM-OOM could dramatically improve the stabilization performance.

Bibliography

- [1] T. P. Heavner, E. A. Donley, F. Levi, G. Costanzo, T. E. Parker, J. H. Shirley, N. Ashby, S. Barlow, and S. R. Jefferts, “First accuracy evaluation of NIST-F2,” *Metrologia*, vol. 51, pp. 174–182, 2014.
- [2] N. Hinkley, J. A. Sherman, N. B. Phillips, M. Schioppo, N. D. Lemke, K. Beloy, M. Pizzocaro, C. W. Oates, and A. D. Ludlow, “An Atomic Clock with 10^{-18} Instability,” *Science Express*, p. 1240420, 2013.
- [3] H. Schnatz, B. Lipphardt, J. Helmcke, F. Riehle, and G. Zinner, “First Phase-Coherent Frequency Measurement of Visible Radiation,” *Phys. Rev. Lett.*, vol. 76, no. 1, pp. 18–21, 1996.
- [4] J. Reichert, R. Holzwarth, T. Udem, and T. Hänsch, “Measuring the frequency of light with mode-locked lasers,” *Optics Communications*, vol. 172, pp. 59–68, 1999.
- [5] D. J. Jones, S. A. Diddams, J. K. Ranka, A. Stentz, R. S. Windeler, J. L. Hall, and S. T. Cundiff, “Carrier-Envelope Phase Control of Femtosecond Mode-Locked Lasers and Direct Optical Frequency Synthesis,” *Science*, vol. 288, no. 5466, pp. 635–640, 2000.
- [6] A. Apolonski, A. Poppe, G. Tempea, C. Spielmann, T. Udem, R. Holzwarth, T. W. Hänsch, and F. Krausz, “Controlling the Phase

- Evolution of Few-Cycle Light Pulses,” *Phys. Rev. Lett.*, vol. 85, no. 4, pp. 740–743, 2000.
- [7] H. R. Telle, G. Steinmeyer, A. E. Dunlop, J. Stenger, D. H. Sutter, and U. Keller, “Carrier-envelope offset phase control: A novel concept for absolute optical frequency measurement and ultrashort pulse generation,” *Appl. Phys. B*, vol. 69, no. 4, pp. 327–332, 1999.
- [8] T. W. Hänsch, “Nobel Lecture: Passion for precision,” *Reviews of Modern Physics*, vol. 78, no. 4, pp. 1297–1309, 2006.
- [9] J. L. Hall, “Nobel Lecture: Defining and measuring optical frequencies,” *Reviews of Modern Physics*, vol. 78, no. 4, pp. 1279–1295, 2006.
- [10] T. J. Kippenberg, R. Holzwarth, and S. A. Diddams, “Microresonator-based optical frequency combs,” *Science*, vol. 332, no. 6029, pp. 555–559, 2011.
- [11] P. Del’Haye, A. Schliesser, O. Arcizet, T. Wilken, R. Holzwarth, and T. J. Kippenberg, “Optical frequency comb generation from a monolithic microresonator,” *Nature*, vol. 450, pp. 1214–1217, 2007.
- [12] M. Yu, Y. Okawachi, A. G. Griffith, M. Lipson, and A. L. Gaeta, “Mode-locked mid-infrared frequency combs in a silicon microresonator,” *Opt. Letters*, vol. 3, no. 8, pp. 854–860, 2016.
- [13] A. E. Siegman, “Lasers,” *University Science Books, Mill Valley, California*, 1986.
- [14] W. R. Bennett, “Background of an inversion: the first gas laser,” *IEEE J. Sel. Top. Quantum Electron.*, vol. 6, no. 6, pp. 869–875, 2000.
- [15] G. Huber, C. Kränkel, and K. Petermann, “Solid-state lasers: status and future [Invited],” *Opt. Soc. Am. B*, vol. 27, no. 11, pp. B93–B105, 2010.

- [16] H. M. Pask, R. J. Carman, D. C. Hanna, A. C. Tropper, C. J. Mackechnie, P. R. Barber, and J. M. Dawes, “Ytterbium-doped silica fiber lasers: versatile sources for the 1-1.2 μm region,” *IEEE J. Sel. Top. Quantum Electron.*, vol. 1, no. 1, pp. 2–13, 1995.
- [17] W. W. Chow and S. W. Koch, “Semiconductor-laser fundamentals,” *Springler, Berlin*, 1999.
- [18] A. Giesen, H. Hügel, A. Voss, K. Wittig, U. Brauch, and H. Opower, “Scalable concept for diode-pumped high power solid-state lasers,” *Appl. Phys. B*, vol. 58, pp. 365–372, 1994.
- [19] J. Limpert, N. Deguil-Robin, I. Manek-Hönninger, F. Salin, F. Röser, A. Liem, T. Schreiber, S. Nolte, H. Zellmer, A. Tünnermann, J. Broeng, A. Petersson, and C. Jakobsen, “High-power rod-type photonic crystal fiber laser,” *Opt. Express*, vol. 13, no. 4, pp. 1055–1058, 2005.
- [20] F. Röser, J. Rothhard, B. Ortac, A. Liem, O. Schmidt, T. Schreiber, J. Limpert, and A. Tünnermann, “131 W 220 fs fiber laser system,” *Opt. Letters*, vol. 30, no. 20, pp. 2754–2756, 2005.
- [21] O. G. Okhotnikov, “Semiconductor disk lasers: Physics and technology,” *John Wiley and Sons*, p. 330, Wiley-VCH, 2010.
- [22] D. E. Spence, P. N. Kean, and W. Sibbett, “60-fsec pulse generation from a self-mode-locked Ti:sapphire laser,” *Opt. Letters*, vol. 16, no. 1, pp. 42–44, 1991.
- [23] U. Keller, K. J. Weingarten, F. X. Kärtner, D. Kopf, B. Braun, I. D. Jung, R. Fluck, C. Hönninger, N. Matuschek, and J. A. der Au, “Semiconductor saturable absorber mirrors (SESAM’s) for femtosecond to nanosecond pulse generation in solid-state lasers,” *IEEE J. Sel. Top. Quantum Electron.*, vol. 2, no. 3, pp. 131–136, 1996.

- [24] J. K. Ranka, R. S. Windeler, and A. J. Stentz, “Visible continuum generation in airsilica microstructure optical fibers with anomalous dispersion at 800 nm,” *Opt. Letters*, vol. 25, no. 1, pp. 25–27, 2000.
- [25] K. Hitachi, A. Ishizawa, T. Nishikawa, M. Asobe, and T. Sogawa, “Carrier-envelope offset locking with a $2f$ -to- $3f$ self-referencing interferometer using a dual-pitch PPLN ridge waveguide,” *Opt. Express*, vol. 22, no. 2, pp. 1629–1635, 2014.
- [26] N. Torcheboeuf, G. Buchs, S. Kundermann, E. Portuondo-Campa, J. Bennis, and S. Lecomte, “Repetition rate stabilization of an optical frequency comb based on solid-state laser technology with an intra-cavity electro-optic modulator,” *Opt. Express*, vol. 25, no. 3, pp. 2215–2220, 2017.
- [27] C.-C. Lee, C. Mohr, J. Bethge, S. Suzuki, M. E. Fermann, I. Hartl, and T. R. Schibli, “Frequency comb stabilization with bandwidth beyond the limit of gain lifetime by an intracavity graphene electro-optic modulator,” *Opt. Letters*, vol. 37, no. 15, pp. 376–379, 2012.
- [28] W. Hänsel, M. Giunta, M. Lezius, M. Fischer, and R. Holzwarth, “Electro-optic modulator for rapid control of the carrier-envelope offset frequency,” *CLEO, San Jose, 2017*, p. SF1C.5, 2017.
- [29] S. Koke, C. Grebing, H. Frei, A. Anderson, A. Assion, and G. Steinmeyer, “Direct frequency comb synthesis with arbitrary offset and shot-noise-limited phase noise,” *Nature Photonics*, vol. 4, pp. 462–465, 2010.
- [30] M. Zimmermann, C. Gohle, R. Holzwarth, T. Udem, and T. W. Hänsch, “Optical clockwork with an offset-free difference-frequency comb: accuracy of sum- and difference-frequency generation,” *Opt. Letters*, vol. 29, no. 3, pp. 310–312, 2004.

- [31] C. Grivas, “Optically pumped planar waveguide lasers: Part ii: Gain media, laser systems, and applications,” *Prog. Quantum Electron.*, vol. 45, pp. 3–160, 2016.
- [32] J.-E. Broquin, “Glass integrated optics: state of the art and position toward other technologies,” *Proc. SPIE*, vol. 6475, p. 647507, 2007.
- [33] D. Geskus, S. Aravazhi, C. Grivas, K. Wörhoff, and M. Pollnau, “Microstructured $\text{KY}(\text{WO}_4)_2:\text{Gd}^{3+}$, Lu^{3+} , Yb^{3+} channel waveguide laser,” *Opt. Express*, vol. 18, no. 9, pp. 8853–8858, 2010.
- [34] F. Chen and J. R. V. de Aldana, “Optical waveguides in crystalline dielectric materials produced by femtosecond-laser micromachining,” *Laser Photon. Rev.*, vol. 8, no. 2, pp. 251–275, 2014.
- [35] T. Calmano and S. Müller, “Crystalline waveguide lasers in the visible and near-infrared spectral range,” *IEEE J. Sel. Top. Quantum Electron.*, vol. 21, no. 1, pp. 401–413, 2015.
- [36] K. Hasse, T. Calmano, B. Deppe, C. Liebald, and C. Kränkel, “Efficient $\text{Yb}^{3+}:\text{CaGdAlO}_4$ bulk and femtosecond-laser-written waveguide lasers,” *Opt. Lett.*, vol. 40, no. 15, pp. 3552–3555, 2015.
- [37] E. Ghibaudo, J.-E. Broquin, and K. Benech, “Integrated optic broadband duplexer made by ion exchange,” *Appl. Phys. Lett.*, vol. 82, no. 8, pp. 3552–3555, 2003.
- [38] J. M. P. Delavaux, S. Granlund, O. Mizuhara, L. Tzeng, D. Barbier, M. Rattay, F. S. Andre, and A. Kevorkian, “Integrated optics erbium-ytterbium amplifier system in 10 Gb/s fiber transmission experiment,” *IEEE Photonics Technology Letters*, vol. 9, no. 2, pp. 247–249, 1997.
- [39] A. Choudhary, A. A. Lagatsky, P. Kannan, W. Sibbett, C. T. A. Brown, and D. P. Shepherd, “Diode-pumped femtosecond solid-state waveguide

- laser with a 4.9 GHz pulse repetition rate,” *Opt. Lett.*, vol. 37, no. 21, pp. 4416–4418, 2012.
- [40] <http://www.schott.com/>.
- [41] A. Choudhary, P. Kannan, J. I. Mackenzie, X. Feng, and D. P. Shepherd, “Ion-exchanged Tm^{3+} :glass channel waveguide laser,” *Opt. Lett.*, vol. 38, no. 7, pp. 1146–1148, 2013.
- [42] F. Gardillou, Y. E. Romanyuk, C. N. Borca, R.-P. Salath, and M. Pollnau, “Lu, Gd codoped $\text{KY}(\text{WO}_4)_2$:Yb epitaxial layers: towards integrated optics based on $\text{KY}(\text{WO}_4)_2$,” *Opt. Lett.*, vol. 32, no. 5, pp. 1317–1319, 2007.
- [43] N. V. Kuleshov, A. A. Lagatsky, A. V. Podlipensky, V. P. Mikhailov, and G. Huber, “Pulsed laser operation of yb-doped $\text{KY}(\text{WO}_4)_2$ and $\text{KGd}(\text{WO}_4)_2$,” *Opt. Lett.*, vol. 22, no. 17, pp. 1317–1319, 1997.
- [44] D. Geskus, E. H. Bernhardt, K. van Dalzen, S. Aravazhi, and M. Pollnau, “Highly efficient Yb^{3+} -doped channel waveguide laser at 981 nm,” *Opt. Express*, vol. 21, no. 11, pp. 1317–1319, 2013.
- [45] K. Suzuki, V. Sharma, J. G. Fujimoto, E. P. Ippen, and Y. Nasu, “Characterization of symmetric [3 3] directional couplers fabricated by direct writing with a femtosecond laser oscillator,” *Opt. Express*, vol. 14, no. 6, pp. 2335–2343, 2006.
- [46] S. Nolte, M. Will, and J. B. A. Tunnermann, “Femtosecond waveguide writing: a new avenue to three-dimensional integrated optics,” *Appl. Phys. A*, vol. 77, no. 1, pp. 109–111, 2003.
- [47] N. D. Psaila, R. R. Thomson, H. T. Bookey, A. K. Kar, N. Chiodo, R. Oselame, G. Cerullo, A. Jha, and S. Shen, “Er:Yb-doped oxyfluoride silicate

- glass waveguide amplifier fabricated using femtosecond laser inscription,” *Appl. Phys. Lett.*, no. 13, p. 131102, 2007.
- [48] T. Calmano, J. Siebenmorgen, A.-G. Paschke, C. Fiebig, K. Paschke, G. Erbert, K. Petermann, and G. Huber, “Diode pumped high power operation of a femtosecond laser inscribed Yb:YAG waveguide laser [invited],” *Optical Materials Express*, vol. 1, no. 3, pp. 428–433, 2011.
- [49] S. Hakobyan, V. J. Wittwer, K. Hasse, C. Kränkel, T. Südmeyer, and T. Calmano, “Highly efficient Q-switched Yb:YAG channel waveguide laser with 5.6 W of average output power,” *Opt. Lett.*, vol. 41, no. 20, pp. 4715–4718, 2016.
- [50] <http://www.rp-photonics.com/>.
- [51] R. Mary, G. Brown, S. J. Beecher, F. Torrisi, S. Milana, D. Popa, T. Hasan, Z. Sun, E. Lidorikis, S. Ohara, A. C. Ferrari, and A. K. Kar, “1.5 GHz picosecond pulse generation from a monolithic waveguide laser with a graphene-film saturable output coupler,” *Opt. Express*, vol. 21, no. 7, pp. 7943–7950, 2013.
- [52] H. Byun, D. Pudo, S. Frolov, A. Hanjani, J. Shmulovich, E. P. Ippen, and F. X. Kärtner, “Integrated 2 GHz femtosecond laser based on a planar Er-doped lightwave circuit,” *CLEO 2010*, p. CFE5, 2010.
- [53] G. Salamu, F. Jipa, M. Zamfirescu, and N. Pavel, “Watt-level output power operation from diode-laser pumped circular buried depressed-cladding waveguides inscribed in Nd:YAG by direct femtosecond-laser writing,” *IEEE Photonics Journal*, vol. 8, no. 1, pp. 1–9, 2016.
- [54] L. McCaughan, “Influence of temperature and initial titanium dimensions of fiber-Ti:LiNbO₃ waveguide insertion loss at $\lambda = 1.3 \mu\text{m}$,” *IEEE J. Quantum Electron.*, vol. 19, no. 2, pp. 131–136, 1983.

- [55] D. J. H. C. Maas, B. Rubin, A. R. Bellancourt, D. Iwaniuk, S. V. Marchese, T. Südmeyer, and U. Keller, “High precision optical characterization of semiconductor saturable absorber mirrors,” *Optics Express*, vol. 16, no. 10, pp. 7571–7579, 2008.
- [56] G. J. Spühler, R. Paschotta, M. P. Kullberg, M. Graf, M. Moser, E. Mix, G. Huber, C. Harder, and U. Keller, “A passively Q-switched Yb:YAG microchip laser,” *Appl. Phys. B*, vol. 72, no. 3, pp. 285–287, 2001.
- [57] Y. Jia, Y. Tan, C. Cheng, J. R. V. de Aldana, and F. Chen, “Q-switched regimes from Nd:YAG ridge waveguides produced by combination of swift heavy ion irradiation and femtosecond laser ablation,” *Opt. Express*, vol. 22, no. 11, pp. 12900–12908, 2014.
- [58] A. Choudhary, S. Dhingra, B. D’Urso, P. Kannan, and D. P. Shepherd, “Graphene Q-switched mode-locked and Q-switched ion-exchanged waveguide lasers,” *IEEE Photonic Tech. Lett.*, vol. 27, no. 6, pp. 7943–7950, 2015.
- [59] Y. Ren, G. Brown, R. Mary, G. Demetriou, D. Popa, F. Torrisi, F. C. A. C. Ferrari, and A. K. Kar, “7.8-GHz Graphene-Based 2- μm Monolithic Waveguide laser,” *IEEE Journal of selected topics in Quant. Electr.*, vol. 21, no. 1, pp. 7943–7950, 2015.
- [60] S. Y. Choi, F. Rotermund, C. Kränkel, and T. Calmano, “Mode-locking of a femtosecond-laser-inscribed Yb:YAG channel waveguide laser using a carbon nanotube saturable absorber,” *CLEO EU 2017*, pp. cj–10–4, 2017.
- [61] A. A. Lagatsky, A. Choudhary, P. Kannan, D. P. Shepherd, W. Sibbett, and C. T. A. Brown, “Fundamentally mode-locked, femtosecond waveguide oscillators with multi-gigahertz repetition frequencies up to 15 GHz,” *Opt. Express*, vol. 21, no. 17, pp. 19608–19614, 2013.

- [62] J. Ye, H. Schnatz, and L. W. Hollberg, “Optical frequency combs: From frequency metrology to optical phase control,” *IEEE J. Sel. Top. Quantum Electron.*, vol. 9, no. 4, pp. 1041–1058, 2003.
- [63] S. A. Diddams, L. Hollberg, and V. Mbele, “Molecular fingerprinting with the resolved modes of a femtosecondlaser frequency comb,” *Nature*, vol. 445, no. 7128, pp. 627–630, 2007.
- [64] S. Schiller, “Spectrometry with frequency combs,” *Opt. Lett.*, vol. 27, no. 9, pp. 766–768, 2002.
- [65] S. A. Diddams, T. Udem, J. C. Bergquist, E. A. Curtis, R. E. Drullinger, L. Hollberg, W. M. Itano, W. D. Lee, C. W. Oates, K. R. Vogel, and D. J. Wineland, “An optical clock based on a single trapped $^{199}\text{Hg}^+$ ion,” *Science*, vol. 293, no. 5531, pp. 825–828, 2001.
- [66] U. Sterr, C. Degenhardt, H. Stoehr, C. Lisdat, H. Schnatz, J. Helmcke, F. Riehle, G. Wilpers, C. Oates, and L. Hollberg, “The optical calcium frequency standards of PTB and NIST,” *C. R. Phys.*, vol. 5, no. 8, pp. 845–855, 2004.
- [67] C.-H. Li, A. J. Benedick, P. Fendel, A. G. Glenday, F. X. Kärtner, D. F. Phillips, D. Sasselov, A. Szentgyorgyi, and R. L. Walsworth, “A laser frequency comb that enables radial velocity measurements with a precision of 1 cm s^{-1} ,” *Nature*, vol. 452, no. 7187, pp. 610–612, 2008.
- [68] T. Steinmetz, T. Wilken, C. Araujo-Hauck, R. Holzwarth, T. W. Hänsch, L. Pasquini, A. Manescau, S. D’Odorico, M. T. Murphy, T. Kentischer, W. Schmidt, and T. Udem, “Laser frequency combs for astronomical observations,” *Science*, vol. 321, no. 5894, pp. 1335–1337, 2008.
- [69] T. M. Fortier, M. S. Kirchner, F. Quinlan, J. Taylor, J. C. Bergquist, T. Rosenband, N. Lemke, A. Ludlow, Y. Jiang, C. W. Oates, and S. A.

- Diddams, “Generation of ultrastable microwaves via optical frequency division,” *Nat. Photonics*, vol. 5, no. 7, pp. 425–429, 2011.
- [70] X. Xie, R. Bouchand, D. Nicolodi, M. Giunta, W. Hnsel, M. Lezius, A. Joshi, S. Datta, C. Alexandre, M. Lours, P.-A. Tremblin, G. Santarelli, R. Holzwarth, and Y. L. Coq, “Photonic microwave signals with zeptosecond-level absolute timing noise,” *Nature Photonics*, vol. 11, no. 1, pp. 44–47, 2017.
- [71] A. Bartels, D. Heinecke, and S. A. Diddams, “10-GHz self-referenced optical frequency comb,” *Science*, vol. 326, no. 5953, p. 681, 2009.
- [72] J. Rauschenberger, T. Fortier, D. Jones, J. Ye, and S. Cundiff, “Control of the frequency comb from a modelocked erbium-doped fiber laser,” *Science*, vol. 10, no. 24, pp. 1404–1410, 2002.
- [73] N. R. Newbury and W. C. Swann, “Low-noise fiber-laser frequency combs,” *J. Opt. Soc. Am. B*, vol. 24, no. 8, pp. 1756–1770, 2007.
- [74] D. C. Heinecke, A. Bartels, and S. A. Diddams, “Offset frequency dynamics and phase noise properties of a self-referenced 10 GHz Ti:sapphire frequency comb,” *Opt. Express*, vol. 19, no. 19, pp. 18440–18451, 2011.
- [75] S. Schilt and T. Sudmeyer, “Carrier-envelope offset stabilized ultrafast diode-pumped solid-state lasers,” *Appl. Sci.*, vol. 5, no. 4, pp. 787–816, 2015.
- [76] K. Grel, V. J. Wittwer, S. Hakobyan, S. Schilt, and T. Sudmeyer, “Carrier envelope offset frequency detection and stabilization of a diode-pumped mode-locked Ti:sapphire laser,” *Opt. Lett.*, vol. 42, no. 6, pp. 1035–1038, 2017.

- [77] M. Endo, I. Ito, and Y. Kobayashi, “Direct 15-GHz mode-spacing optical frequency comb with a Kerr-lens mode-locked Yb:Y₂O₃ ceramic laser,” *Opt. Express*, vol. 23, no. 2, pp. 1276–1282, 2015.
- [78] A. Klenner, M. Golling, and U. Keller, “A gigahertz multimode-diode-pumped Yb:KGW enables a strong frequency comb offset beat signal,” *Opt. Express*, vol. 21, no. 8, pp. 10351–10357, 2013.
- [79] S. A. Meyer, T. M. Fortier, S. Lecomte, and S. A. Diddams, “A frequency-stabilized Yb:KYW femtosecond laser frequency comb and its application to low-phase-noise microwave generation,” *Appl. Phys. B*, vol. 112, no. 4, pp. 565–570, 2013.
- [80] A. Klenner, S. Schilt, T. Südmeyer, and U. Keller, “Gigahertz frequency comb from a diode-pumped solid-state laser,” *Opt. Express*, vol. 22, no. 25, pp. 31008–31019, 2014.
- [81] A. Klenner, A. S. Mayer, A. R. Johnson, K. Luke, M. R. E. Lamont, Y. Okawachi, M. Lipson, A. L. Gaeta, and U. Keller, “Gigahertz frequency comb offset stabilization based on supercontinuum generation in silicon nitride waveguides,” *Opt. Express*, vol. 24, no. 10, pp. 11043–11053, 2016.
- [82] A. S. Mayer, A. Klenner, A. Johnson, K. Luke, M. Lamont, Y. Okawachi, M. Lipson, A. Gaeta, and U. Keller, “Low-noise Gigahertz Frequency Comb from diode-Pumped Solid-State Laser using Silicon Nitride Waveguides,” *Advanced Solid State Lasers (Optical Society of America, 2015)*, p. AT4A.5, 2015.
- [83] S. A. Meyer, J. A. Squier, and S. A. Diddams, “Diode-pumped Yb:KYW femtosecond laser frequency comb with stabilized carrier-envelope offset frequency,” *Eur. Phys. J. D*, vol. 48, no. 1, pp. 19–26, 2008.
- [84] M. C. Stumpf, S. Pekarek, A. E. H. Oehler, T. Südmeyer, J. M. Dudley, and U. Keller, “Self-referencable frequency comb from a 170-fs, 1.5- μ m

-
- solid-state laser oscillator,” *Appl. Phys. B*, vol. 99, no. 3, pp. 401–408, 2010.
- [85] S. Schilt, N. Bucalovic, V. Dolgovskiy, C. Schori, M. C. Stumpf, G. D. Domenico, S. Pekarek, A. E. H. Oehler, T. Südmeyer, U. Keller, and P. Thomann, “Fully stabilized optical frequency comb with sub-radian CEO phase noise from a SESAM-modelocked 1.5- μm solid-state laser,” *Opt. Express*, vol. 19, no. 24, pp. 24171–24181, 2011.
- [86] C.-C. Lee, Y. Hayashi, D. Hou, K. Silverman, A. Feldman, T. Harvey, R. Mirin, and T. R. Schibli, “Highly phase-coherent stabilization of carrier-envelope-offset frequency with graphene modulator on SESAM,” *Conference on Lasers and Electro-Optics (2016) (Optical Society of America, 2016)*, p. SM3H.7, 2016.
- [87] T. D. Shoji, W. Xie, K. L. Silverman, A. Feldman, T. Harvey, R. P. Mirin, and T. R. Schibli, “Ultra-low-noise monolithic mode-locked solid-state laser,” *Optica*, vol. 3, no. 9, pp. 995–998, 2016.
- [88] S. Schilt, N. Bucalovic, L. Tombez, V. Dolgovskiy, C. Schori, G. D. Domenico, M. Zaffalon, and P. Thomann, “Frequency discriminators for the characterization of narrow-spectrum heterodyne beat signals: application to the measurement of a sub-hertz carrier-envelope-offset beat in an optical frequency comb,” *Rev. Sci. Instrum.*, vol. 82, no. 12, p. 123116, 2011.
- [89] A. Schlatter, S. C. Zeller, R. Grange, R. Paschotta, and U. Keller, “Pulse-energy dynamics of passively mode-locked solid-state lasers above the Q-switching threshold,” *J. Opt. Soc. Am. B*, vol. 21, no. 8, pp. 1469–1478, 2004.

- [90] F. Emaury, A. Diebold, A. Klenner, C. J. Saraceno, S. Schilt, T. Südmeyer, and U. Keller, “Frequency comb offset dynamics of SESAM modelocked thin disk lasers,” *Opt. Express*, vol. 23, no. 17, pp. 21836–21856, 2015.
- [91] G. D. Domenico, S. Schilt, and P. Thomann, “Simple approach to the relation between laser frequency noise and laser line shape,” *Appl. Opt.*, vol. 49, no. 25, pp. 4801–4807, 2010.
- [92] V. Dolgovskiy, N. Bucalovic, P. Thomann, C. Schori, G. D. Domenico, and S. Schilt, “Cross-influence between the two servo loops of a fully stabilized Er: fiber optical frequency comb,” *J. Opt. Soc. Am. B*, vol. 29, no. 10, pp. 2944–2957, 2012.
- [93] D. A. Howe, D. U. Allan, and J. A. Barnes, “Properties of Signal Sources and Measurement Methods,” *Proceedings of the 35th Annual Frequency Control Symposium (IEEE, 1981)*, pp. 669–716, 1981.
- [94] R. W. P. Drever, J. L. Hall, F. V. Kowalski, J. Hough, G. M. Ford, A. J. Munley, and H. Ward, “Laser phase and frequency stabilization using an optical resonator,” *Appl. Phys. B*, vol. 31, no. 2, pp. 97–105, 1983.
- [95] H. R. Telle, B. Lipphardt, and J. Stenger, “Kerr-lens, mode-locked lasers as transfer oscillators for optical frequency measurements,” *Appl. Phys. B*, vol. 74, no. 1, pp. 1–6, 2002.
- [96] M. Beck, A. Cox, T. Pltzing, M. Indlekofer, T. Mandhyani, P. Leiprecht, and A. Bartels, “Turn-key 1 GHz Ti:sapphire frequency comb with enhanced offset locking bandwidth,” *8th Frequency Standard and Metrology Symposium (2015)*, vol. D04, pp. 669–716, 2015.
- [97] D. Matei, T. Legero, S. Häfner, C. Grebing, R. Weyrich, W. Zhang, L. Sonderhouse, J. Robinson, J. Ye, F. Riehle, and U. Sterr, “1.5 μm Lasers with Sub-10 mHz Linewidth,” *Physical Review Letters*, vol. 118, no. 26, p. 263202, 2017.

- [98] W. F. Walls, “Cross-correlation phase noise measurements,” *Proceedings of the 1992 IEEE Frequency Control Symposium*, pp. 257–261, 1992.
- [99] B. R. Washburn, W. C. Swann, and N. R. Newbury, “Response dynamics of the frequency comb output from a femtosecond fiber laser,” *Opt. Express*, vol. 13, no. 26, pp. 10622–10633, 2005.
- [100] L. Karlen, G. Buchs, E. Portuondo-Campa, and S. Lecomte, “Efficient carrier-envelope offset frequency stabilization through gain modulation via stimulated emission,” *Opt. Letters*, vol. 41, no. 2, pp. 376–379, 2016.
- [101] M. Hoffmann, S. Schilt, and T. Südmeyer, “CEO stabilization of a femtosecond laser using a SESAM as fast opto-optical modulator,” *Opt. Express*, vol. 21, no. 24, pp. 30054–30064, 2013.
- [102] N. Bucalovic, V. Dolgovskiy, M. C. Stumpf, C. Schori, G. D. Domenico, U. Keller, S. Schilt, and T. Südmeyer, “Effect of the carrier-envelope-offset dynamics on the stabilization of a diode-pumped solid-state frequency comb,” *Opt. Letters*, vol. 37, no. 21, pp. 4428–4430, 2012.
- [103] A. Klenner and U. Keller, “All-optical Q-switching limiter for high-power gigahertz modelocked diode-pumped solid-state lasers,” *Opt. Express*, vol. 23, no. 7, pp. 8532–8544, 2015.
- [104] A. S. Mayer, C. Phillips, and U. Keller, “10-GHz straight-cavity SESAM-modelocked Yb:CALGO laser enabled by cascading of second-order nonlinearities,” *ASSL 2017 Nagoya, Japan*, p. ATh1A.3, 2017.

Curriculum Vitae

Name Sargis Hakobyan
Date of Birth 16/05/1991
Nationality Armenia

Education

2017-present Post Doctoral researcher at École Polytechnique Fédérale de Lausanne (EPFL), Neuchâtel, Switzerland
2013-2017 Doctoral studies at University of Neuchâtel, Switzerland
2011-2013 Master studies at École Polytechnique Fédérale de Lausanne (EPFL), Lausanne, Switzerland
2007-2011 Bachelor studies at Yerevan State University, Yerevan, Armenia

Research Experience

2013-2017 Research assistant at Laboratoire Temps-Fréquence, University of Neuchâtel, Neuchâtel, Switzerland
2012-2013 Research assistant at Laboratory of Physics of Nanostructures, EPFL, Lausanne, Switzerland

Acknowledgments

I thank,

Thomas, for being a great professor and supervising me over the past four years, and for motivating me the most.

Stéphane, for being an excellent scientific teacher, and for revealing the world of ultralow noise to me.

Kutan, for being a great friend and an office mate for the entire time, I will have a lot good memories from my PhD thanks to him.

Valentin, for his constant and selfless support, and for teaching a lot of technical skills without which it would have been impossible to work efficient.

Loïc, William, and Pierre, to be great colleagues and creating the fun atmosphere that was very important for me.

Bertrand, for teaching me waveguides, and being a great party mate.

Nayara, Clément, and Norbert, to be great team mates to party and travel all around the world.

Maxim, François, and other LTF members, for being very positive and supportive.

My parents, for their unconditional love and support.

My wife Zara, for believing in me, and being with me the entire time, I love you.